# Exploring Yaw and Roll Dynamics of Ground Vehicles Using TS Fuzzy Approach and a Novel Method for Stability Analysis Based on Lyapunov Exponents

by

Ali Reza Armiyoon

A thesis submitted to
The Faculty of Graduate Studies of
The University of Manitoba
in partial fulfillment of the requirements
of the degree of

Doctor of Philosophy

Department of Mechanical Engineering
The University of Manitoba
Winnipeg, Manitoba, Canada
August 2015

Thesis advisor
**Christine Q. Wu**

Author
**Ali Reza Armiyoon**

**Exploring Yaw and Roll Dynamics of Ground Vehicles Using TS Fuzzy Approach and a Novel Method for Stability Analysis Based on Lyapunov Exponents**

# Abstract

Vehicle yaw stabilization and rollover prevention are two key factors in safety of vehicles. Designing a controller that can address both of the above safety concerns is of interest. In addition, it is essential that the performance of such a controller is evaluated properly. This can be done using a proper stability analysis. The above research problem is challenging for two reasons. First, maintaining both of the objectives, yaw stabilization and rollover mitigation, is contradictory at some instances, specifically when the vehicle is close to the verge of wheel lift-off. Second, the complexity of the dynamics of vehicle systems, which mostly arises from tire dynamics, makes the problems of controller design and stability analysis more challenging.

In this Ph.D. thesis, a novel method for stability analysis of dynamical systems using the concept of Lyapunov exponents is proposed. The proposed method for stability analysis does not have the limitations of the current methods, and more specifically, can identify boundaries of the whole stability regions of attractors in a dynamical system. Furthermore, this method is computationally efficient and can be applied to general forms of nonlinear systems. The proposed stability analysis scheme is applied to the closed loop systems of ground vehicles with T-S fuzzy controllers for the purpose of evaluating and comparing the performance of the systems. The T-S fuzzy controllers integrate yaw stabilization and rollover avoidance. The ground vehicles that are studied in this research consist of torsionally flexible and torsionally rigid vehicles, which have differences in their dynamics because of the torsional compliance in their frames. The torsional compliance plays an important role in the dynamics, specifically for long vehicles, leading to different rollover indexes in the front and rear axles of the vehicles. The T-S fuzzy controllers are capable of prioritizing the contradictory objectives, and capturing all the essential complexities of dynamics of the systems.

# Acknowledgments

I wish to express my deepest gratitude to my advisor, Prof. Christine Wu, for her continued support and guidance of this research. Prof. Wu always had a positive and constructive approach, and by her enthusiasm and her encouragements taught me how to face the challenges in my research.

I would like to extend my sincere appreciation to my committee members, Prof. Subramaniam Balakrishnan, Prof. Shaahin Filizadeh, Prof. Abba Gumel, and Prof. Sherif Sherif, for their valuable feedback, and for the time they spent for evaluating this thesis.

I would also like to thank Prof. Amir Khajepour, who is one of the leading researchers in the area of vehicle dynamics and control, for his excellent questions and incisive comments. It was my pleasure and a moment of excitement when I found out that Prof. Khajepour was selected as the external referee of my thesis.

I would like to acknowledge the help of my friends Dr. Amir Fassih, Dr. Masoumeh Esfandiari, Dr. Mansoor Alghooneh, and Mr. Damon Bazargan in the application of control theory, Mr. Ali Azimi in implementing the method for calculating the Jacobian Matrix, and Mr. Hamidreza Nasrinpour, Mr. Siavash Malektaji, and Mr. Hamed Janani in assisting me in understanding the concepts of Monte Carlo Techniques and SVM algorithms.

I am immensely grateful to my dearest friends who contributed in my life during my stay in Winnipeg, including but not limited to, Javad, Mansoor, Ali Azimi, Masoud, Ehsan Alishahi, Damon, Elahe Ebrahimnia, Masoumeh Esfandiari, and many others.

I would also like to acknowledge the financial support of the Natural Sciences and Engineering Research Council (NSERC) of Canada, and the University of Manitoba.

Last, but certainly not least, I would like to send my love to my family, who are although away from me, but have always had unconditional support and encouragement. Specifically my parents whom I cannot thank enough for everything that they have done for me.

*This thesis is dedicated to my parents and all the friends who contributed in my life during my stay in Winnipeg.*

# Contents

# List of Figures

# List of Tables

# Nomenclature

## Acronyms and Abbreviations

| | |
|---|---|
| BoA | Basin of Attraction |
| CN1, CN2 | Controller#1, Controller#2 |
| CDF, PDF | Cumulative and probability distribution function |
| GSR | Gram-Schmidt reorthonormalization |
| HSUV | Heavy Single Unit Vehicle |
| LMI | Linear Matrix Inequality |
| LE | Lyapunov Exponent |
| MF | Membership Function |
| $RI$ | Rollover index |
| ST1, ST2 | Strategy#1, Strategy#2 |
| SVM | Support vector machine |
| TRV, TFV | Torsionally rigid and flexible vehicles |

## Greek Symbols

| | |
|---|---|
| $\zeta$ | A random number used in the Monte Carlo method |
| $\boldsymbol{\gamma}$ | A set of vectors for storing the principal axes in calculation of LEs |
| $\boldsymbol{\Omega}_{ad}$ | Admissible region of the stability analysis |
| $\boldsymbol{\sigma}^j$ | An orthogonal set of vector used in GSR process of calculating LEs |
| $\alpha$ | Configuration parameter of the double pendulum |
| $\omega_c$ | Cut-off frequency of the filter used in the TFV model |
| $\tilde{p}$ | External force of the double pendulum |

| | |
|---|---|
| $\theta_1$, $\theta_2$ | Generalized coordinates of the double pendulum |
| $\boldsymbol{\zeta}$ | Integration of the error between the actual value and the desired value in control systems |
| $\psi(.,.)$ | Kernel functions in SVM calculations |
| $\lambda$ | Lyapunov exponents |
| $\kappa$, $\mu$ | Premise (scheduling) variables and fuzzy sets in the T-S fuzzy system |
| $\phi$ | Roll angles in the vehicle models |
| $\boldsymbol{\omega}_{i,j}$ | Rotational velocities of masses of the TFV model $i = s, u$, $j = f, r$ |
| $\eta_1$, $\eta_2$ | Scaling factors for adjusting probabilities of the events |
| $\beta$ | Side slip angle in vehicle models |
| $\boldsymbol{\Psi}_t$ | State transition matrix of the linearized system in calculation of LEs |
| $\delta$ | Steering angle in vehicle models |
| $\psi$ | Yaw angle of a vehicle |

## Subscripts and Superscripts

| | |
|---|---|
| $(.)_f$, $(.)_r$ | Front and rear portion of the heavy single unit vehicle |
| $(.)_L$, $(.)_R$ | Left and right side of the vehicles |
| $(.)_s$, $(.)_u$ | Sprung and unsprung mass of the vehicles |

## Roman Symbols

| | |
|---|---|
| $P$ | A common positive definite matrix in LMI approach |
| $\mathbf{z}$ | A function in the feature space in SVM calculations |
| $K_{us}$ | A measure for quantifying understeer/oversteer quality of vehicles |
| $\mathbf{p}$ | Array of parameters of a dynamical system |
| $B_y$, $C_y$, $D_y$, $E_y$ | Coefficients of Pacejka magic formula |
| $M_z$ | Controlling yaw moments |
| $C_\alpha$ | Cornering stiffness of tires |
| $P(x)$, $p(x)$ | Cumulative and probability distribution function of the variable $x$ |
| $G(\mathbf{x})$ | Decision function in a SVM problem |

| | |
|---|---|
| $n$ | Dimension of a dynamical system |
| $a$, $b$ | Distance from c.g. of vehicles to front and rear axles |
| $q_k$, $Q_k$ | Generalized coordinates and external forces in Lagrange equation |
| $h$ | Height properties in the vehicle system |
| $z_{i,j}$ | Heights of masses of the TFV model $i = s, u$, $j = f, r$ |
| $\mathbf{u}$, $\mathbf{w}$, $\mathbf{y}$ | Input, output, and disturbance in the control systems |
| $\mathbf{J}$ | Jacobian matrix of a dynamical system |
| $a_y$ | Lateral acceleration of the vehicles |
| $v_x$, $v_y$ | Longitudinal and lateral velocity of vehicles |
| $F(s)$ | Low pass filter function of the complex variable $s$ |
| $C_{ax,f}^{LB}$, $C_{ax,i}^{UB}$ | Lower and upper bounds of axle's force, $F_y^{ax,i}$, in the vehicle models,$i = f, r$ |
| $m$ | Mass properties used the vehicle systems and the double pendulum system |
| $A', A'', B', E', C$ | Matrices of the state space form of the vehicle systems |
| $w_1$ | Minimum number of points found in each iteration |
| $I_i$ | Moments of inertia of the vehicle, $i = z, x, xz$ |
| $E_i$ | Mutually exclusive events in the Monte Carlo method |
| $p$, $c$ | Nondimensional parameters of the double pendulum |
| $F_{z,i}$, $F_{z0,i}$ | Normal force and nominal value of normal force on tires, $i = f, r$ |
| $Y_1^j$, $Y_e^j$ | Position vector of the $j^{th}$ center point and the comparing points |
| $\mathbf{Q}$, $\mathbf{R}$ | Positive definite matrices used as design parameters of the controllers |
| $p_i$ | Probability of the $i^{th}$ event in the Monte Carlo method |
| $p_m$ | Probability that the $m^{th}$ point in the grid is selected |
| $\tilde{r}$ | Resolution of the admissible region |
| $t_r$, $t_s$, $MP$ | Rise time, settling time, and overshoot of the response of a system |
| $\mathbf{x}$, $\mathbf{f}$ | State vector and state vector function |
| $F_y^{axle}$ | Sum of tire lateral forces in an axle of a vehicle |
| $K_{s,i}, C_{s,i}$ | Suspension stiffness and suspension damping of an axle of the TRV, $i = f, r$ |

| | |
|---|---|
| $\mathbb{R}^n$, $\mathbb{Z}$ | The $n$-dimensional space and feature space used in SVM calculations |
| $x$, $y$, $z$ | The attached coordinates to the vehicle dynamic systems |
| $E_m$ | The event that the $m^{th}$ point in the grid is selected $m = 1, 2, \ldots, N$ |
| $X$, $Y$, $Z$ | The inertia coordinates of the vehicle dynamic systems |
| $\mathbf{BN}^i$ | The set that includes all the boundary points found for the $i^{th}$ attractor |
| $A_1^j$ | The set that includes the center points, $j = 1, \ldots, L$ |
| $A_e^j$ | The set that includes the comparing point of the $j^{th}$ center point, $j = 1, \ldots, L$ and $e = 2, \ldots, q+1$ |
| $u_1$ | Threshold for the number of consecutive iterations that the number of found points is less than $w_1$ |
| $t$ | Time in dynamical systems |
| $F_x$, $F_y$ | Tire longitudinal and lateral forces |
| $k$, $\tilde{c}$ | Torsion spring and damper of the double pendulum |
| $T$ | Track width of the vehicle models |
| $\mathbf{V}_{i,j}$ | Translational velocities of masses of the TFV model $i = s, u$, $j = f, r$ |
| $\mathbf{e}_j$ | Unit vector in the direction of the $j^{th}$ state of a dynamical system |
| $l$ | Wheel base of the vehicle |
| $r$, $r_d$ | Yaw rate and desired value for yaw rate in vehicle models |

# Chapter 1

# Introduction

## 1.1 Motivation

Active control of vehicle dynamics have been a major area of research for the last decades as it is used for enhancement of vehicle safety. The safety issue is crucially important for general public and governments and has drawn special attention. In terms of dynamics of vehicles, the yaw and roll motions have significant effects on safety of vehicles. Controlling yaw motion is important because it determines the desired path of the vehicle. A fluctuating or a slow response of yaw motion can be dangerous specially in emergency cases such as an obstacle avoidance. Moreover, drivers prefer vehicles that are fast in response and are easy to maneuver. For the purpose of safe maneuvering of vehicles and providing the drivers with better feeling of driving, i.e., better quality of maneuverability, yaw motion must be controlled.

On the other hand, the most important safety concern is rollover. Nowadays, there are many regulations in place that mandate the use of rollover prevention systems in vehicles. In spite of the use of such systems, rollover is still one of the most fatal and most tragic events of vehicle accidents. Only 3% of all accidents involve rollover crashes, which account for 31% of occupant fatalities [4]. Therefore, addressing this issue is also of crucial importance.

An important part of study of any dynamical system, such as yaw and roll dynamics

of ground vehicles, is stability analysis. Proper stability analysis must provide enough information about the nature of a system, such as the whole stability region of an attractor, in a computationally efficient way. Finding the whole stability region of an attractor can be highly beneficial in some cases such as comparing performances of two control systems. Most of the existing methods are not capable of providing the whole stability region. In addition, finding the whole stability region is not trivial when the dynamics of a system is complex. A majority of the current methods are not applicable to highly complex systems. Therefore, developing a method that can identify boundaries of the whole stability region of an attractor is desirable.

In this research, vehicles with torsionally flexible structures are also of interest. Examples of torsionally flexible vehicles (TFV) are heavy single unit vehicles (HSUV). Torsionally flexible vehicles, as opposed to torsionally rigid vehicles (TRV), are mostly long vehicles. The significance of the torsional compliance in the frame comes into account due to the excessive length of such vehicles. In addition, TFVs have relatively high center of gravities which makes them more vulnerable to rollover events. Thus, studying the nature of rollover in TFVs is imperative to avoid such tragic events.

## 1.2 Literature Review

### 1.2.1 Yaw Motion Control and Rollover Prevention of Ground Vehicles

Controlling the yaw and roll motions are equally important as the lack of any of the two can have detrimental effects on the performance of a vehicle, and eventually on safety. Therefore, integration of controlling both of the motions is critical. A serious challenge in controlling both of the motions is the contradictory nature of the two dynamics. Obviously, one of the basic functions of vehicles is maneuvering according to the desire of the driver. When a driver maneuvers a vehicle, the vehicle becomes closer to the wheel lift-off situation

in comparison with the case of straight line motion. However, rollover prevention is not a concern when the vehicle is away from the limits of wheel lift-off. On the other hand, when the vehicle is close to the margins of wheel lift-off, as it is shown in the results and discussion chapter, tracking a desired value of yaw rate can contribute to occurrence of wheel lift-off. In such circumstances, maintaining both of the objectives, following a desired yaw rate, and preventing wheel lift-off from happening, at the same time is not possible. That means there must be a compromise between maneuverability and rollover prevention.

In this section, the application of active control systems designed for the purpose of yaw stabilization and rollover prevention is reviewed. First, a history of using active control systems in passenger cars, as a large group of TRVs, as well as TFVs, is presented, and next, the recent advancements in such control algorithms are reviewed.

**Background on Development of Active Control Systems for Ground Vehicles**

The contributions on vehicle dynamics and control research are highly impressive. Active control of vehicle dynamics dates back to 1980s [5; 6; 7; 8] and 1990s [9; 10; 11; 12; 13; 14; 15] as safety of vehicles have been an important issue for the last decades. Sampson surveyed that until 1980s most of the research on active safety and control was conducted in railway industry [16]. Inspired from railway machinery, Goodall and Kortüm reviewed the state-of-the-art developments in active control of ground vehicles in 1983 [5]. In 1989 an air spring control system was introduced to improve handling and ride comfort of a ground vehicle [8]. Lang and Walz (1991) studied an active roll reduction system using a complex multi-body model to reduce the body roll angle in cornering [17]. Sharp and Pan (1993) designed an anti-roll bar system with rotary actuators, and studied the effects of limitations of control hardware on active roll control of an automobile [18]. An integrated control strategy was introduced by Gordon in 1996 in which the body pitch and the roll attitude angles, and the body bounce motion were controlled. This controller that was designed based on low-speed motions showed enhancements in the aforementioned properties [19]. Darling et al. (1997) investigated the use of a standard anti-roll bar equipped with rotary hydraulic actuators to

reduce the body roll. However, performance of the actuators in severe maneuvers was not satisfactory [20].

**Contributions on Control of Heavy Single Unit Vehicles**

The above mentioned research was performed on passenger cars[1]; however, the research on active safety of heavy vehicles was not as fast-growing as it was for passenger cars. In 1993, Dunwoody and Froese, investigated the potential benefits of using an active roll controller to enhance the roll performance of a tractor semi-trailer by the aid of simulations [21]. The feasibility of reducing the roll angle of commercial vehicles by applying an active roll stabilizer system was investigated by Kusahara in 1994 [22]. This study was performed on a medium-duty truck, with the primary objective of resolving the conflicting relationship between ride comfort and handling. The effect of rear-axle steering on vehicle controllability and stability was also investigated in this study [22]. Although Nissan performed research in the yaw control of medium-duty trucks [23; 24], it was not until 1995 that a roll control system was implemented on a heavy vehicle. A set of switchable air springs and dampers, designed by Mercedes-Benz, was installed and tested on a single unit two-axle medium-duty truck. Using the measurements of driver inputs and other on-board sensors, this system enhanced the roll behavior of the vehicle [25]. Dorling, in 1996, investigated the simultaneous control of pitch, bounce, roll, and yaw motions in his PhD thesis, and focused more on the design of a roll control system for a single unit vehicle [26].

Lin et al. studied the use of an active roll control system for a single unit truck to reduce the lateral load transfer effects in response to steering inputs. They designed a proportional-derivative (PD) lateral acceleration feedback controller [11]. In another study, the results of the PD controller were compared to those of a linear quadratic optimal controller, which was also designed to regulate the load transfer ratio. Although the optimal controller showed

[1]The main group of torsionally rigid vehicles (TRVs) are passenger cars. Similarly a large group of torsionally flexible vehicles (TFVs) are heavy single unit vehicles. Therefore, these terms and their associated examples are interchangeably used in the thesis.

better performance, the PD controller was attractive because of its simple instrumentation requirements [27]. They also extended their work to enhancement of the roll stability of a tractor semi-trailer system. The key idea in their controller was that the vehicle body must turn into the corner, which creates a stabilizing roll moment. They suggested that the torsional compliance of the vehicle frames may have a significant effect on the performance of the roll active safety systems [28].

Sampson et. al introduced models of single unit and articulated heavy vehicles which included the torsional compliance of the frame [2; 16; 29]. As will be discussed later, the inclusion of the compliance is imperative in analyzing the dynamics of such vehicles. This model separates the masses and other properties of the vehicle into front and rear portions as well as sprung and unsprung portions, which results in a model with four masses. The structure compliance is considered as a set of springs and dampers connecting the front and rear sprung masses. More details about this model will be given in Section 4.1.2. Other contributions of Sampson and Cebon were developing LQR and LQG controllers for the active roll control of a single unit truck [2]. They implemented a controller with similar structure into an articulated vehicle in a set of experiments [30].

A challenge in this research is the complex nature of tire forces. The complexity arises from different phenomena such as the nonlinear behavior of tires, the saturation of the forces, and the loss of the forces in an axle due to lateral load transfer effects [3]. The existence of such complex properties demands using a sophisticated method which is able to handle all these issues. The nonlinear properties of tires are not included in the model introduced by Sampson and Cebon in [2] and the subsequent research for HSUVs. Furthermore, in the existing models, the roll angles are assumed to be small; however, in occasions like wheel lift-off such angles may have relatively high values. Therefore, the nonlinear effects of the roll angles must be considered in developing the model as well. Thus, there is a need to extend the existing models of torsionally flexible vehicles to include such important sources of nonlinearity. In this research, the model presented in [2] is utilized as the basis for developing a model that includes the aforementioned properties.

Gaspar et al. investigated the use of a combined control structure to prevent rollover of heavy vehicles. In their research, they used a reduced version of Sampson's model [16], in which the compliance of the frame was not considered. The controllers were based on the Linear Parameter Varying (LPV) model of yaw-roll dynamics, where the forward velocity and the lateral load transfer ratio at the rear axle were the scheduling parameters. In their first attempt in 2005, an active brake control system was proposed to reduce the risk of rollover in heavy vehicles [31]. They extended the proposed controller by combining the brake control system with an active anti-roll bar system in 2006 [32; 33]. A fault detection and identification (FDI) filter, which identifies different actuators' failure, was added to the control structure [34]. LPV modeling was also used by Baslamısh in 2007 with the same control techniques [35].

Yu et al. reported that there is a scarcity of the studies on handling behavior of commercial vehicles, specifically transit buses. They performed an experimental study and analyzed steady-state and transient response of a typical 12-meter transit bus in 2007 [36]. In 2009, Boada et al. proposed a reinforcement learning algorithm using neural networks to improve the roll stability of a heavy single unit vehicle [37]. They used the same model as Sampson's [29]. Gauchía et al. studied the influence of several parameters on the roll stability and the structure stress level of buses in a lane change maneuver in 2010. In their simulation-based analysis, they used the model introduced in [29] to prevent the effects of excessive roll motions on the structure by means of an active roll control system [38].

In 2011, Gauchía et al. introduced a new mathematical model that estimates the threshold of lateral acceleration for buses. This limit is normally obtained by means of rollover tests, which are costly. The proposed model simulated the rollover test, and included the effect of the changes in the position of the center of gravity [39]. A hydro-pneumatic passive suspension system with focus on heavy vehicles was introduced by Cao et al. in 2010. To evaluate ride comfort and handling of the vehicle, and suspension anti-roll and anti-pitch characteristics under various road excitations and steering/braking maneuvers, a comprehensive vehicle model was developed for a heavy single unit vehicle. In their model, the

effect of structure flexibility is not included [40].

A front active steering and braking system was designed by Akhmetov et al. in 2013 for heavy single unit vehicles based on a reference trajectory generation technique. The controllers were designed based on simple dynamic models, and the performance of the controllers were examined by an 8-DOF model, which is similar to Sampson's model [41]. Imine et al. have developed an active steering assistance system to avoid rollover of heavy vehicles using a single body model in 2012. The states of the system are estimated using a high-order sliding mode observer and a twisting algorithm is utilized as the control method [42]. They have also presented a rollover risk prediction algorithm based on high-order sliding mode observers for heavy vehicles in 2014 [43].

Most of the control algorithms for yaw and roll dynamics of torsionally flexible vehicles, which consider the torsional compliance, are either linear, or do not consider the essential nonlinearities in the system. There is a need to develop an integrated control algorithm for yaw stabilization and rollover prevention of TFVs. Such a controller must be capable of capturing the important complexities in dynamics of the vehicle in normal driving conditions and wheel lift-off situations.

### Recent Advancements in Yaw Stabilization and Rollover Prevention of Ground Vehicles

Most of the control methods that are used for torsionally rigid vehicles can be used for torsionally flexible vehicles as well, with some modifications. In the following paragraphs, recent advancements in the yaw rate control and rollover prevention of torsionally rigid vehicles are reviewed.

Maneuverability, i.e. good quality of the yaw rate following, and rollover prevention are mostly dealt with separately in the literature [44; 45]. A model predictive envelope controller for enhancement of handling was introduced in 2013, which bounds the vehicle motion within a stable region of the state space [46] . In [47], a robust on-off switched braking control was designed for rollover prevention in 2014.

Although the contributions in this field are impressive, there are fewer pieces of research that integrate control of maneuverability and rollover prevention [48; 49; 50; 51]. In 2010, a unified chassis controller for rollover prevention and lateral stability was proposed by Yoon et al. where integration is performed through switching among several control modes [51]. The problem with switching controllers in [47] and [51] is that they create discontinuity in the system. This can make the stability analysis rather challenging. For example, finding a Lyapunov function for a discontinuous system is not straightforward, and Lyapunov exponents cannot be used for such a system. In 2013, Rajamani and Piyabongkarn introduced an integrated system for yaw stabilization and rollover prevention using a technique of reducing the longitudinal speed of the vehicle before entering a sharp curve [49]. Although this approach is effective, it directly interferes with the intention of the driver and he/she may resist reducing the speed of the vehicle. In one of the recent works, Alberding et al. proposed a nonlinear hierarchical control allocation system for integration of yaw stabilization and rollover prevention in 2014 [52]. In their controller, a rollover prevention measure was considered as a constraint on the control allocation problem. The control system consists of a high level controller and a control allocation system, which uses an optimized PI controller to regulate the error of the yaw rate with respect to a reference. The rollover prevention constraint is a critical roll angle, and the roll angle of the vehicle is monitored and controlled to be away from this limit. Although the research work is valuable, the choice of a critical roll angle as the indicator of the rollover threat is not ideal. They have also provided a comprehensive survey on integration of rollover prevention and yaw stabilization [52].

T-S fuzzy systems have the capacity to perform integration of control objectives with a high level of accuracy in representing and controlling the complex dynamics of a system [53; 54]. Dahmani et al. have proposed a T-S fuzzy controller for rollover mitigation in 2014. In their work, linear models of tire lateral forces are used and the changes in the forces are considered as uncertainties [55]. Although this approach has some benefits, the author believes that the better approach for modeling the dynamics of the system is to use a comprehensive model that can capture the complexities of tire dynamics as they are readily

available. Besides, if a proper model is not available for a specific vehicle, there are some algorithms that can be employed for estimating tire forces [56]. In addition, the control method proposed by Dahmani et al. has only one objective, which is minimizing the rollover index (RI) [55]. One problem with this approach is that it is neither necessary nor efficient to focus on rollover prevention unless the vehicle is close to the margins of wheel lift-off. T-S fuzzy approaches also have a stability proof for zero-initial conditions. Although this is a significant advantage comparing with other control algorithms, the stability proof is not extended to cases with non-zero-initial conditions.

### 1.2.2 Stability Analysis of Nonlinear Dynamical Systems

Nonlinear dynamical systems are widely present in different fields including biological science, engineering, economics, mathematics, etc. In general, all real world dynamical systems are nonlinear [57]. Stability analysis of a dynamical system consists of finding the attractors of a system, which can be fixed points, limit cycles, toruses, or strange attractors, determining the stability [2] nature of the attractors, and last but not least, identifying the basin of attraction (BoA) of each attractor. A basin of attraction of an attractor is defined as a set of initial conditions for which the system approaches the corresponding attractor. There has been much effort in developing approaches to find boundaries of BoAs. Such approaches can be categorized into two groups: Non-Lyapunov-based (NLB) methods, and Lyapunov-function-based (LFB) methods. Recently, Lyapunov-exponents-based (LEB) methods have been developed in Nonlinear System Research Laboratory (NSRL) at University of Manitoba [58; 59].

Most methods of the NLB group are based on simulations [60; 61; 62; 63; 64; 65]. The work in [66; 67] is based on topological approaches like the viability theory. Genesio et al., used the trajectory reversal method [68], in which the trajectories of the systems are used to find a part of the BoA. In spite of their low computational load, the drawback of

[2] In this research, stability means stability in the sense of Lyapunov. For more information about the definition of Laypunov stability please refer to [57]

simulation-based methods is their dependence on the initial conditions.

Significant research has been carried out on developing LFB methods [69]. The general idea behind the methods of this category consists of two steps. The first step is to derive a Lyapunov function using Lyapunov's direct method. This function gives an initial estimate for the BoA of interest, which is often a part of the whole BoA [70]. The second step is to enlarge the region defined by the Lyapunov function using different methods such as optimization techniques.

Most of the research in LFB group can be further classified into three areas: firstly, to broaden the class of nonlinear systems that can be analyzed using the same class of Lyapunov functions; secondly, to enlarge the class of Lyapunov functions that are used as the initial estimates; finally, to improve the optimization techniques used for enlarging the regions found as a part of the whole BoA.

There are contributions toward extending the type of dynamical systems under study using the same class of Lyapunov functions; however, most of the research in this area is limited to some specific types, like polynomial systems [71; 72; 73]. Enlarging the class of Lyapunov functions as the base estimate for a BoA is another way to enhance the performance of the LFB approach. Balestrino [74] pointed out that the first choice of Lyapunov function, which is the basis for the optimization process, has significant effects on the geometry of the BoA. Therefore, it is imperative that the first estimate is chosen properly. To that end, one approach is to form a Lyapunov function by combining different Lyapunov functions [74; 75; 76; 77; 78].

Regarding the research in the third area, which is improving the optimization techniques, Linear Matrix Inequalities (LMI) [79; 80; 81] and Bilinear Matrix Inequalities (BMI) [71] together with Sum-of-Square (SOS) programming technique [72; 78; 82; 83; 84] are extensively used in the literature. The aim is to enlarge the region that is identified as a part of a BoA of a system by Lyapunov functions. Most of the applications are restricted to specific types of dynamical systems [71; 72]. One problematic issue is a rapid growth in the number of optimization decision variables for which point-wise maximums of polynomial Lyapunov

functions is proposed in [85] as a solution.

Although LFB methods have a strong mathematical basis, one challenge is that it is extremely difficult to establish the initial estimate since there is no constructive way to derive a Lyapunov function for general nonlinear systems. Another important fact is that the LFB methods are not capable of finding the entire BoA of a system, and propose an estimation of the BoA. This estimated region might be close to the whole BoA, or might be a small portion of it. This problem is caused by the fact that Lyapunov functions are not exclusive about the region that they define as a part of the BoA. That is, no conclusion can be made for the regions outside of the estimated BoA by a Lyapunov function.

The concept of Lyapunov exponents, on the other hand, is a constructive and powerful tool for stability analysis, which can be applied to a vast range of nonlinear systems. This concept has been established in NSRL as a practical tool for performing stability analysis. The invariant property of Lyapunov exponents, i.e., Lyapunov exponents are independent from initial conditions, within the same basin of attraction, is the foundation of this approach [86; 58; 87; 88; 89]. A new method, named the BoA edge algorithm, was introduced in [59] that is based on Lyapunov exponents and the gift wrapping algorithm. This method searches for the boundary of the BoA by testing a geometrically iterated set of initial conditions and calculating the respective Lyapunov exponents for them. Although the BoA edge algorithm can provide the boundary of a BoA for a given attractor, it is computationally inefficient and intensive. Such an algorithm is able to find the entire stability region provided that the region has a closed boundary. However, if the boundary consists of disconnected parts, the proposed algorithm fails.

It is worth mentioning that there are methods for finding BoAs of a dynamical system using experimental data [90; 91; 92] which are off the scope of this research.

## 1.3 Research Needs and Challenges of the Research

From the above discussions and the review of literature, the following research needs and challenges are identified:

1. Integration of yaw stabilization and rollover prevention is critical. Satisfying both of the objectives can be contradictory in some occasions. Therefore, there must be a compromise between obtaining each objective at the right time.

2. Important nonlinear effects such as tire nonlinearities are not included in the existing models for TFVs. There is a need to extend the existing models to a model that includes such essential nonlinearities.

3. T-S fuzzy algorithm is an effective method for solving a complex integration problem with contradictory objectives. It can also be effective in modeling and control of systems with complicated nonlinearities with a great accuracy.

4. The methods that are proposed for control of TFVs either use linear algorithms or do not include the essential nonlinearities in the system. Besides, there is a lack of integrated control of yaw stabilization and rollover avoidance for such vehicles.

5. A comprehensive stability analysis can be used for comparing the performance of control systems. As the stability analysis of T-S fuzzy approach is restricted to zero-initial conditions, it cannot provide such information. Therefore, there is a need for a proper stability analysis tool which can guarantee the stability and robustness of a control system.

6. The current methods for identifying stability regions are not capable of finding the entire stability region of an attractor in a computationally efficient way. Therefore, it is extremely valuable if one can establish a stability analysis tool that is invariant, can identify the whole region of a BoA, is applicable to a broad range of dynamical systems including highly complex systems, and at the same time has lower computational load.

7. Some methods of LFB group provide an expression for the boundaries of parts of BoAs. However, such methods have the limitations mentioned before. It is highly desirable if a mathematical expression can be obtained for the boundaries of BoAs. These expressions can be used for monitoring or control purposes.

## 1.4 Objectives of the Research

In this PhD thesis, the stability analysis and control of yaw and roll dynamics of torsionally rigid and torsionally flexible vehicles considering the effects of torsional compliance in their frames are studied. The goal of this research is to devise tools to enhance the behaviour of such vehicles in terms of yaw stability and rollover resistance to contribute to safer their operation.

To that end, a reliable controller that addresses both yaw stability and rollover prevention, as well as a stability analysis scheme that can be used for studying highly complex systems, such as vehicle dynamics systems, are needed. A T-S fuzzy controller is proposed, which prioritizes the two contradictory objectives, maneuverability and rollover prevention, and satisfies each objective according to the situation of the vehicle. When the vehicle is in normal driving conditions, the focus of the controller is on enhancement of yaw stability of the vehicle and assisting the driver to perform their desired maneuver. As the vehicle starts to approach the limits of wheel lift-off, the priority is given to rollover resistance and the controller attempts to prevent wheel lift-off. This control strategy not only provides the driver with high quality of maneuverability in normal driving conditions, but also reduces the chance of rollover. Furthermore, the stability analysis method must be able to provide the entire stability region in an efficient way. A novel approach for identifying the entire BoA of an attractor using the concept of Lyapunov exponents and Monte Carlo techniques is proposed in this thesis. This method is not limited to vehicle systems and can be implemented to a broad range of nonlinear dynamic systems.

In addition, a necessary step in achieving the goal is constructing a suitable model for

dynamics of such vehicles. An extension of the existing model in [2] for TFVs is presented in this research. The extended model benefits from a nonlinear tire model and other nonlinear effects which are necessary to study the behavior of the vehicle in situations like wheel lift-off.

# Chapter 2

# Theoretical Preliminaries

In this chapter all the required preliminaries of the research work are described. First, the concept of Lyapunov exponents as the stability analysis tool is explained. Next, the Monte Carlo principle is discussed, which is a powerful technique utilized to reduce the computational load of the stability analysis. A general description of support vector machine (SVM) learning algorithm is provided; SVM is used to classify the obtained data from the stability analysis. Finally, the control methods that are used in this research including T-S fuzzy approach and optimal linear quadratic regulators are described in this chapter.

## 2.1 Lyapunov Exponents

The concept of Lyapunov (characteristic) exponents is known to be one of the most powerful and constructive tools for detecting chaotic behaviors, and has been exploited in the last decade for dynamical system stability analyses. Lyapunov Exponents, $\lambda_i$ , $(i = 1, ..., n)$, are defined as the average exponential rates of convergence or divergence of two close orbits [93]. Consider an $n$-dimensional smooth dynamical system as:

$$\dot{\mathbf{x}}(t) = \mathbf{f}(\mathbf{x}(t)) \tag{2.1}$$

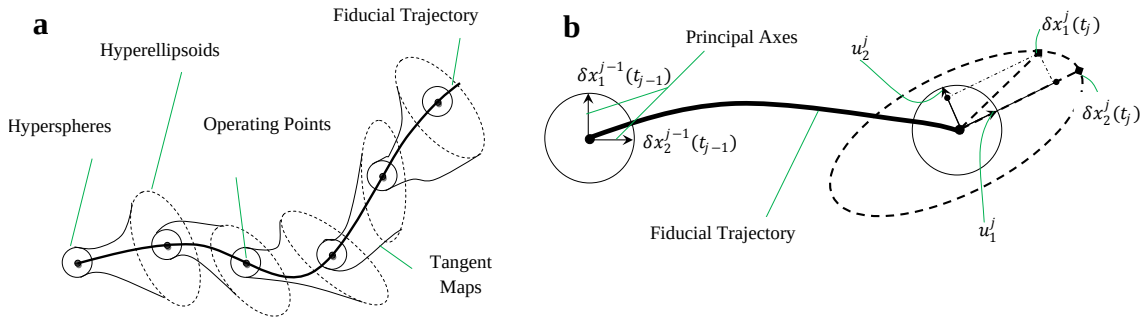


Figure 2.1: a) The schematic diagram of calculating LE b) The schematic diagram of GSR

where $\mathbf{x} \in \mathbb{R}^n$ is the state vector, and $\mathbf{f}(\mathbf{x}(t))$ is a continuous and differentiable vector function. Due to the deforming nature of the flow of the system, any infinitesimal $n$-sphere of initial conditions becomes an $n$-ellipsoid. Monitoring the long term evolution of such an $n$-sphere is the basic idea of calculating Lyapunov exponents. Figure 2.1-a demonstrates the process of calculating Lyapunov exponents. The $i^{th}$ Lyapunov exponent of the system is defined in terms of the length of principal axes as follow:

$$\lambda_i = \lim_{t\to\infty} \frac{1}{t} \ln \frac{||\delta x_i(t)||}{||\delta x_i(t_0)||}, \qquad i = 1, ..., n \tag{2.2}$$

where $||\delta x_i(t)||$ and $||\delta x_i(t_0)||$ denote the magnitudes of the $i^{th}$ principal axis at time $t$ and $t_0$, respectively, as indicated in Figure 2.1-b. According to this definition, Lyapunov exponents of a system quantify the contracting or expanding nature of the system in different directions. One important characteristic of Lyapunov exponents is that they are global properties of a system and independent from initial conditions (the invariant property). This independence is a consequence of a theorem of Oseledec [94].

The sign of Lyapunov exponents determines the dynamics of a system qualitatively. If all the Lyapunov exponents of a system are negative, the attractor is an exponentially stable fixed point. Any time-dependent continuous dynamical system that does not have a fixed point will have at least one zero exponents. For the systems with an exponentially stable limit cycle, the largest Lyapunov exponents is zero, which corresponds to the slow changes in the magnitude of principal axis tangent to the flow. Similarly, if the first two largest

Lyapunov exponents are zero, the system has a stable two-torus. Finally, any system that has at least one positive exponent is defined to be chaotic provided that some other conditions are satisfied [93].

In the process of calculating Lyapunov exponents, the centers of the $n$-ellipsoids are on a trajectory, known as the fiducial trajectory, which is defined by the action of the nonlinear equations of motion on a set of initial conditions. The points on the surface of the sphere, which are infinitesimally away from the fiducial trajectory, are defined by the action of the linearized form of (2.1). The principal axes that are initially orthonormal vector frame attached to the fiducial trajectory are defined by the linearized equations. This results in the following set of equations:

$$\left\{ \begin{array}{c} \dot{\mathbf{x}}(t) \\ \dot{\mathbf{\Psi}}_t \end{array} \right\} = \left\{ \begin{array}{c} \mathbf{f}(\mathbf{x}(t)) \\ \mathbf{J}(\mathbf{x}(t))\, \mathbf{\Psi}_t \end{array} \right\} \tag{2.3}$$

In the above equation, $\mathbf{\Psi}_t$ is the state transition matrix of the linearized system $\delta x(t) = \mathbf{\Psi}_t\, \delta x(0)$, and $\mathbf{J}(\mathbf{x}(t))$ is the Jacobian matrix of the system. The initial conditions for (2.3) are as follow:

$$\left\{ \begin{array}{c} \mathbf{x}(0) \\ \mathbf{\Psi}_t(t_0) \end{array} \right\} = \left\{ \begin{array}{c} \mathbf{x}_0 \\ \mathbf{I} \end{array} \right\} \tag{2.4}$$

Figure 2.1-a shows a schematic diagram of the process of calculating Lyapunov Exponents. If (2.4) is used, after a number of iterations the principal axes lie in the direction of the most rapid growth. In the long run, the vectors become indistinguishable. Therefore, Gram-Schmidt reorthonormalization (GSR) procedure is applied to reset the vectors to an orthogonal set $\boldsymbol{\sigma}^j = [\boldsymbol{\sigma}_1^j, ..., \boldsymbol{\sigma}_n^j]$, which spans the same subspace. Let us consider $[\delta \mathbf{x}_1^j(t_j), ..., \delta \mathbf{x}_n^j(t_j)] = [\boldsymbol{\gamma}_1, ..., \boldsymbol{\gamma}_n]$, for the sake of simplicity. The formulation of GSR is given as:

$$
\begin{aligned}
\boldsymbol{\sigma}_1^j &= \frac{\boldsymbol{\gamma}_1}{||\boldsymbol{\gamma}_1||} \\
\boldsymbol{\sigma}_2^j &= \frac{\boldsymbol{\gamma}_2 - \langle \boldsymbol{\gamma}_2, \boldsymbol{\sigma}_1^j \rangle \boldsymbol{\sigma}_1^j}{||\boldsymbol{\gamma}_2 - \langle \boldsymbol{\gamma}_2, \boldsymbol{\sigma}_1^j \rangle \boldsymbol{\sigma}_1^j||} \\
&\vdots \\
\boldsymbol{\sigma}_n^j &= \frac{\boldsymbol{\gamma}_n - \langle \boldsymbol{\gamma}_n, \boldsymbol{\sigma}_{n-1}^j \rangle \boldsymbol{\sigma}_{n-1}^j - .., - \langle \boldsymbol{\gamma}_2, \boldsymbol{\sigma}_1^j \rangle \boldsymbol{\sigma}_1^j}{||\boldsymbol{\gamma}_n - \langle \boldsymbol{\gamma}_n, \boldsymbol{\sigma}_{n-1}^j \rangle \boldsymbol{\sigma}_{n-1}^j - .., - \langle \boldsymbol{\gamma}_2, \boldsymbol{\sigma}_1^j \rangle \boldsymbol{\sigma}_1^j||}
\end{aligned}
\tag{2.5}
$$

With the aid of GSR, for a finite time, Lyapunov exponents, $\boldsymbol{\lambda}$, are calculated as:

$$
\lambda_i \approx \frac{1}{M\,\Delta t} \sum_{j=1}^{M} \ln ||\boldsymbol{\sigma}_i^j||\,, \quad i = 1, ..., n \tag{2.6}
$$

where $M$ is the number of iterations, and $\Delta t$ is the time step. A schematic of GSR process is illustrated in Figure 2.1-b.

**Note:** The computational approach for calculating LEs has been under review for several decades [95; 93], and the procedure is proven to be computationally accurate and precise. The key in calculating LEs is to understand that the deviations from the fiducial trajectory can be as small as computer limitations allow [93]. Another important thing to note is that the use of linearized equations for constructing the transition matrix is not mandatory. Instead a higher order polynomial of Taylor expansion of the system can be used. In addition, another way to ensure that the numerical error is as low as possible is to reduce the time step of the integration. This is the time that the fiducial trajectory is solved alongside the locally linearized equations of the transition matrix. After each time step, the GSR method is employed and the principal axes are reorthonormalized. Therefore, if the time step is small enough, the error of calculation is minimum. In this research, the time step is varied between $10^{-6}$ to $10^{-3}$ for different systems. The results of the codes for calculating LEs have been verified by those of the classical systems in the literature [95; 96]

## 2.2 The Monte Carlo Principle and Inverse Transform Sampling Method

Monte Carlo methods are statistical sampling techniques that have been used for solving many quantitative problems in science, engineering, and economics [97]. One purpose of Monte Carlo principle is to produce a set of samples, $\{\mathbf{x}^{(i)}\}_{i=1}^{L}$ (sample points in the state space in this research), from a given probability density, $p(x)$ [98; 99]. Despite the fact that Monte Carlo methods were developed to simulate random processes, they have been frequently applied to problems that do not have a probabilistic interpretation, and have become helpful computational tools in scientific research [100].

Consider $n$ independent and mutually exclusive events as $E_1$, ..., $E_n$ which have probabilities as $p_1$, ..., $p_n$, respectively, with the property that $p_1 + ... + p_n = 1$. If a random number, $\zeta$, uniformly distributed over the interval $[0\,,\,1)$, satisfies the following inequality,

$$p_1 + ... + p_{i-1} \leqslant \zeta < p_1 + ... + p_i \tag{2.7}$$

it determines the event $E_i$. Let us assign a variable $x$ on the interval $0 \leqslant x < n$ to the above events, with the assumption that $i-1 \leqslant x < i$ represents the event $E_i$. Assume that the variable $x$ has a probability density function (PDF), $p(x)$, defined as:

$$p(x) = p_i, \quad (i-1 \leqslant x < i)\,, \quad i = 1, ..., n \tag{2.8}$$

Thus, as shown in Figure 2.2-a, $p(x)$ is composed of step functions that their summation is equal to 1 since $p_1 + ... + p_n = 1$. The cumulative (probability) distribution function (CDF) of $p(x)$ is:

$$\zeta = P(x) = \int_0^x p(s)\,ds \quad (0 \leqslant x < n) \tag{2.9}$$

Since the function $p(x)$ is discrete, $P(x)$ has a form of monotonically increasing piece-wise-smooth-line such that $P(0) = 0$, $P(n) = 1$, as illustrated in Figure 2.2-b. Equation

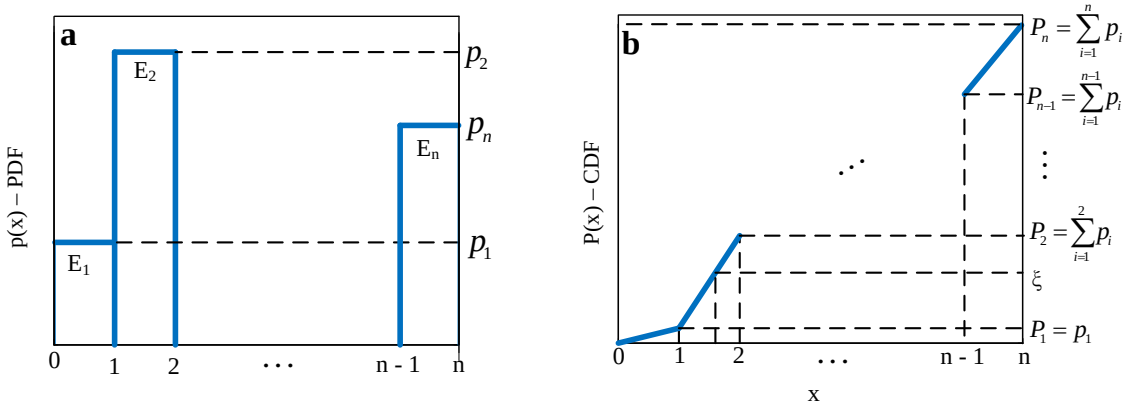


Figure 2.2: a) probability density function (PDF), $p(x)$, b) Cumulative distribution function (CDF), $P(x)$

(2.9) determines $x$ as a function of $\zeta$ such that, if $\zeta$ is uniformly distributed over $[0\,,\,1)$, $x$ falls in the interval $i-1 \leq x < i$ with frequency $p_i$. Therefore, by inverting the function in (2.9) the uniformly distributed variable, $\zeta$, is transformed to the variable $x$ with the desired distribution, $p(x)$. One important property of Monte Carlo methods arises from the fact that they position the samples in regions of high probability [101].

As an example, consider $p(x) = e^{-x}$ as the desired density function. Using (2.9), the desired distribution function is found as $P(x) = 1 - e^{-x}$. The inverse function, defining the relation between $\zeta$ and $x$, can be obtained as: $P^{-1}(\zeta) = -\ln(1-\zeta)$. This process is depicted in Figure 2.3 where points are distributed uniformly on the vertical axis, $\zeta$. On the horizontal axis the transformed variable $x$ is illustrated which clearly does not have a uniform but exponential distribution.

## 2.3 Support Vector Machine (SVM) Learning Algorithm

The support vector machine (SVM) learning algorithms are new classification methods, which have been introduced for solving pattern recognition problems based on the idea of

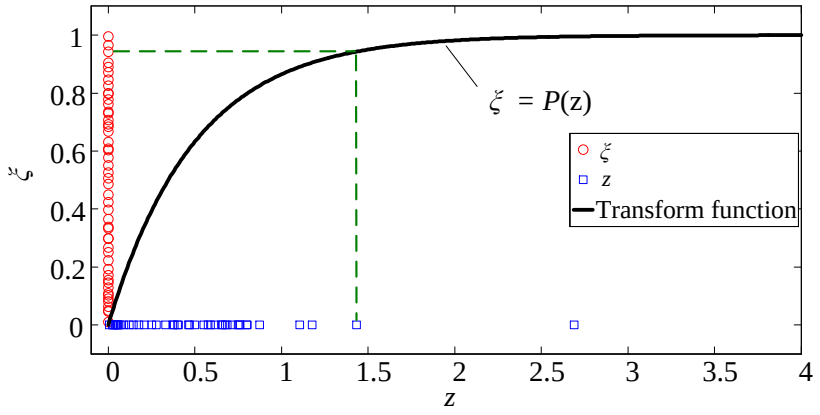


Figure 2.3: Example of standard sampling method - transferring a uniformly distributed variable $z$ to $y$ with exponential distribution.

structural risk minimization. It is stated in the literature that SVMs have shown higher performance than the traditional methods, and are among the best supervised machine learning algorithms [102]. An SVM is a two-class classifier that maps the input points into a high-dimensional feature space, and maximizes the margin between two classes in the space by a separating hyperplane. The resulted optimal hyperplane is a combination of some of the input points called support vectors [103; 104; 105; 106].

Consider a set of $l$ labeled training points and their associated labels as

$$(\mathbf{x}_1, \gamma_1), ..., (\mathbf{x}_l, \gamma_l) \tag{2.10}$$

The training points $\mathbf{x}_i \in \mathbb{R}^n$, where $n$ indicates the dimension of the space of $\mathbf{x}$, may belong to either of the two classes which is indicated as $\gamma_i \in \{-1, 1\}$ for $i = 1, ..., l$. Since it is too restrictive to search for a suitable hyperplane in the input space, a solution is to map the input space into a higher dimension feature space. Suppose $\mathbf{z} = \varphi(\mathbf{x})$ represents the feature space where $\varphi$ is a mapping from $\mathbb{R}^n$ to a feature space $\mathbb{Z}$. The aim of SVM is to find the hyperplane such that the inputs $\mathbf{x}_i$ can be separated according to the following function

$$G(\mathbf{x}) = \sum_{i=1}^{l} \alpha_i \, \gamma_i \, \psi(\mathbf{x}, \mathbf{x}_i) + b \tag{2.11}$$

where $\alpha_i$ are positive real constants, $b$ is a real constant, $\psi(.,.)$ are called kernel functions, and $\mathbf{x}_i$ are the training points. The choices for kernels can be polynomials of any order, radial basis functions (RBF), and multilayer perceptron. For more details refer to [102; 103; 104; 105; 106; 107; 108; 109].

## 2.4 T-S Fuzzy Approach

Fuzzy ideas are known for being capable of modeling and controlling systems with complex nonlinear dynamics. Among different rule-based fuzzy methods, T-S fuzzy approach is the bridge between the classical control theories, and the conventional fuzzy approaches. The classical control theories are mostly tedious and impractical, and the conventional fuzzy approaches suffer from lack of a proper stability analysis and a systematic methodology to construct fuzzy models.

There are different methods for representing nonlinear systems using T-S fuzzy approach. One approach is sector nonlinearity, which provides a precise representation of the nonlinear model. To be able to use sector nonlinearity approach, the nonlinear terms must be bounded either locally or globally. Another approach is dynamic linearization, which is based on Taylor series expansion on multiple operating points [110]. In this research we use sector nonlinearity approach as it can better represent the dynamics system.

A typical T-S fuzzy model has the following format:

$$\textbf{Fuzzy rule } i : \text{If } \kappa_1 \text{ is } \mu_{i,1},\ \kappa_2 \text{ is } \mu_{i,2},\ ...,\ \kappa_p \text{ is} \mu_{i,p} \text{ Then}$$

$$\begin{cases} \dot{\mathbf{x}}(t) = A_i \, \mathbf{x}(t) + B_i \, \mathbf{u}(t) + E_{x,i} \, \mathbf{w}(t) \\ \qquad\qquad\qquad\qquad\qquad\qquad\qquad\qquad i = 1,\ ...,\ q \\ \mathbf{y}(t) = C_i \, \mathbf{x}(t) + D_i \, \mathbf{u}(t) + E_{y,i} \, \mathbf{w}(t) \end{cases} \tag{2.12}$$

where $\mathbf{x}$ is the state vector, $\mathbf{u}$ is the input vector, $\mathbf{w}$ is the disturbance vector, $A_i$, $B_i$, $E_{x,i}$, $C_i$, $D_i$, and $E_{y,i}$ are constant matrices, $q$ is the number of subsystems, and finally, $\kappa_j$ and $\mu_{i,j}$, $j = 1, ..., p$, are premise (scheduling) variables and fuzzy sets, respectively. By blending the subsystems, the T-S fuzzy system is inferred as follow:

$$\begin{cases} \dot{\mathbf{x}}(t) = \sum_{i=1}^{r} h_i(\boldsymbol{\kappa})(A_i\,\mathbf{x}(t) \;+\; B_i\,\mathbf{u}(t) \;+\; E_{x,i}\,\mathbf{w}(t)) \\ \mathbf{y}(t) = \sum_{i=1}^{r} h_i(\boldsymbol{\kappa})(C_i\,\mathbf{x}(t) \;+\; D_i\,\mathbf{u}(t) \;+\; E_{y,i}\,\mathbf{w}(t)) \end{cases} \tag{2.13}$$

where

$$\boldsymbol{\kappa} = [\kappa_1\,\kappa_2,\ ...,\ \kappa_p], \quad \nu_i = \prod_{j=1}^{p} \mu_{i,j} \quad h_i(\boldsymbol{\kappa}) = \frac{\nu_i}{\sum_{i=1}^{r} \nu_i} \qquad i = 1,\ ...,\ q \tag{2.14}$$

and $h_i$ are called fuzzy weighting functions.

Stability analysis of T-S fuzzy systems is performed using Linear Matrix Inequality (LMI) approach. The first step is to cast an LMI problem that includes the conditions for stability of all the subsystems. Being based on Lyapunov's direct method, the LMI problem provides a quadratic Lyapunov function which is valid for all the subsystems of the fuzzy model. For more details about the stability analysis of T-S fuzzy systems, see [111; 112; 113; 114; 53]. In this research, we use the following theorem for the stability proof of the fuzzy system:

**Theorem:** For a given positive constant $\gamma > 0$, the continuous-time unforced form of fuzzy system (2.13), i.e $\mathbf{u}(t) = 0$, is stable with $\gamma$-disturbance attenuation, that is $\|\mathbf{y}\|_2 < \gamma\,\|\mathbf{w}\|_2$ for all nonzero $\mathbf{w} \in [0,\ \mathbf{N}]$ ($\mathbf{N}$ is a finite positive number) under zero initial conditions if there exists a common positive definite matrix $P$ such that

$$\begin{bmatrix} A_i\,P + A_i^T\,P + C^T\,C & P\,E_{x,i} + C^T\,E_{y,i} \\ E_{x,i}^T\,P + E_{y,i}^T\,C & -(\gamma^2\mathbf{I} + D^T D) \end{bmatrix} < 0 \qquad i = 1,\ ...,\ q \tag{2.15}$$

For the proof of the theorem refer to [112]. This theorem can determine whether a fuzzy system, as a combination of a number of subsystems, is able to stabilize the plant.

# Chapter 3

# Fundamental Research on Identifying Boundaries of BoAs of Dynamical Systems

As mentioned in Chapter 1, there is a need for developing a method that is capable of identifying the whole stability region of an attractor in a computationally efficient way. In this chapter, the proposed method for identifying boundaries of stability regions is presented. The method utilizes three concepts: Lyapunov exponents, Monte Carlo methods, and support vector machine learning algorithm, which are described in detail in Chapter 2. The proposed method is applied to three case studies to demonstrate its effectiveness. This method can be used for stability analysis of a large number of dynamical systems. In addition, a new computational approach for calculating Lyapunov exponents (LEs) is introduced, which is a practical alternative for the conventional way of calculating LEs. Such a computational method is useful when finding an analytical form for the Jacobian matrix of a system is impractical. In this research, such a method is used in the stability analysis of the vehicle systems with the fuzzy controllers.

# 3.1 Identifying Boundaries of BoAs of a Dynamical System Using Lyapunov Exponents and Monte Carlo Techniques

The proposed method uses Lyapunov exponents as the measure for determining stability of a system. The main idea of the proposed method is that within the same BoA [1] of an exponentially stable attractor, Lyapunov exponents remain constant. The challenge is to identify the specific regions that contain boundaries of the BoAs, named boundary regions. In such regions, two close points as the initial conditions might exhibit different Lyapunov exponents spectra. The Monte Carlo method, described in Chapter 2, is used to target areas that have higher probabilities to be on the boundary regions. The search for the boundary regions is performed in an iterative learning process, which leads to a fine region surrounding the boundary of interest. The details of the method are described in the following subsections.

## 3.1.1 Forming a Grid in an Admissible Region

Having a general insight about the dynamics of a system, an admissible region, $\mathbf{\Omega}_{ad}$, in the state space can be determined, as shown in Figure 3.1, which includes the attractors of interest and their corresponding BoAs. A grid in $\mathbf{\Omega}_{ad}$ is formed with a desired resolution, $\tilde{r}$. To obtain reasonable results, the grid must be fine enough. In each cell of the grid one point, $\mathbf{x}$, located in the center of it, is considered to represent that specific cell. The stability analysis is performed in $\mathbf{\Omega}_{ad}$.

## 3.1.2 Primary Stability Analysis

The primary stability analysis includes finding the attractors of interest and determining the stability or instability by calculating Lyapunov exponents for such attractors. Such an

[1] Basin of attraction (BoA) and stability region have been used interchangeably in the literature for the same concept. In this thesis, we use them with the same meaning.

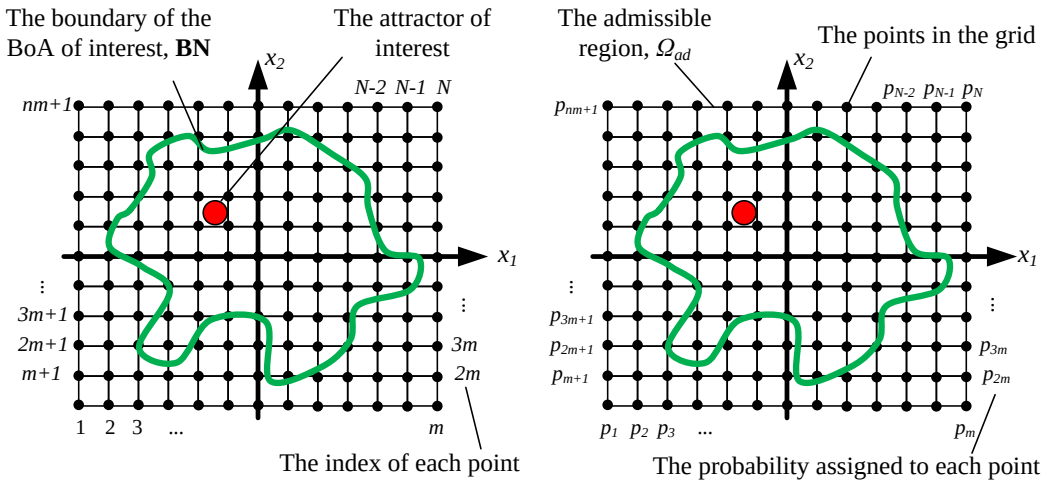


Figure 3.1: A schematic representation of forming a grid in an admissible region, $\Omega_{ad}$, and indexing and assigning probabilities to each point in the grid

analysis is crucial as it provides insights into the nature of the attractors. Assuming that the system has $s$ attractors with different Lyapunov exponents spectrum in $\mathbf{\Omega}_{ad}$, there are $s$ spectra of Lyapunov exponents:

$$\mathbf{\Lambda}^{ref} = \{\boldsymbol{\lambda}_1^{ref}, \boldsymbol{\lambda}_2^{ref}, ..., \boldsymbol{\lambda}_s^{ref}\} \tag{3.1}$$

where $\boldsymbol{\lambda}_i^{ref}$, $i = 1, ..., s$ is the Lyapunov spectrum of the $i^{th}$ attractor. Lyapunov exponents are calculated following the procedure discussed in Section 2.1. Using the proposed method, for each attractor, a set, $\mathbf{BN}^i$, $i = 1, \ldots, s$, is identified, which contains the points belonging to boundary regions of the BoA of the $i^{th}$ attractor, as shown in Figure 3.1. It is stated later that these points are stored as pairs of points which satisfy certain criteria in a comparison process.

### 3.1.3 Locating the Points in the Boundary Region

All points in the grid are assigned probabilities to be a part of boundaries of the BoAs. To use the Monte Carlo technique, described in Section 2.2, the points in the grid are indexed by integers, $m$, as depicted in Figure 3.1. This process yields to the sequence of the form

$1, 2, \ldots, N$, with $N$ being the total number of points in the grid. Using this transformation, we define a sequence of $N$ mutually exclusive events $E_1, \ldots, E_N$ that have probabilities $p_1, \ldots, p_N$, where the event $E_m$, $m = 1, 2, \ldots, N$ represents the situation that the $m^{th}$ point belongs to a boundary region.

Assigning a variable $z$ on the interval $0 < z < N$ to the events $E_1, ..., E_N$, with the agreement that $m - 1 < z < m$ represents the event $E_m$, a probability distribution function $p(z)$ is constructed by the definition

$$p(z) = p_m, \qquad m - 1 < z < m, \quad m = 1, 2, \ldots, N \tag{3.2}$$

Therefore, using (2.9) the corresponding CDF is found as:

$$\zeta = P(z) = \int_0^z p(\tau)\, d\tau \tag{3.3}$$

The probabilities are equal in the first iteration, i.e., $p(z) = \frac{1}{N}$ , which results in a CDF with a constant slope as $P(z) = \frac{z}{N}$. Probabilities for the further iterations are updated through a learning process that will be discussed later.

Suppose that we need to select $L$ points from the grid according to the probability distribution, $p(z)$. First, $L$ uniformly distributed random real numbers, $\zeta$, in the interval $[0, 1)$ are generated. Using the inverse of the CDF in (3.3), $z = P^{-1}(\zeta)$, $L$ real numbers with the desired distribution in the interval $(1, N]$ are obtained. Given the condition that $m - 1 < z < m$ represents the event $E_m$, the real numbers are converted to integers, $m$. These integers are considered as the indices of the points in the grid, and represent $L$ points in $\mathbf{\Omega}_{ad}$ with the desired distribution, $p(z)$. Such points are named center points, $A_1^j$, $j = 1, \ldots, L$, as shown in Figure 3.2 (See the sets **1** and **2**). For each center point, $q$ points, $A_e^j$, $e = 2, \ldots, q+1$, named comparing points, are selected in their $r$-neighborhood, i.e.,

$$\| Y_1^j - Y_e^j \| < r, \quad j = 1, ..., L, \quad e = 2, \ldots, q+1 \tag{3.4}$$

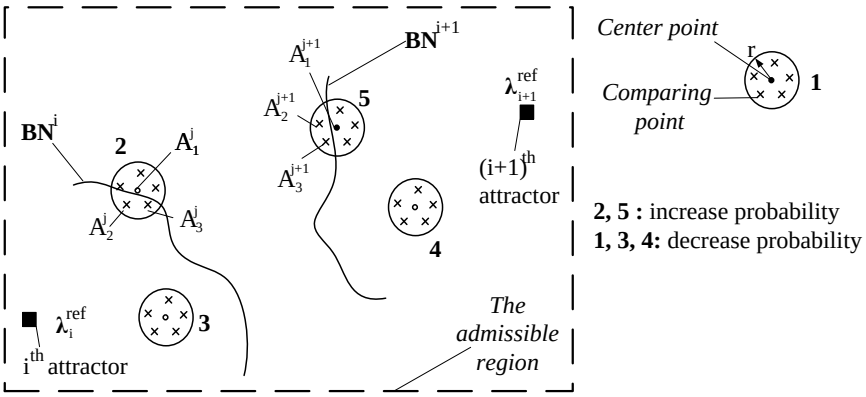


Figure 3.2: A schematic representation of the process of updating the PDF in each iteration based on the calculation of Lyapunov exponents for the center and comparing points.

where $r > \tilde{r} > 0$, $Y_1^j$ is the position vector of the center point, and $Y_e^j$ are the position vectors of the comparing points. Each center point, together with its comparing points are used as initial conditions for the calculation of Lyapunov exponents.

To locate the boundary points:

- All the center points and comparing points are stored in a set, $\mathbf{A}$, with the size $[L\times(q+1)]$, as follow:

$$\mathbf{A} = \begin{Bmatrix} A_1^1 & A_2^1 & ... & A_{q+1}^1 \\ \vdots & \vdots & ... & \vdots \\ A_1^j & A_2^j & ... & A_{q+1}^j \\ \vdots & \vdots & ... & \vdots \\ A_1^L & A_2^L & ... & A_{q+1}^L \end{Bmatrix} \tag{3.5}$$

- Lyapunov exponents are calculated with all the points in $\mathbf{A}$ as initial conditions. The corresponding Lyapunov exponents spectrums are stored in a set $\mathbf{LE^A}$ of the same size as $\mathbf{A}$, i.e., $[L\times(q+1)]$:

$$\mathbf{LE^A} = \begin{Bmatrix} \boldsymbol{\lambda}_1^1 & \boldsymbol{\lambda}_2^1 & ... & \boldsymbol{\lambda}_{q+1}^1 \\ \vdots & \vdots & ... & \vdots \\ \boldsymbol{\lambda}_1^j & \boldsymbol{\lambda}_2^j & ... & \boldsymbol{\lambda}_{q+1}^j \\ \vdots & \vdots & ... & \vdots \\ \boldsymbol{\lambda}_1^L & \boldsymbol{\lambda}_2^L & ... & \boldsymbol{\lambda}_{q+1}^L \end{Bmatrix} \tag{3.6}$$

- Performing the comparisons: Consider an arbitrary pair of points from the $j^{th}$ row of $\mathbf{A}$ as $\{A_k^j,\, A_h^j\}$, $k,\, h\, =\, 1,\, \ldots,\, q+1,\, k \neq h$. The sufficient condition that this pair belongs to the boundary region of the $i^{th}$ attractor is one of the following:

$$\begin{aligned} \boldsymbol{\lambda}_k^j = \boldsymbol{\lambda}_i^{ref} \text{ and } \boldsymbol{\lambda}_h^j \neq \boldsymbol{\lambda}_k^j \\ \boldsymbol{\lambda}_h^j = \boldsymbol{\lambda}_i^{ref} \text{ and } \boldsymbol{\lambda}_h^j \neq \boldsymbol{\lambda}_k^j \end{aligned} \tag{3.7}$$

  Thus, to investigate that the selected points in $\mathbf{A}$ belong to any of the boundary regions, we need to perform such a comparison for any possible pairs from each row of $\mathbf{A}$ with the Lyapunov spectrum of each attractors, $\boldsymbol{\lambda}_i^{ref}$, $i\, =\, 1,\, ...,\, s$. This leads to a set, $\boldsymbol{\Delta}$, of three-element sets which has the following size: $[s \times L \times M]$, and is written as:

$$\boldsymbol{\Delta}^i = \begin{Bmatrix} \left\{\, \boldsymbol{\lambda}_i^{ref}, \boldsymbol{\lambda}_1^1, \boldsymbol{\lambda}_2^1 \,\right\} & \left\{\, \boldsymbol{\lambda}_i^{ref} \boldsymbol{\lambda}_1^1 \boldsymbol{\lambda}_3^1 \,\right\} & ... & \left\{\, \boldsymbol{\lambda}_i^{ref}, \boldsymbol{\lambda}_q^1, \boldsymbol{\lambda}_{q+1}^1 \,\right\} \\ \vdots & \vdots & ... & \vdots \\ \left\{\, \boldsymbol{\lambda}_i^{ref}, \boldsymbol{\lambda}_1^j, \boldsymbol{\lambda}_2^j \,\right\} & \left\{\, \boldsymbol{\lambda}_i^{ref}, \boldsymbol{\lambda}_1^j, \boldsymbol{\lambda}_3^j \,\right\} & ... & \left\{\, \boldsymbol{\lambda}_i^{ref}, \boldsymbol{\lambda}_q^j, \boldsymbol{\lambda}_{q+1}^j \,\right\} \\ \vdots & \vdots & ... & \vdots \\ \left\{\, \boldsymbol{\lambda}_i^{ref}, \boldsymbol{\lambda}_1^L, \boldsymbol{\lambda}_2^L \,\right\} & \left\{\, \boldsymbol{\lambda}_i^{ref}, \boldsymbol{\lambda}_1^L, \boldsymbol{\lambda}_3^L \,\right\} & ... & \left\{\, \boldsymbol{\lambda}_i^{ref}, \boldsymbol{\lambda}_q^L, \boldsymbol{\lambda}_{q+1}^L \,\right\} \end{Bmatrix} \tag{3.8}$$

$$\boldsymbol{\Delta} \,=\, \{\boldsymbol{\Delta}^1,\, \boldsymbol{\Delta}^2,\, ...,\, \boldsymbol{\Delta}^s\}\,, \quad i = 1,\, 2,\, ...,\, s$$

with the size of $\boldsymbol{\Delta}^i$ being $[L \times M]$, and $M = \frac{q(q+1)}{2}$ being the number of possible pairs formed by the elements of each row of $\mathbf{A}$.

For each element in $\mathbf{\Delta}$, and its corresponding pair of point, $\{A_k^j,\, A_h^j\}$, $k,\, h = 1, \ldots, q+1$, $k \neq h$, two cases are possible:

- **Case 1:** $\{A_k^j,\, A_h^j\}$ belongs to the boundary region of the $i^{th}$ attractor. In this case one of the sufficient conditions mentioned in (3.7) is satisfied. The corresponding points, $A_k^j$ and $A_h^j$, are stored in $\mathbf{BN}^i$, $i = 1, ..., s$.

  For instance, in the set **2** of Figure 3.2, the points $A_2^j$ and $A_3^j$ are on the same side of the boundary, $\mathbf{BN}^i$, whereas the point $A_1^j$ is on the other side. Thus, for $\{A_1^j,\, A_2^j\}$

  $$\boldsymbol{\lambda}_2^j = \boldsymbol{\lambda}_i^{ref}\, and\, \boldsymbol{\lambda}_2^j \neq \boldsymbol{\lambda}_1^j \tag{3.9}$$

  and for $\{A_1^j,\, A_3^j\}$

  $$\boldsymbol{\lambda}_3^j = \boldsymbol{\lambda}_i^{ref}\, and\, \boldsymbol{\lambda}_3^j \neq \boldsymbol{\lambda}_1^j \tag{3.10}$$

  Therefore, $\{A_1^j,\, A_2^j\}$ and $\{A_1^j,\, A_3^j\}$ are stored in $\mathbf{BN}^i$.

- **Case 2:** $\{A_k^j,\, A_h^j\}$ does not belong to any of the boundary regions. The possible scenarios are:

  - $\boldsymbol{\lambda}_k^j = \boldsymbol{\lambda}_h^j = \boldsymbol{\lambda}_i^{ref}$, which means $A_k^j$ and $A_h^j$ belong to the BoA of the $i^{th}$ attractor, but not to any boundary region. An example of this case is any pair of points chosen from the set **3** in Figure 3.2.
  - $\boldsymbol{\lambda}_k^j = \boldsymbol{\lambda}_h^j$ and $\boldsymbol{\lambda}_k^j \neq \boldsymbol{\lambda}_i^{ref}$ and $\boldsymbol{\lambda}_h^j \neq \boldsymbol{\lambda}_i^{ref}$, which means $A_k^j$ and $A_h^j$ belong to the same BoA, but not the BoA of the $i^{th}$ attractor, and obviously, not to any boundary region of interest. An example of this case is any pair of points chosen from the set **4** in Figure 3.2.
  - $\boldsymbol{\lambda}_k^j \neq \boldsymbol{\lambda}_h^j$ and $\boldsymbol{\lambda}_k^j \neq \boldsymbol{\lambda}_i^{ref}$ and $\boldsymbol{\lambda}_h^j \neq \boldsymbol{\lambda}_i^{ref}$ which means $A_k^j$ and $A_h^j$ belong to a boundary region, but not the boundary region of the $i^{th}$ attractor. For example, this case happens for the sets $\{A_1^{j+1},\, A_2^{j+1}\}$ and $\{A_1^{j+1},\, A_3^{j+1}\}$, indicated in Figure 3.2 as set **5**, which belong to the boundary region of the $(i+1)^{th}$ attractor, not to that of the $i^{th}$ attractor.

**A Special Case - the System Has Only One Attractor of Interest**

In this case the set of reference Lyapunov exponents has only one element, $\mathbf{\Lambda}^{ref} = \{\boldsymbol{\lambda}^{ref}\}$, and the number of boundary regions is reduced to one set, **BN**, as well. With $L$ center points, and $q$ associated comparing points to each of the center points, the sets **A**, and $\mathbf{LE^A}$ remain the same as described before. Since there is only one $\boldsymbol{\lambda}^{ref}$, the size of $\mathbf{\Delta}$ is reduced to $[L \times M]$, and $\mathbf{\Delta}$ has the following form:

$$\mathbf{\Delta} = \begin{Bmatrix} \left\{ \boldsymbol{\lambda}^{ref}, \boldsymbol{\lambda}_1^1, \boldsymbol{\lambda}_2^1 \right\} & \left\{ \boldsymbol{\lambda}^{ref}, \boldsymbol{\lambda}_1^1, \boldsymbol{\lambda}_3^1 \right\} & ... & \left\{ \boldsymbol{\lambda}^{ref}, \boldsymbol{\lambda}_q^1, \boldsymbol{\lambda}_{q+1}^1 \right\} \\ \vdots & \vdots & ... & \vdots \\ \left\{ \boldsymbol{\lambda}^{ref}, \boldsymbol{\lambda}_1^j, \boldsymbol{\lambda}_2^j \right\} & \left\{ \boldsymbol{\lambda}^{ref}, \boldsymbol{\lambda}_1^j, \boldsymbol{\lambda}_3^j \right\} & ... & \left\{ \boldsymbol{\lambda}^{ref}, \boldsymbol{\lambda}_q^j, \boldsymbol{\lambda}_{q+1}^j \right\} \\ \vdots & \vdots & ... & \vdots \\ \left\{ \boldsymbol{\lambda}^{ref}, \boldsymbol{\lambda}_1^L, \boldsymbol{\lambda}_2^L \right\} & \left\{ \boldsymbol{\lambda}^{ref}, \boldsymbol{\lambda}_1^L, \boldsymbol{\lambda}_3^L \right\} & ... & \left\{ \boldsymbol{\lambda}^{ref}, \boldsymbol{\lambda}_q^L, \boldsymbol{\lambda}_{q+1}^L \right\} \end{Bmatrix} \tag{3.11}$$

$$j = 1,\ 2,\ ...,\ L$$

For each element in $\mathbf{\Delta}$ the possible cases of the comparison are:

- **Case 1:** $\{A_k^j,\ A_h^j\}$ belongs to the boundary region, **BN**, provided that one of the following conditions is satisfied:

$$\begin{aligned} \boldsymbol{\lambda}_k^j = \boldsymbol{\lambda}^{ref} \text{ and } \boldsymbol{\lambda}_h^j \neq \boldsymbol{\lambda}_k^j \\ \boldsymbol{\lambda}_h^j = \boldsymbol{\lambda}^{ref} \text{ and } \boldsymbol{\lambda}_h^j \neq \boldsymbol{\lambda}_k^j \end{aligned} \tag{3.12}$$

- **Case 2:** $\{A_k^j,\ A_h^j\}$ does not belong to the boundary region, **BN**. The possible scenarios are:
  - $\boldsymbol{\lambda}_k^j = \boldsymbol{\lambda}_h^j = \boldsymbol{\lambda}^{ref}$ which means $\{A_k^j,\ A_h^j\}$ are inside the BoA of interest.
  - $\boldsymbol{\lambda}_k^j = \boldsymbol{\lambda}_h^j$ and $\boldsymbol{\lambda}_k^j \neq \boldsymbol{\lambda}^{ref}$ and $\boldsymbol{\lambda}_h^j \neq \boldsymbol{\lambda}^{ref}$, which means $\{A_k^j,\ A_h^j\}$ are outside the BoA of interest.
  - $\boldsymbol{\lambda}_k^j \neq \boldsymbol{\lambda}_h^j$ and $\boldsymbol{\lambda}_k^j \neq \boldsymbol{\lambda}^{ref}$ and $\boldsymbol{\lambda}_h^j \neq \boldsymbol{\lambda}^{ref}$, which means $\{A_k^j,\ A_h^j\}$ are outside the BoA of interest (they belong to the boundary region of another attractor).

### 3.1.4 Updating the Probability Distribution Based on the Observation and Storing the Boundary Points

After calculating Lyapunov exponents for a number of points in $\mathbf{\Omega}_{ad}$, we gain more information about the probability distribution through the above learning process. Therefore, some heuristic rules are used to update the probability distribution in the grid after the observation in each iteration. For each element in $\mathbf{\Delta}$, and their corresponding pair of points, $\{A_k^j,\, A_h^j\}$, these cases are considered:

- If $\{A_k^j,\, A_h^j\}$ belongs to the boundary regions:
  - the probabilities of the points in an $r$-neighborhood of the associated center point, $A_1^j$ as
    $$\mathbf{\Omega}_r^j = \{\mathbf{x}|\ \parallel Y_1^j - Y_{\mathbf{x}} \parallel < r,\, \mathbf{x} \neq A_k^j,\, \mathbf{x} \neq A_h^j\} \tag{3.13}$$
    (where $Y_1^j$ is the position vector of the center point, and $Y_{\mathbf{x}}$ is the position vector of $\mathbf{x}$) is increased by a case-dependent scaling factor, $\eta_1$, since the chance to find more points that belong to the boundary regions is relatively high in that area.
  - the probabilities of $\{A_k^j,\, A_h^j\}$ are set to zero. This guarantees that they are not reselected in the next iterations, since they have already been stored in one of the boundary sets, $\mathbf{BN}^i$, $i = 1, ..., s$.
- If $\{A_k^j,\, A_h^j\}$ does not belong to the boundary regions, their probabilities are decreased by a case-dependent scaling factor, $\eta_2$.

At the end of the updating process, the obtained PDF is normalized to ensure that the condition $p_1 + p_2 + ... + p_N = 1$ is satisfied. The PDF is updated in each iteration by the described process, and based on the updated PDF, a new CDF is calculated for the next iteration. Therefore, CDF changes in each iteration as the program learns more about the probability distribution. Figure 3.3 shows a schematic graph of a CDF. The straight line belongs to the first iteration in which every point in the grid has the same probability, and

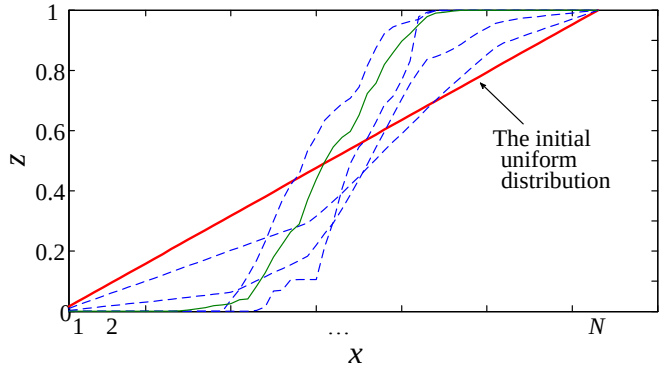


Figure 3.3: A schematic cumulative distribution function (CDF) that is updated in each iteration based on the observation from the state space.

the CDF has a constant slope. As the program runs for some iteration, the probability distribution changes. The described procedure is repeated for a number of iterations, and at the end of this process the algorithm finds the boundary regions with appropriate accuracy.

The criteria for terminating the program is that if after a minimum number of iterations, which can be determined based on the system's specifications, the number of boundary points found in $u_1$ consecutive iterations is less than $w_1$, the program stops.

### 3.1.5 Classifying the Gathered Data Using SVM

As mentioned in section 1.2.2, it is practically impossible to find a close-form solution that describes the boundary of a BoA using analytical approaches if the system is complex. Therefore, it is extremely valuable if one can find a mathematical representation for the boundaries, for example, for monitoring or control purposes. For instance, if the objective of a controller is to simply maintain the states of a system in the BoA of an attractor, having a mathematical expression is highly beneficial. Similarly, for monitoring purposes, using a mathematical expression, it can be easily determined whether a system is operating within boundaries or not.

Here, SVM is employed to classify the collected data, and to find a mathematical representation for the boundaries. Given that the $s$ boundary regions, $\mathbf{BN}^i$, $i = 1, ..., s$, are identified, we have $s$ separate classification problems. The stored data in each boundary

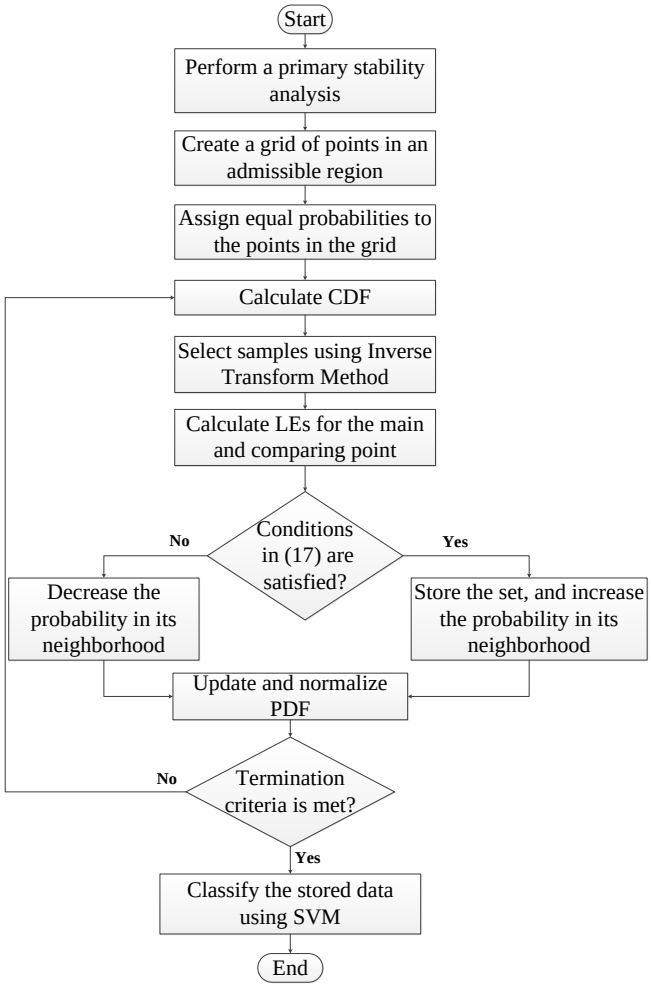


Figure 3.4: The flow chart of the algorithm ($I$ is the counter of the iterations, and $P$ is the total number of iterations)

sets, $\mathbf{BN}^i$, $i = 1, ..., s$ is classified into two groups: points that belong to the BoA, i.e., they have the same Lyapunov exponents spectrum as that of the corresponding attractor; and points that do not belong to the basin, which obviously have a different Lyapunov spectrum. Based on the shape of the boundary, type of the Kernel function is decided, and the SVM algorithm provides a decision function that separates the two classes. This decision function might have error in separating the points; however, using a more suitable function for the specific problem may reduce the error.

The decision function can be used for the above mentioned applications. One of the important properties of the expressions that SVM provides is that they separate the state

space into two regions: the region of the points of class#1, and the region of the points of class#2. In the application of this research, the function separates the state space into two areas: points that are inside a BoA, and points that are outside the BoA, which is decided based on the sign of the mathematical expression. For example, for the points inside the BoA, the expression is positive, and for the points outside the BoA, the expression is negative. This property of the expression obtained by SVM, makes the monitoring or control process extremely simple.

*Remark 1.* It is not always straightforward to find a mathematical expression for a boundary of a BoA using SVM. If the boundary has a complex shape, the optimization problem of SVM might not converge to a solution. However, there is always the possibility that there exists a form of kernel function that can be used for the problem, and coming up with a proper kernel function might need intuition and trial and error.

*Remark 2.* Note that there are some limitations for the use of Lyapunov exponents as the stability measure. One of the limitations of the concept of Lyapunov exponents is that it can only be used for stability analysis of exponentially stable attractors. Another limitation is that in some rare cases, the Lyapunov spectra of two attractors might be the same. In such cases, it is not possible to use Lyapunov exponents to distinguish the BoAs of the two attractors. However, the idea of reducing the load of computations by the aid of Monte Carlo techniques is not limited to the use of Lyapunov exponents and can be used with other stability analysis tools. For instance, if using simulation is intended, the same concept can be utilized to reduce the computational load.

The flowchart shown in Figure 3.4 illustrates the procedure of the proposed method.

## 3.2 System and Structural Stability Analysis of Dynamical Systems Using the Proposed Method

In this section, performance of the proposed method for finding boundaries of stability regions is demonstrated using three case studies. The first case study is a well-known classical dynamical system, called Lienard system. The second case study is a 2-DOF lateral dynamics model of a ground vehicle. For these two case studies the boundaries of the system stability regions are determined. The last case study is a follower-loaded double pendulum system, for which the boundaries of structural stability analysis are determined. Such a double pendulum has been used for vibration and dynamics analysis.

### 3.2.1 System Stability Analysis of a Lienard System

Consider a Lienard system as [115; 116; 117]

$$\begin{aligned} \dot{x} &= y - 0.32x^5 - \tfrac{4}{3}x^3 + 0.8x \\ \dot{y} &= -x \end{aligned} \tag{3.14}$$

where $x$ and $y$ are the sates of the system. It has been proved that the attractors of this system are two limit cycles and a fixed point at the origin, which are depicted in Figure 3.5. The fixed point is exponentially stable as the Lyapunov exponents are: $\boldsymbol{\lambda}_1 = \{-0.4, -0.4\}^T$. The first limit cycle is a repeller, while the second limit cycle is an attractor [115]. As mentioned in section 2.1, if the largest Lyapunov exponent is zero, the attractor is a limit cycle. The Lyapunov exponents associated with the stable limit cycle are: $\boldsymbol{\lambda}_2 = \{0.00, -2.98\}^T$.

The stability and instability of the attractors is also demonstrated in Figure 3.5 where two trajectories initiating from close initial conditions on the edge of the first limit cycle are depicted in the insert **M**. The trajectory with initial conditions $A_1^{j+1} = (0, -1.0415)$, which is in solid black line, approaches the fixed point, while the trajectory initiating from $A_2^{j+1} = (0, -1.0420)$, which is in dashed black line, approaches the second limit cycle.

Following up the above discussion, the boundary between the BoA of the fixed point

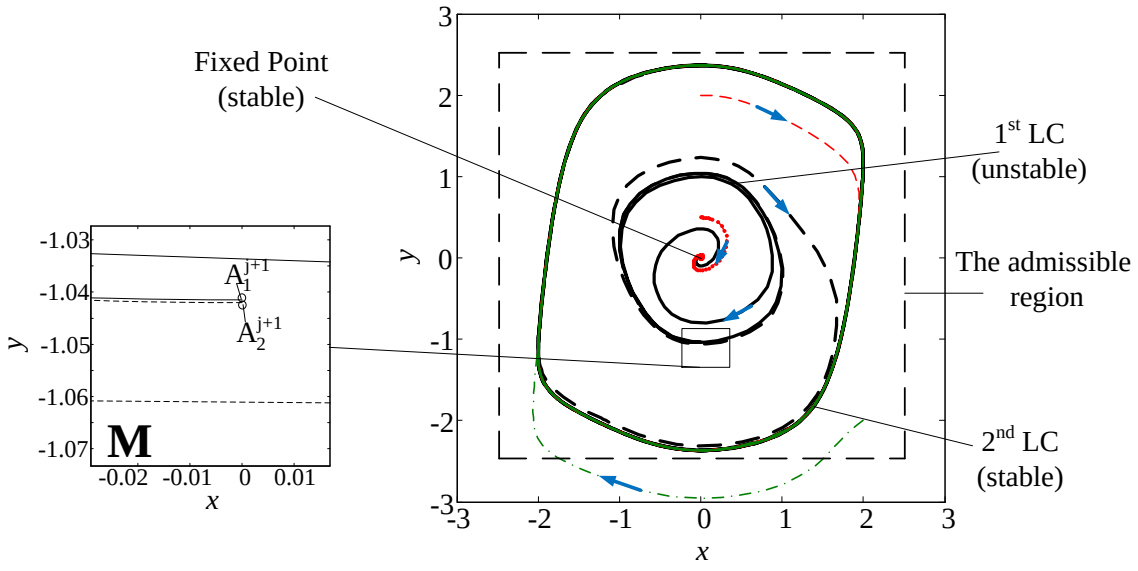


Figure 3.5: The attractors of the system, and trajectories in different regions of the admissible region

and the BoA of the second limit cycle is the first limit cycle [115]. Let us define the region surrounded by the first limit cycle as $\mathbf{\Omega}_1$, the set of points that define the first limit cycle as $\mathbf{\Omega}_{FLC}$, and the region of the whole state space as $\mathbf{\Omega}_s$. The BoA of the fixed point is

$$\mathbf{\Omega}_{FP} = \{\mathbf{x} | \, \mathbf{x} \in \mathbf{\Omega}_1, \, \mathbf{x} \neq \mathbf{0}\} \tag{3.15}$$

where $\mathbf{x} = (x, \, y)$. The BoA of the second limit cycle is

$$\mathbf{\Omega}_{SLC} = \{\mathbf{x} | \, \mathbf{x} \in \mathbf{\Omega}_s, \, \mathbf{x} \notin \mathbf{\Omega}_{FP}, \, \mathbf{x} \notin \mathbf{\Omega}_{FLC}\} \tag{3.16}$$

The proposed method is employed to find the boundary of the BoA of the origin, and the results are shown in Figure 3.6. The problem is defined as the special case, described in section 3.1.3, i.e., there is one attractor of interest, which is the fixed point with Lyapunov exponents spectrum, $\boldsymbol{\lambda}^{ref} = \{-0.40, \, -0.40\}^T$, as the reference. The search for the boundary, **BN**, is performed in an admissible region as:

$$\mathbf{\Omega}_{ad} = \{(x, \, y) \, | \, -2.5 < x < 2.5, -2.5 < y < 2.5\} \tag{3.17}$$

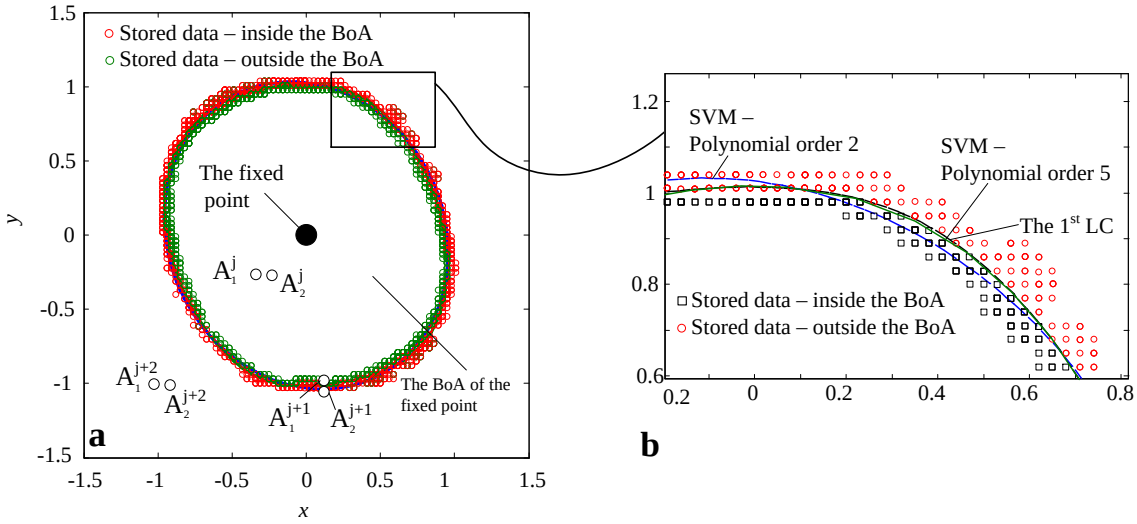


Figure 3.6: a) Comparison of SVM - polynomial order 2, and polynomial order 5 with the first limit cycle b) The stored data in **BN**

depicted in Figure 3.5, with the resolution $\tilde{r} = 0.03$ of the unit length of the state space, which creates a grid of $N = 27,889$ points. Thus, the probability distribution function for each point in the grid is: $p(z) = 3.58 \times 10^{-5}$, in the first iteration. In each iteration, $L = 50$ center points with $q = 2$ comparing points associated with each center point are selected, which results in calculation of Lyapunov exponents for 150 points. Some examples of paired points for performing the comparisons, $\{A_1^j, A_2^j\}$, ..., $\{A_1^{j+2}, A_2^{j+2}\}$, are shown in Figure 3.6-a. The following situations are likely to happen:

- $\boldsymbol{\lambda}_1^j = \boldsymbol{\lambda}_2^j = \boldsymbol{\lambda}^{ref}$, which means that the corresponding points, $\{A_1^j, A_2^j\}$, are inside the BoA of the fixed point, but not in the boundary region. The probabilities of these points are decreased by a scaling factor, $\eta_2 = 0.95$.

- $\boldsymbol{\lambda}_1^{j+1} = \boldsymbol{\lambda}^{ref}$ and $\boldsymbol{\lambda}_2^{j+1} \neq \boldsymbol{\lambda}^{ref}$, which means the corresponding points, $\{A_1^{j+1}, A_2^{j+1}\}$, shown also in the insert **M** of Figure 3.5, are in the boundary region, and will be stored in **BN**. The probabilities of these points are increased by a scaling factor, $\eta_1 = 1.2$.

- $\boldsymbol{\lambda}_1^{j+2} \neq \boldsymbol{\lambda}^{ref}$ and $\boldsymbol{\lambda}_2^{j+1} \neq \boldsymbol{\lambda}^{ref}$, which means the corresponding points, $\{A_1^{j+2}, A_2^{j+2}\}$, are outside the BoA of the fixed point. The probabilities of these points are decreased

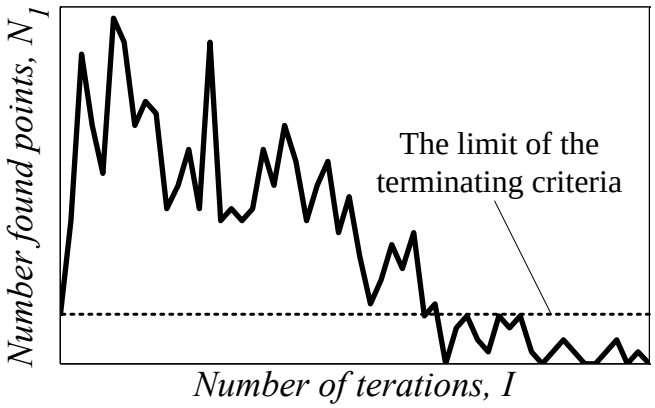


Figure 3.7: Number of boundary points found in each iteration - $I$ is the number of iteration, and $N_1$ is the number of the found point in the associated iteration

by a scaling factor, $\eta_2$.

After these changes in the probabilities of the selected points in each iteration, the PDF is updated according to the described process, and then normalized to satisfy the condition: $p_1 + p_2 + ... + p_N = 1$.

Figure 3.7 shows the number of points that have been found in each iteration. At the end of the process the number of found points decreases. The reason for that can be the fact that the boundary becomes closer to be complete considering that the algorithm does not reselect the already found points. The program stops after 40 iterations, according to the terminating criteria described in section 3.1.4 with $u_1 = 4$ and $w_1 = 5$, which is found to be enough to determine the boundary region with adequate accuracy. This makes the total number of calculations $6,000$ which is 21.5% of the total number of points in the grid. 540 points that belong to the boundary region are determined that are shown in Figure 3.6-a.

The found points are fed into the SVM algorithm as the inputs to find an expression for the boundary, and a polynomial of order 2 is obtained. The kernel function used for deriving this polynomial has the following form:

$$\psi(\mathbf{x}, \mathbf{x}_i) \; = \; \mathbf{x}\,\mathbf{x}_i(1 + \mathbf{x}\,\mathbf{x}_i) \tag{3.18}$$

where $\mathbf{x} = (x,\, y)$ is the state vector of the system, and $\mathbf{x}_i$ are the training data of the

SVM problem which are the gathered data in **BN**. The decision function, which defines the boundary between the two basins of attraction, has the following form:

$$G(\mathbf{x}) = G(x,\, y) = 14.45x^2 \,+\, 3.21x\,y \,-\, 0.03x \,+\, 12.36y^2 \,+\, 0.05y \,-\, 13.05 \tag{3.19}$$

The above decision function, which represents the boundary appropriately, is depicted in Figure 3.6. From the view point of the classification problem, this decision function has an error in classifying the data of **BN**. The error is defined as

$$error = \frac{number\,of\,incorrectly\,classified\,points\,in\,\mathbf{BN}}{the\,total\,number\,of\,points\,in\,\mathbf{BN}} \tag{3.20}$$

With the function in (3.19) the error in classification is about 22%. This amount of error is not a serious concern, since the training data is so condensed in a fine boundary region. However, if more accuracy is demanded, we can increase the order of the polynomial, or use another form of kernel function. In this case study, a polynomial of order 5 gives more accuracy with less than 4% error. Both of the polynomials together with the first limit cycle are demonstrated in Figure 3.6-b. The polynomial of order 5 is closer to the limit cycle and shows a better performance in classifying the data.

### 3.2.2 System Stability Analysis of a Lateral Vehicle Dynamics Model

The second case study is a 2-DOF vehicle lateral dynamics model. The degrees of freedom of the system are side slip angle, $\beta$, and yaw rate, $r$, with steering angle $\delta = 0$. The equations of motion are written in the subsequent equations [3; 118; 119]:

$$\begin{aligned}
\dot{\beta} \;=\; & \frac{1}{m\,v_x}\,[-m\,v_x\,r \,+\, F_{z,f}\,\sin(\,C_T\,\arctan(\,B_T\,(\delta - \beta + \tfrac{a}{v_x}r)\,)\,) \\
& \qquad + F_{z,r}\,\sin(\,C_T\,\arctan(\,-B_T\,(\beta + \tfrac{b}{v_x}r))] \\
\dot{r} \;=\; & \frac{1}{I_z}\,[a\,F_{z,f}\,\sin(\,C_T\,\arctan(\,B_T\,(\delta - \beta + \tfrac{a}{v_x}r)\,) \\
& \qquad - b\,F_{z,r}\,\sin(\,C_T\,\arctan(\,-B_T\,(\beta + \tfrac{b}{v_x}r))]
\end{aligned} \tag{3.21}$$

| Parameter | Value | Unit | Description |
|---|---|---|---|
| $m$ | 1300 | $kg$ | total mass |
| $I_z$ | 2500 | $kg.m^2$ | moment of inertia about $x$ axis |
| $a$ | 1.2 | $m$ | distance from c.g. to front axle |
| $b$ | 1.3 | $m$ | distance from c.g. to rear axle |
| $v_x$ | 20 | $\frac{m}{s}$ | forward velocity |
| $C_T$ | 1.307 | | a coefficient of Pacejka model |
| $B_T$ | 13.330 | | a coefficient of Pacejka model |

Table 3.1: The parameters of the vehicle of case study 2 [1]

The parameters of the vehicle are given in Table 3.1, and Figure 3.8 shows a schematic of the vehicle dynamic model. With $\delta = 0$, the expected path of the vehicle is a straight line, and the initial conditions can be assumed as some disturbances that may cause the vehicle to deviate from the path.

Equation (3.21) provides a basic nonlinear model that can represent vehicle's behavior in lateral and yaw motions with many simplifying assumptions. However, for the sake of performing stability analysis, it is a complicated and highly nonlinear system. Finding a Lyapunov function for such a system is challenging, which may suggest that using Lyapunov's second method is not feasible for this case study. Thus, a practical alternative is to use the proposed method for stability analysis. To apply the proposed method to this problem, the admissible region is considered as:

$$\boldsymbol{\Omega}_{ad} = \left\{ (\beta\,(rad),\, r\,(rad/s)) \,|\, -\frac{\pi}{2} < \beta < \frac{\pi}{2},\, -\pi \,< r < \pi \right\} \tag{3.22}$$

In this region, the system has one equilibrium at the origin, which is the attractor of interest. Using an optimization algorithm to search for other possible fixed points in the admissible region, it is proved that there is no other fixed point in $\boldsymbol{\Omega}_{ad}$ than the origin. Lyapunov exponents of the system are: $\boldsymbol{\lambda}^{ref} = \{-5.59,\, -7.00\}^T$, which indicates that the origin is exponentially stable.

The results of the trajectory analysis are illustrated in Figure 3.9. Such results are

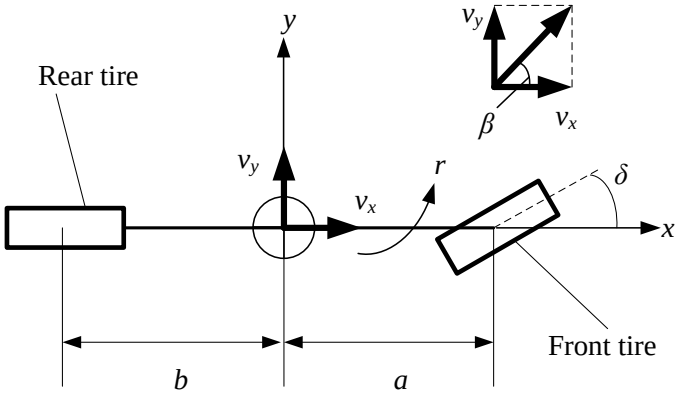


Figure 3.8: A schematic of the vehicle dynamic model

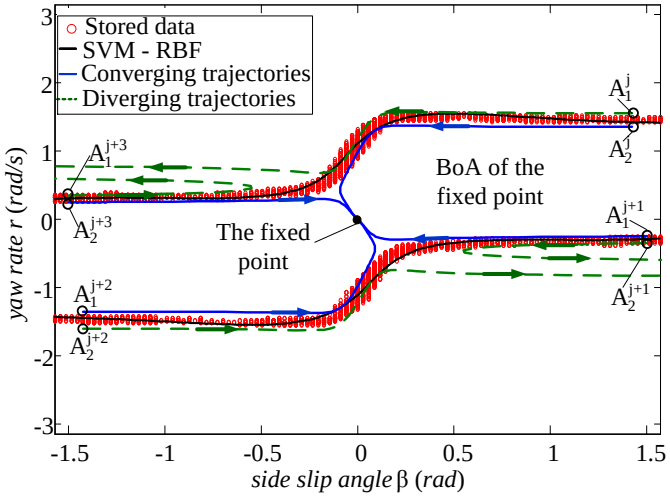


Figure 3.9: Trajectory analysis for the vehicle system compared with the results of the proposed method

comparable to the work of Ko and Lee [120; 121] in which they have used a trajectory reversing technique to find the stability region of a mid-size car.

The boundaries of the BoA of the equilibrium point are found using the proposed method. The resolution of the grid in $\mathbf{\Omega}_{ad}$ is 0.02, which creates a grid of $N = 49,770$ points. In each iteration, Lyapunov exponents have been calculated for 240 center points and comparing points, including $L = 80$ center points, each of which are accompanied by $q = 2$ comparing

points. The program stops after 48 iterations, which is enough to identify the fine boundary regions. This makes the total number of calculations $11,520$ which is $23.14\%$ of the total number of points in the grid. 815 points have been identified to be in the boundary regions that are shown in Figure 3.9.

To demonstrate the accuracy of the results, some trajectories of the system are also drawn in Figure 3.9. These trajectories initiate from pairs of close initial conditions on the edge of the boundary regions, $\left\{A_1^j,\, A_2^j\right\}$, ..., $\left\{A_1^{j+3},\, A_2^{j+3}\right\}$, located at different parts of the admissible region. The converging and diverging trajectories are illustrated in continuous and dashed lines, respectively. For example, the trajectory starting from $A_1^j = (1.425,\, 1.515)$ which is in dotted line, moves close to the trajectory initiating from $A_2^j = (1.425,\, 1.425)$ until some point on the boundary, and then it starts deviating from the other trajectory and moves to the left side of the state space, while the trajectory of $A_2^j$ converges to the origin. The same manner can be seen with other pairs as depicted in Figure 3.9.

### 3.2.3 Structural Stability Analysis of a Follower-Loaded Double Pendulum

In this section, the efficiency of the method with a structural stability analysis is examined. Figure 3.10 shows a schematic of a double pendulum system, called follower-loaded double pendulum, with external force, $\tilde{p}$, which its configuration is specified by another parameter, $\alpha$. The rods are mass-less that are connected to two masses $2m$ and $m$. The system has two degrees of freedom indicated by $\theta_1$ and $\theta_2$, which are the angles shown in the figure. Both sets of the torsion spring and dampers, located at the joints, have the same values, $k$ and $\tilde{c}$. More information about the model can be found in [122; 123]. Using Lagrange equations, the equations of motion of the system are derived as follow:

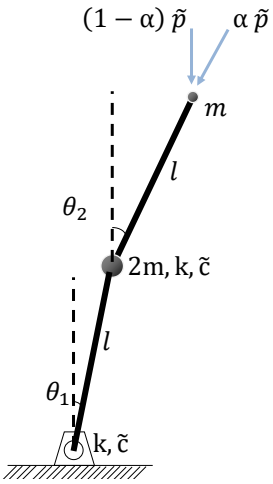


Figure 3.10: The schematic of the follower-loaded double pendulum

$$
\begin{aligned}
&3\ddot{\theta}_1 + [\cos(\theta_1 - \theta_2)\,\ddot{\theta}_2 + \sin(\theta_1 - \theta_2)\,\dot{\theta}_2^2] + 2c\dot{\theta}_1 - c\dot{\theta}_2 + 2\theta_1 - \theta_2 \\
&\qquad = p\,[(1-\alpha)\,\sin(\theta_1) + \alpha\,\sin(\theta_1 - \theta_2)] \\
&\ddot{\theta}_2 + [\cos(\theta_1 - \theta_2)\,\ddot{\theta}_1 - \sin(\theta_1 - \theta_2)\,\dot{\theta}_1^2] + c\dot{\theta}_2 - c\dot{\theta}_1 - \theta_1 + \theta_2 \\
&\qquad = p\,(1-\alpha)\,\sin(\theta_2)
\end{aligned}
\tag{3.23}
$$

where $p = \frac{\tilde{p}\,l}{k}$, and $c = \frac{\tilde{c}}{\sqrt{k\,m\,l^2}}$. The state vector of the system is $\mathbf{x} = \left\{\theta_1,\, \dot{\theta}_1,\, \theta_2,\, \dot{\theta}_2\right\}^T$.

The system alternates between approaching to a trivial equilibrium point in the origin [122; 123], and different limit cycles depending on the values of $p$ and $\alpha$. A fundamental question is that in what ranges of $p$ and $\alpha$, the system approaches to the fixed point or to the limit cycles. Since $p$ and $\alpha$ are two parameters of the system, to answer that question a structural stability analysis in the parametric space, $\mathbb{R}^2$, defined by $p$ and $\alpha$ must be performed.

A linear analysis based on Routh-Hurwitz criteria is performed in [122; 123] that results in finding the boundaries depicted in Figure 3.11 by solid black lines. The region that this analysis identifies as the BoA of the fixed point is $\mathbf{\Omega}_1 \cup \mathbf{\Omega}_2$ which is illustrated by right-tilted lines.

The nonlinear stability analysis using the proposed method has been conducted for this

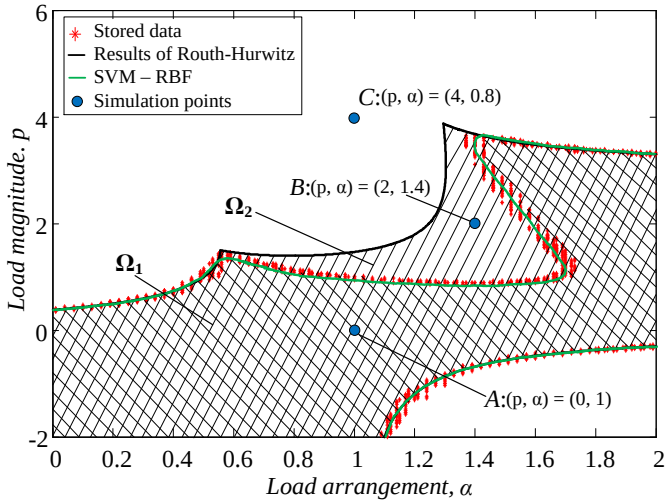


Figure 3.11: Comparison between the result of Routh-Hurwitz analysis and the results of the proposed method - region $\mathbf{\Omega}_1$ is obtained by the algorithm; region $\mathbf{\Omega}_1 \cup \mathbf{\Omega}_2$ is obtained by Routh-Hurwitz method.

system as well. The characteristics of the computations for performing the analysis are similar to the preceding case studies except that the admissible region in the parametric space is

$$\mathbf{\Omega}_{ad} = \{(p,\, \alpha)\,|\, 0 < p < 2,\; -2 < \alpha < 8\} \tag{3.24}$$

with a resolution of $\tilde{r} = 0.03$. As mentioned earlier, to investigate the changes in dynamics of the system due to perturbations in the parameters, the initial conditions are fixed as: $\mathbf{x}_0 = \{0.01,\, 0.01,\, 0.01,\, 0.01\}^T$. The results of the nonlinear analysis are also demonstrated in Figure 3.11 where the stars are the found points in the boundary regions. The region that the nonlinear analysis suggests as the BoA of the fixed point is $\mathbf{\Omega}_1$ which is also depicted by right- and left-tilted lines in the figure.

Comparing the results of the two analyses, a difference can be noticed between the region resulted from the proposed method as the BoA of the fixed point, $\mathbf{\Omega}_1$, and the region that Routh-Hurwitz analysis identifies as the basin, $\mathbf{\Omega}_1 \cup \mathbf{\Omega}_2$. The area in which the results of the two analyses do not match is marked in Figure 3.11 as $\mathbf{\Omega}_2$.

To investigate this disagreement further, time histories and trajectories of three points,

marked as $A$, $B$ and $C$ in Figure 3.11, are plotted in Figures 3.12 - 3.14. These points are located in different areas of the parametric space. The time history and trajectory of the system for point $A$ are illustrated in Figure 3.12-a and b, respectively. Both of the plots show that the system ultimately converges to the fixed point. Lyapunov exponents of the system are $\boldsymbol{\lambda}_A = \{-0.01, -0.02, -0.03, -0.04\}^T$, which also proves that the system has an exponentially stable equilibrium point.

On the other hand, the system shows oscillatory behavior in the region identified as $\boldsymbol{\Omega}_2$ in Figure 3.11. The results of the simulations show that for point $B$, located in $\boldsymbol{\Omega}_2$, not only the system is not attracted to the origin, but also starts oscillating as shown in the time history in Figure 3.13-a, and moves in a closed orbit in the state space of the system as illustrated in Figure 3.13-b. In this case, Lyapunov spectrum of the system is $\boldsymbol{\lambda}_B = \{0.00, -0.03, -0.04, -0.05\}^T$. Since the largest Lyapunov exponent is zero, the attractor of the system is an exponentially stable limit cycle. These facts prove that point $B$ does not belong to the BoA of the fixed point.

Finally, the results for point $C$, shown in Figure 3.14, are quite comparable to those for point $B$. Lyapunov exponents are $\boldsymbol{\lambda}_C = \{0.00, -0.03, -0.04, -0.06\}^T$. Thus, in spite of slight differences between the two latter cases, which are apparently due to the change in the parameters, their qualitative behaviors are the same, and we can conclude that they belong to a same BoA.

Upon the above discussion, the simulation results show that the outcome of the linear analysis is not valid for the whole area that it indicates as the BoA. Furthermore, the results of simulation agree with the nonlinear analysis of the proposed method which indicates that the method is more reliable, and can anticipate the behavior of systems more accurately.

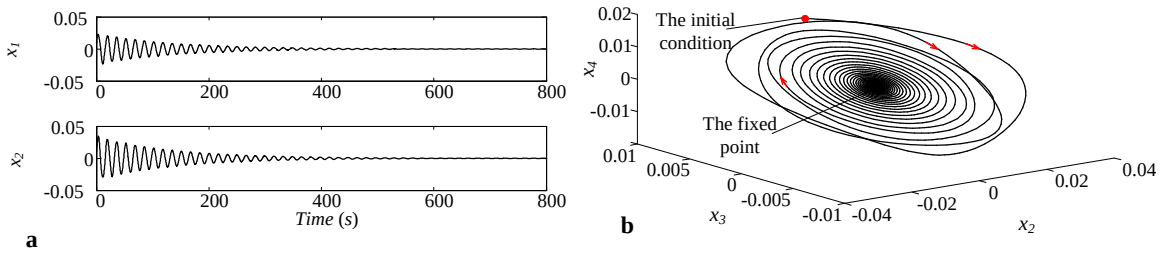


Figure 3.12: a) Time history b) trajectory of the double pendulum system for point $A$ in shown in Figure 3.11

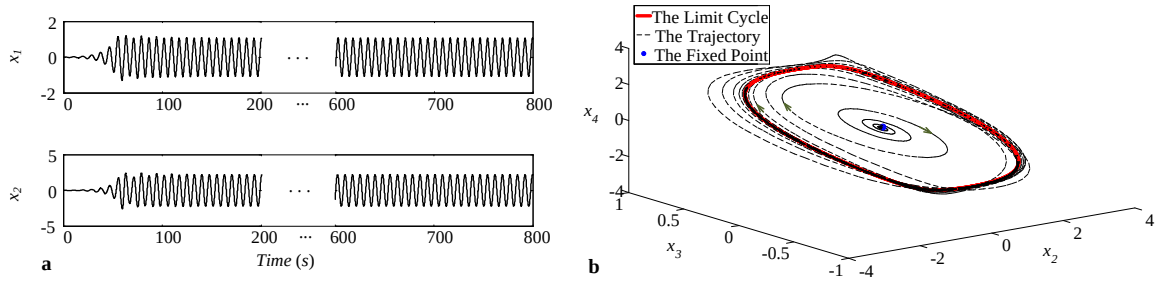


Figure 3.13: a) Time history b) trajectory of the double pendulum system for point $B$ in shown in Figure 3.11

## 3.3 A New Computational Approach for Calculating Lyapunov Exponents

Calculating Lyapunov exponents normally requires evaluating Jacobian matrix of the nonlinear system. In some cases that the nonlinear system has complex and lengthy terms, finding the closed form of a Jacobian matrix can be time-consuming or impractical. In such cases there is also the possibility of having an error in the calculation process of the Jacobian matrix. For instance the nonlinear equations of motion of the vehicle systems in this research are of high orders ($4^{th}$ and $8^{th}$ orders). In addition, the Pacejka tire model, used in this research, is highly complex, which makes deriving the closed form of the Jacobian matrix more difficult.

In order to avoid such difficulties, a new computational approach is introduced in this thesis. The new approach evaluates the Jacobian matrix at each time instance without

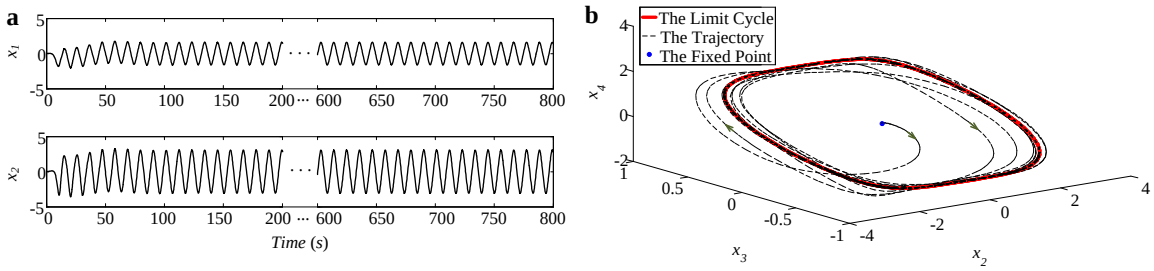


Figure 3.14: a) Time history b) trajectory of the double pendulum system for point $C$ shown in Figure 3.11

requiring the closed form of the Jacobian matrix. Consider a dynamical system as:

$$\dot{\mathbf{x}} = \mathbf{f}(\mathbf{x}, \mathbf{p}) \tag{3.25}$$

where $\mathbf{p}$ is an array of parameters of the system. To calculate the Jacobian matrix numerically, the Taylor expansion of the $i^{th}$ nonlinear equation, $f_i(\mathbf{x}, \mathbf{p})$, about point $\mathbf{x}$ is written as:

$$f_i(\mathbf{x} + \Delta\mathbf{x}, \mathbf{p}) = f_i(\mathbf{x}, \mathbf{p}) + \sum_{j=1}^{n} \frac{\partial f_i}{\partial x_j} \Delta x_j + O(\Delta x^2) \tag{3.26}$$

Neglecting the higher order terms, we can write the above equation as:

$$\mathbf{f}(\mathbf{x} + \Delta\mathbf{x}, \mathbf{p}) \approxeq \mathbf{f}(\mathbf{x}, \mathbf{p}) + \mathbf{J}(\mathbf{x}, \mathbf{p})\Delta\mathbf{x} \tag{3.27}$$

In (3.27), $\mathbf{J}$ is the Jacobian matrix of size $(n \times n)$ composed of the partial derivatives as:

$$J_{ij} = \frac{\partial f_i}{\partial x_j} \tag{3.28}$$

The Jacobian matrix can be estimated using (3.27) as:

$$\mathbf{J}(\mathbf{x}, \mathbf{p}) = \frac{\mathbf{f}(\mathbf{x} + \Delta\mathbf{x}, \mathbf{p}) - \mathbf{f}(\mathbf{x}, \mathbf{p})}{\Delta\mathbf{x}} \tag{3.29}$$

Based on the above equation and finite difference approximation [124], each element of the Jacobian matrix can be approximated by:

$$\frac{\partial f_i}{\partial x_j} \approx \frac{f_i(\mathbf{x} + \mathbf{e}_j h, \mathbf{p}) - f_i(\mathbf{x}, \mathbf{p})}{h} \tag{3.30}$$

where $h$ is a small perturbation, and $\mathbf{e}_j$ is a unit vector in the direction of $x_j$. Therefore, if the parameters of the system, $\mathbf{p}$, are fixed, the Jacobian matrix can be calculated using (3.30) provided that the value of $h$ is small enough.

**Note:** The above-mentioned approach for calculating the Jacobian matrix computationally instead of deriving a closed form for it does not affect the process of calculating Lyapunov exponents. In other words, the process of calculating Lyapunov exponents is independent from the method of calculating the Jacobian matrix. The benefit of using this approach is to find the Jacobian matrix for complex systems, such as the systems of this research, in a more efficient way.

## 3.4 Summary

As mentioned in Chapter 1, using Lyapunov-function-based methods is not practical if the system includes complex dynamics. Besides, the load of computation of Lyapunov-exponents-based methods is a drawback on the methods of this group. In this chapter, a novel method for identifying boundaries of stability regions (BoAs) is presented. This method uses the concept of Lyapunov exponents as the stability analysis tool. With the aid of Monte Carlo techniques the algorithm targets the regions in the state space which contain the boundaries of BoAs. This is accomplished through an iterative learning process. The load of computation is increased in the case studies of this chapter by more than 70%. Support vector machine learning algorithm is employed to provide an expression for the boundaries of stability regions. Such expressions can be highly beneficial for control and monitoring purposes.

# Chapter 4

# Design of a Multi-objective T-S Fuzzy Control for Yaw Stabilization and Rollover Prevention of Ground Vehicles

In this chapter, the methodology of the T-S fuzzy control scheme for yaw stabilization and rollover prevention is described. First, the vehicle dynamics models that are used in this research are presented, and the methodology is then explained in great details. This chapter includes three major parts: in the first part, the vehicle dynamics model of torsionally rigid vehicles (TRV) and torsionally flexible vehicles (TFV), used in this research, are described (Refer to 4.2 for more detail). Next, a T-S fuzzy controller for yaw stabilization and rollover prevention of a TRV with a 4 dimensional state space model is described. Finally, a T-S fuzzy controller with the same objectives for a TFV with a 8 dimensional state space model, including the torsional compliance of the frame, is detailed.

## 4.1 Vehicle Dynamics Models

Having a proper model that represents the dynamics of a system is a crucial step for analyzing it. The model has to be accurate enough so that it represents all the important aspects of the dynamics, yet must not be too complex that demands a complicated or intensive analysis or design procedure. The complexity of a model is dictated by the purpose of the study. For example, if enhancement of ride comfort is intended, the model must include bounce and pitch motions, since the vertical acceleration of the vehicle is a key factor. However, if roll stability analysis is desired, the side slip angle, the yaw rate, and the roll dynamics of the vehicle play significant roles.

The purpose of this section is to present suitable models for yaw-roll stability analysis and control of a torsionally rigid vehicle (TRV) and a torsionally flexible vehicle (TFV). One property of TRVs is that since their structures is rigid enough, the roll angle in the structure can be considered unchanged throughout the length of the vehicle. Therefore, for modeling the roll motion of the sprung mass one generalized coordinate, which is the roll angle, $\phi$, is enough. On the other hand, in the case of a torsionally flexible vehicle roll angles in the front and rear parts of the vehicle can have different values. Such a phenomenon can be seen in harsh maneuvers, and plays a significant role in the dynamics of such vehicles. In harsh maneuvers, it may be noticed that, for example, one of the front wheels of the vehicle are off the ground, while the rear wheel(s) on the same side are still on the ground. This behaviour makes the dynamics of TFVs more complicated and significantly different from those of TRVs.

### 4.1.1 The Model of a Torsionally Rigid Vehicle Dynamics

A proper model that can be used for designing a controller with the purpose of yaw and roll control must include lateral and roll dynamics of the vehicle. The model that is used in this thesis includes the side slip angle, $\beta$, the yaw rate, $r$, and the roll angle, $\phi$, as the generalized coordinates. The equations of motion of the system are derived as follow:

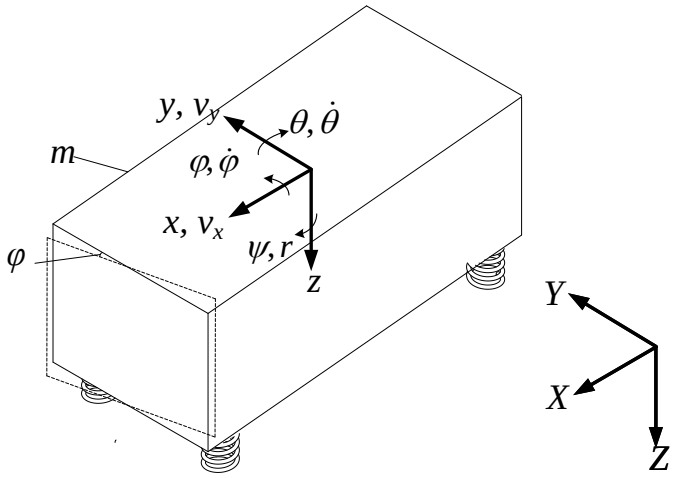


Figure 4.1: The schematic of a torsionally rigid vehicle

$$\begin{cases} mv_x(\dot{\beta}+r) = F_{y,f} + F_{y,r} \\ I_z\dot{r} = a\,F_{y,f} \;-\; b\,F_{y,r} \\ (I_x + m_s h_s)\ddot{\phi} - I_{xz}\dot{r} + m_s h_s v_x(\dot{\beta}+r) = -(K_{s,f} + K_{s,r} - m_s g h_s)\phi - (C_{s,f} + C_{s,r})\dot{\phi} \end{cases} \tag{4.1}$$

where $F_{y,f}$ and $F_{y,r}$ are sum of tire lateral forces in front and rear axles, respectively. Other terms of (4.1) than the lateral forces, $F_{y,f}$ and $F_{y,r}$, are linear terms, and it is the tire model that indicates the complexity of the equations of motion. A schematic of a TRV is shown in Figure 4.1.

In this research, for both cases of TRVs and TFVs, we use two models for different purposes: a linear model and a nonlinear model. The nonlinear model includes the well-known comprehensive tire model, Pacejka magic formula, which captures most of the important properties of the dynamics of tires, and reads as:

$$F_y = D_y \sin\left[C_y \arctan\left(B_y\,\alpha - E_y\left(B_y\,\alpha - \arctan B_y\,\alpha\right)\right)\right] \tag{4.2}$$

The coefficients $B_y$, $C_y$, $D_y$, and $E_y$ are complex expressions of the states of the system.

Such expressions are derived using the results of numerous experiments with the aid of numerical methods. Some of the coefficients have physical meanings as well, such as $D_y$ which represents the normal force on the tire [3]. More details about the tire model is given in Appendix B. The nonlinear model is used for two purposes. Firstly, to create an accurate model of the dynamics of the vehicle used as the plant in the control loop, and secondly, as the basis for defining the bounds of the nonlinear terms, which are the nonlinear forces of tires, based on sector nonlinearity approach [110].

On the other hand, the linear model is used for creating subsystems of the T-S fuzzy model, as the control methods that are used for designing controllers for each subsystem are linear. The linear model includes a linear tire model which reads as follow:

$$F_y = C_\alpha \, \alpha \tag{4.3}$$

where $C_\alpha$ is the cornering stiffness of tires, and $\alpha$ is the side slip angles of each axle which are written as:

$$\begin{cases} \alpha_f = \delta - \beta - \dfrac{a\, r}{v_x} \\ \alpha_r = -\beta + \dfrac{b\, r}{v_x} \end{cases} \tag{4.4}$$

Substituting the terms of the linear tire model in (4.1), the state space form of the equations is written as:

$$\begin{cases} A' \, \dot{\mathbf{x}} = A'' \, \mathbf{x} \, + \, B' \, u \, + \, E' \, \delta \\ \\ \mathbf{y} = C \, \mathbf{x} \end{cases} \tag{4.5}$$

where $\mathbf{x} = \left\{ \beta \; r \; \phi \; \dot{\phi} \right\}^T$ is the state vector, $u$ is the control input, $\delta$ is the driver's steering command, and $A'$, $A''$, $B'$, and $E'$ are written as follow:

$$A' = \begin{bmatrix} m\,v_x & 0 & 0 & m_s\,h_s \\ 0 & I_z & 0 & -I_{xz} \\ 0 & 0 & 1 & 0 \\ m_s\,v_x\,h_s & -I_{xz} & 0 & m_s\,h_s^2 + I_x \end{bmatrix}$$

$$A'' = \begin{bmatrix} -C_{\alpha_f} - C_{\alpha_r} & -mv_x - \frac{aC_{\alpha_f} - bC_{\alpha r}}{v_x} & 0 & 0 \\ bC_{\alpha_r} - aC_{\alpha_f} & -\frac{C_{\alpha_f}\,a^2 + C_{\alpha_r}\,b^2}{v_x} & 0 & 0 \\ 0 & 0 & 0 & 1 \\ 0 & -m_s v_x h & a''_{4,3} & a''_{4,4} \end{bmatrix} \tag{4.6}$$

$$a''_{4,3} = m_s g h - K_{s2} - K_{s1}, \quad a''_{4,4} = -C_{s1} - C_{s2}$$

$$B' = \begin{bmatrix} 0 & 1 & 0 & 0 \end{bmatrix}^T, \quad E' = \begin{bmatrix} C_{\alpha_f} & a\,C_{\alpha_f} & 0 & 0 \end{bmatrix}^T$$

Finally, by multiplying both sides of the first equation in (4.5) by $(A')^{-1}$ the final form of the state space equations are derived as follow:

$$\begin{cases} \dot{\mathbf{x}} = A\,\mathbf{x} + B\,u + E\,\delta \\ \mathbf{y} = C\,\mathbf{x} \end{cases} \tag{4.7}$$

### 4.1.2 The Model of a Torsionally Flexible Vehicle Dynamics

As discussed before, it is imperative to include the torsional compliance in modeling the dynamics of torsionally flexible vehicles. There have been efforts for developing a proper model that can represent the behavior of TFVs. The best existing models are proposed by Sampson and Cebon in [2], which have been repeatedly used in the literature.

#### An Extension of the Torsionally Flexible Vehicle Dynamics Model

In this research, a model for torsionally flexible vehicles is developed using the main idea in [2], which is separating the masses of the front and rear parts of the vehicle, and using a set of a spring and a damper to model the flexibility of the structure, as shown in

| Parameter | Value | Description |
|---|---|---|
| $m_s$ | 1300 $kg$ | sprung mass |
| $m_u$ | 170 $kg$ | unsprung mass |
| $I_z$ | 2500 $kg.m^2$ | yaw moment of inertia |
| $I_x$ | 750 $kg.m^2$ | roll moment of inertia |
| $I_{xz}$ | 150 $kg.m^2$ | yaw-roll moment of inertia |
| $T$ | 1.4 $m$ | track width |
| $a$ | 1.2 $m$ | C.G. to front axle |
| $b$ | 1.3 $m$ | C.G. to rear axle |
| $K_{s,i}$ | 22500 $\frac{N.m}{rad}$ | Suspension stiffness of an axle |
| $C_{s,i}$ | 1300 $\frac{N.m.s}{rad}$ | Suspension damping of an axle |
| $h$ | 0.6 $m$ | height of C.G. from ground |
| $h_s$ | 0.4 $m$ | C.G. of $m_s$ to C.G. of $m_u$ |
| $h_u$ | 0.3 $m$ | C.G. of $m_u$ from ground |
| $v_x$ | 20 $\frac{m}{s}$ | longitudinal velocity |
| $C_{ax,f}^{LB}$ | 7286.8 $\frac{N}{rad}$ | lower bound of $F_y^{ax,f}$ |
| $C_{ax,f}^{UB}$ | 33743 $\frac{N}{rad}$ | upper bound of $F_y^{ax,f}$ |
| $C_{ax,r}^{LB}$ | 6715.2 $\frac{N}{rad}$ | lower bound of $F_y^{ax,r}$ |
| $C_{ax,r}^{UB}$ | 32991 $\frac{N}{rad}$ | upper bound of $F_y^{ax,r}$ |

Table 4.1: The parameters of the torsionally rigid vehicle used for designing the T-S fuzzy controller [1]

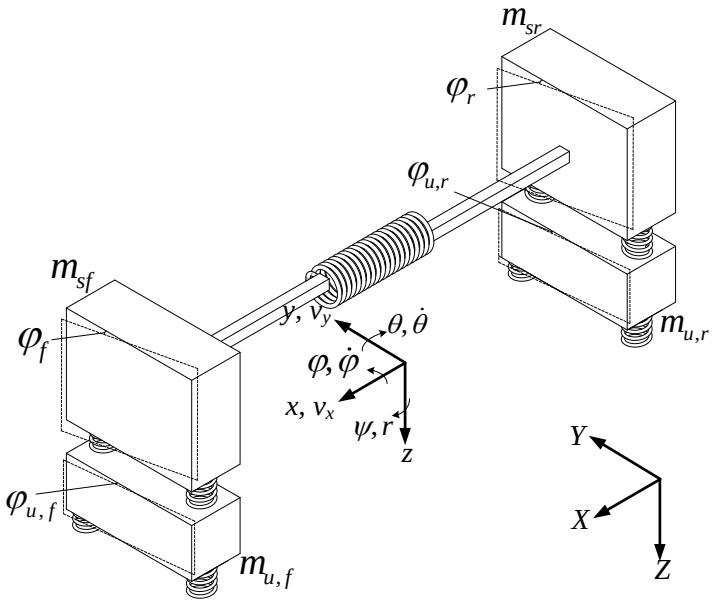


Figure 4.2: The schematic of a torsionally flexible vehicle

Figure 4.2. In the model that is introduced here, we exploit the nonlinear Pajecka tire model represented in (4.2). For details about the Magic Formula refer to Appendix B. Furthermore, the velocity terms of different masses in the model are also nonlinear in the current model. This is important if the model is used for situations with high lateral accelerations since the values of roll angles are not small in such occasions. Therefore, this model can be considered as an extension of the model in [2].

As illustrated in Figure 4.2, the model consists of four masses: the front unsprung mass, $m_{u,f}$, the rear unsprung mass, $m_{u,r}$, the front sprung mass, $m_{s,f}$, and the rear sprung mass, $m_{s,r}$. The model has 6 generalized coordinates including the lateral velocity, $v_y$, the yaw rate, $r$, the roll angle of the front unsprung mass, $\phi_{u,f}$, the roll angle of the rear unsprung mass, $\phi_{u,r}$, the roll angle of the front sprung mass, $\phi_f$, and the roll angle of the rear sprung mass, $\phi_r$. The sprung masses can roll due to the existence of a suspension system in the front and rear axles, as well as the flexibility of the structure. The roll angles of the unsprung masses happen due to the torsional compliance of the tires. However, tires are considered rigid in the vertical direction, which means that unsprung masses are not suspended.

The driving forces, $F_x$, are evenly distributed on both sides of the axles, so that they do not create a yaw moment. The lateral load transfer effects are considered in this study as well. The forward speed of the vehicle, $v_x$, can be assumed as a constant in studying the yaw-roll dynamics of a vehicle system. This avoids unnecessary nonlinearities, which makes the system more complicated.

**Deriving the Equations of Motion**

The equations of motion of the vehicle are formulated using Lagrange equation. To use Lagrange equation, the terms of kinetic and potential energies and a dissipation function that includes the energy losses due to damper elements must be considered. To find the external generalized forces, $Q_k$, associated with the generalized coordinates, $q_k$, the concept of virtual work is employed. The first step is to derive the velocity terms of each mass of the vehicle, which are as follow:

$$\mathbf{V}_{u,f} = \{v_x,\, v_y + a\, r,\, 0\}^T, \quad \boldsymbol{\omega}_{u,f} = \left\{\dot{\phi}_{u,f},\, 0,\, r\right\}^T$$

$$\mathbf{V}_{u,r} = \{v_x,\, v_y - b\, r,\, 0\}^T, \quad \boldsymbol{\omega}_{u,r} = \left\{\dot{\phi}_{u,r},\, 0,\, r\right\}^T$$

$$\mathbf{V}_{s,f} = \left\{ \begin{array}{c} v_x + h_f\, r\, \sin\,\phi_f \\ v_y + a\, r - h_f\, \dot{\phi}_f\, \cos\,\phi_f \\ h_f\, \dot{\phi}_f\, \sin\,\phi_f \end{array} \right\}, \quad \boldsymbol{\omega}_{s,f} = \left\{ \begin{array}{c} \dot{\phi}_f + \dot{\phi}_{u,f} \\ 0 \\ r \end{array} \right\} \tag{4.8}$$

$$\mathbf{V}_{s,r} = \left\{ \begin{array}{c} v_x + h_r\, r\, \sin\,\phi_r \\ v_y - b\, r - h_r\, \dot{\phi}_r\, \cos\,\phi_r \\ h_r\, \dot{\phi}_r\, \sin\,\phi_r \end{array} \right\}, \quad \boldsymbol{\omega}_{s,r} = \left\{ \begin{array}{c} \dot{\phi}_r + \dot{\phi}_{u,r} \\ 0 \\ r \end{array} \right\}$$

All the variables of the equations in this section, including the above velocity terms, are defined in Nomenclature. The kinetic energy of the system is then written as:

$$\begin{aligned} T = \frac{1}{2} \textstyle\sum_k m_k\, \mathbf{V}_k^2 + \frac{1}{2} \textstyle\sum_k [I_{xx,k}\, \omega_{x,k}^2 + I_{y,k}\, \omega_{y,k}^2 + I_{z,k}\, \omega_{z,k}^2 \\ -2(I_{xy,k}\, \omega_{x,k}\, \omega_{y,k} + I_{yz,k}\, \omega_{y,k}\, \omega_{z,k} + I_{xz,k}\, \omega_{x,k}\, \omega_{z,k})], \\ k = \{u, r\},\, \{u, f\},\, \{f\},\, \{r\} \end{aligned} \tag{4.9}$$

The potential energy of the vehicle system is composed of torsional spring terms, and the gravitational potential energies due to the height of the masses. These heights are derived as:

$$\begin{aligned} -z_{u,f} &= h_u \cos\phi_{u,f} \\ -z_{u,r} &= h_u \cos\phi_{u,r} \\ -z_{s,f} &= h_u \cos\phi_{u,f} + h_f \cos(\phi_{u,f} + \phi_f) \approx h_u + h_f \cos\phi_f \\ -z_{s,r} &= h_u \cos\phi_{u,r} + h_r \cos(\phi_{u,r} + \phi_r) \approx h_u + h_r \cos\phi_r \end{aligned} \tag{4.10}$$

Thus, the potential energy of the system is written as follow:

$$\begin{aligned} U = & -m_{u,f}\, g\, z_{u,f} - m_{u,r}\, g\, z_{u,r} - m_{s,f}\, g\, z_{s,f} - m_{s,r}\, g\, z_{s,r} \\ & + \tfrac{1}{2} k_b (\phi_f - \phi_r)^2 + \tfrac{1}{2} k_{u,f} \phi_{u,f}^2 + \tfrac{1}{2} k_{u,r} \phi_{u,r}^2 \\ & + \tfrac{1}{2} k_f (\phi_f - \phi_{u,f})^2 + \tfrac{1}{2} k_r (\phi_r - \phi_{u,r})^2 \end{aligned} \tag{4.11}$$

Considering the viscous damping, the dissipation function is written as follow:

$$\begin{aligned} D = & \tfrac{1}{2} C_b (\dot{\phi}_f - \dot{\phi}_r)^2 + \tfrac{1}{2} C_{u,f} \dot{\phi}_{u,f}^2 + \tfrac{1}{2} C_{u,r} \dot{\phi}_{u,r}^2 \\ & + \tfrac{1}{2} C_{\alpha_f} (\dot{\phi}_f - \dot{\phi}_{u,f})^2 + \tfrac{1}{2} C_{\alpha_r} (\dot{\phi}_r - \dot{\phi}_{u,r})^2 \end{aligned} \tag{4.12}$$

The modified form of Lagrange equation for $v_y$ and $r$ and other generalized coordinates of a vehicle system read as [3]:

$$\begin{aligned} & \frac{d}{dt}\frac{\partial T}{\partial v_y} + r\frac{\partial T}{\partial v_x} = Q_{v_y} \\ & \frac{d}{dt}\frac{\partial T}{\partial r} - v_y\frac{\partial T}{\partial v_x} + v_x\frac{\partial T}{\partial v_y} = Q_r \\ & \frac{d}{dt}\frac{\partial T}{\partial \dot{\phi}_k} - \frac{\partial T}{\partial \phi_k} + \frac{\partial U}{\partial \phi_k} = Q_k, \qquad k = \{u,r\},\ \{u,f\},\ \{f\},\ \{r\} \end{aligned} \tag{4.13}$$

The generalized forces are found using the concept of virtual work:

$$\Delta W = \sum_{k=1}^{6} Q_k\, \Delta q_k \tag{4.14}$$

where $\Delta q_k$ are the generalized coordinates [1]. The generalized forces are obtained by virtual displacements in the generalized coordinates:

$$\begin{aligned} \Delta W = & \sum F_y\, \Delta y + \sum M_z\, \Delta\psi + \sum M_{\phi_{u,f}}\, \Delta\phi_{u,f} \\ & + \sum M_{\phi_{u,r}}\, \Delta\phi_{u,r} + \sum M_{\phi_f}\, \Delta\phi_f + \sum M_{\phi_r}\, \Delta\phi_r \end{aligned} \tag{4.15}$$

Equating (4.14) and (4.15), the generalized forces are found as:

$$\begin{aligned} & Q_{v_y} = F_{y,f} + F_{y,r} \qquad && Q_r = a\, F_{y,f} - b\, F_{y,r} \\ & Q_k = 0, \qquad k = f, r \\ & Q_{u,f} = -R\, F_{y,f} \qquad && Q_{u,r} = -R\, F_{y,r} \end{aligned} \tag{4.16}$$

[1] Pacejka calls the coordinate $y$, a quasi-coordinate since $y$ cannot be obtained by integrating $v$. For more information, please refer to [3]

| Parameter | Value | Description |
|---|---|---|
| $m$ | 14193 $kg$ | Mass of the vehicle |
| $m_s$ | 12487 $kg$ | Sprung mass of the vehicle |
| $m_{u,f}$ | 706 $kg$ | Front unsprung mass |
| $m_{u,r}$ | 1000 $kg$ | Rear unsprung mass |
| $I_z$ | 34917 $kg.m^2$ | Yaw moment of inertia of the vehicle |
| $I_x$ | 24201 $kg.m^2$ | Roll moment of inertia |
| $I_{xz}$ | 4200 $kg.m^2$ | Yaw-roll moment of inertia |
| $a$ | 1.95 $m$ | Distance from C.G. to front axle |
| $b$ | 1.54 $m$ | Distance from C.G. to rear axle |
| $h$ | 1.15 $m$ | Height of C.G. of sprung mass from roll center |
| $h_u$ | 1.68 $m$ | Height of C.G. of unsprung mass from ground |
| $K_f$ | $700 \times 10^3 \frac{N.m}{rad}$ | Front suspension stiffness |
| $K_r$ | $470 \times 10^3 \frac{N.m}{rad}$ | Rear suspension stiffness |
| $K_{t,f}$ | $2800 \times 10^3 \frac{N.m}{rad}$ | Front tire roll stiffness |
| $K_{t,r}$ | $2700 \times 10^3 \frac{N.m}{rad}$ | Rear tire roll stiffness |
| $l_f$ | $200 \times 10^3 \frac{N.m.s}{rad}$ | Suspension damping of front axle |
| $l_r$ | $200 \times 10^3 \frac{N.m.s}{rad}$ | Suspension damping of front axle |
| $l_b$ | $0 \frac{N.m.s}{rad}$ | Torsional damping of the frame |
| $K_b$ | $47698 \frac{N.m}{rad}$ | Torsional stiffness of the frame |
| $R$ | 1.15 $m$ | Height of roll axis from ground |
| $C_{\alpha_f}$ | $387.12 \times 10^3$ | Front tire cornering stiffness |
| $C_{\alpha_r}$ | $283.12 \times 10^3$ | Rear tire cornering stiffness |

Table 4.2: The parameters of the torsionally flexible vehicle used for designing the T-S fuzzy controller [2]

The side slip angle of a vehicle, $\beta$, is defined as: $\beta = tan^{-1}\frac{v_y}{v_x}$. For small values of $\beta$, it is valid to assume: $\beta \approx \frac{v_y}{v_x}$. The largest values of side slip angles in simulations of this research is not more than $0.4\,rad$. With $\beta = 0.4\,rad$, such an assumption creates less than 5% error. To have similar form of equations as those in [2], $v_y$ is replaced by $\beta$. Finally, the equations of motion of the system are derived by substituting (4.9), (4.11), (4.12), and (4.16) into the modified Lagrange equations, (4.13) as:

$$
\begin{aligned}
&mv_x(\dot{\beta}+r)+m_{s,f}h_f\ddot{\phi}_f+m_{s,r}h_r\ddot{\phi}_r = F_{y,f}+F_{y,r}\\
&I_{zz}\dot{r}-I_{xz,f}\ddot{\phi}_f-I_{xz,r}\ddot{\phi}_r = a\,F_{y,f}-b\,F_{y,r}\\
&I_{xx,f}\ddot{\phi}_f-I_{xz,f}\dot{r}+m_{s,f}\,h_f v_x\,(\dot{\beta}+r) = m_{s,f}gh_f\sin\phi_f-k_f(\phi_f-\phi_{u,f})\\
&\qquad\qquad -C_{\alpha_f}(\dot{\phi}_f-\dot{\phi}_{u,f})-k_b(\phi_f-\phi_r)-C_b(\dot{\phi}_f-\dot{\phi}_r)\\
&I_{xx,r}\ddot{\phi}_r-I_{xz,r}\dot{r}+m_{s,r}\,h_r v_x\,(\dot{\beta}+r) = m_{s,r}gh_r\sin\phi_r-k_r(\phi_r-\phi_{u,r})\\
&\qquad\qquad -C_{\alpha_r}(\dot{\phi}_r-\dot{\phi}_{u,r})+k(\phi_f-\phi_r)+C_b(\dot{\phi}_f-\dot{\phi}_r)\\
&m_{u,f}v_x(h_u-R)(\dot{\beta}+r) = -R\,F_{y,f}+m_{u,f}gh_u\phi_{u,f}-k_{u,f}\phi_{u,f}\\
&\qquad\qquad +k_f(\phi_f-\phi_{u,f})+C_{\alpha_f}(\dot{\phi}_f-\dot{\phi}_{u,f})\\
&m_{u,r}v_x(h_u-R)(\dot{\beta}+r) = -R\,F_{y,r}+m_{u,r}gh_u\phi_{u,r}-k_{u,r}\phi_{u,r}\\
&\qquad\qquad +k_r(\phi_r-\phi_{u,r})+C_{\alpha_r}(\dot{\phi}_r-\dot{\phi}_{u,r})
\end{aligned}
\tag{4.17}
$$

**State Space Form of the Equations**

Like the case of the TRV, the state space representation of the equations can be obtained by using a linear tire model as (4.3). The associated matrices $A'$, $A''$, $B'$ and $E'$ in (4.5) are given in the subsequent equations. Following the same procedure, the state space model will have the same form as (4.7). Such a state space form is used for design of the subsystems of the T-S fuzzy controller.

$$
A' = \begin{pmatrix}
m\,v_x & 0 & 0 & m_{s,f}\,h_f & 0 & m_{s,r}\,h_r & 0 & 0\\
0 & I_{zz} & 0 & -I_{xz,f} & 0 & -I_{xz,r} & 0 & 0\\
0 & 0 & 1 & 0 & 0 & 0 & 0 & 0\\
m_{s,f}\,v_x\,h_f & -I_{xz,f} & 0 & I_{xx,f} & 0 & 0 & -l_f & 0\\
0 & 0 & 0 & 0 & 1 & 0 & 0 & 0\\
m_{s,r}\,v_x\,h_r & -I_{xz,r} & 0 & 0 & 0 & I_{xx,r} & 0 & -l_r\\
m_{u,f}\,v_x\,(R-h_{u,f}) & 0 & 0 & 0 & 0 & 0 & -l_f & 0\\
m_{u,r}\,v_x\,(R-h_{u,r}) & 0 & 0 & 0 & 0 & 0 & 0 & -l_r
\end{pmatrix}
\tag{4.18}
$$

$$A'' = \begin{pmatrix} -C_{\alpha_f} - C_{\alpha_r} & -m\,v_x - \frac{a\,C_{\alpha_f} - b\,C_{\alpha_r}}{v_x} & 0 & 0 & 0 & 0 & 0 & 0 \\ b\,C_{\alpha_r} - a\,C_{\alpha_f} & -\frac{a^2\,C_{\alpha_f} + b^2\,C_{\alpha_r}}{v_x} & 0 & 0 & 0 & 0 & 0 & 0 \\ 0 & 0 & 0 & 1 & 0 & 0 & 0 & 0 \\ 0 & -m_{s,f}\,v_x\,h_f & a''_{3,4} & -l_b - l_f & K_b & l_b & K_f & 0 \\ 0 & 0 & 0 & 0 & 0 & 1 & 0 & 0 \\ 0 & -m_{s,r}\,v_x\,h_r & K_b & l_b & a''_{5,6} & -l_b - l_r & 0 & K_r \\ -R\,C_{\alpha_f} & a''_{2,7} & -K_f & -l_f & 0 & 0 & a''_{7,7} & 0 \\ -R\,C_{\alpha_r} & a''_{2,8} & 0 & 0 & -K_r & -l_r & 0 & a''_{8,8} \end{pmatrix}$$

$$\begin{aligned} a''_{3,4} &= m_{s,f}\,g\,h_f - K_f - K_b & a''_{5,6} &= m_{s,r}\,g\,h_r - K_r - K_b \\ a''_{2,7} &= -m_{u,f}\,v_x\,(R - h_{u,f}) - \tfrac{a\,R\,C_{\alpha_f}}{v_x} & a''_{7,7} &= K_f + K_{t,f} - m_{u,f}\,g\,h_{u,f} \\ a''_{2,8} &= \tfrac{b\,R\,C_{\alpha_r}}{v_x} - m_{u,r}\,v_x\,(R - h_{u,r}) & a''_{8,8} &= K_r + K_{t,r} - m_{u,r}\,g\,h_{u,r} \end{aligned} \tag{4.19}$$

$$B' = \begin{bmatrix} 0 & 1 & 0 & 0 & 0 & 0 & 0 & 0 \end{bmatrix}^T, \quad E' = \begin{bmatrix} C_{\alpha_f} & a\,C_{\alpha_f} & 0 & 0 & 0 & 0 & R\,C_{\alpha_f} & 0 \end{bmatrix}^T \tag{4.20}$$

**Nonlinear Tire Models**

The tire lateral force depends on many variables such as the normal force on the tire, $F_z$, the side slip angle, $\beta$, the camber angle of the tire, $\gamma$ etc. Among them, $F_z$ and $\beta$ have the most significant effects on the lateral force. Sampson and Cebon in [2] have also considered the effect of changes in the tire cornering stiffness, $C_\alpha$, and accordingly the tire lateral force with variations in the normal force, $F_z$, by a quadratic function. The tire cornering stiffness is then defined as:

$$C_\alpha = \frac{F_y}{\alpha} = c_1 \times F_z + c_2 \times F_z^2 \tag{4.21}$$

where $c_1$ and $c_2$ are two parameters, and $\alpha$ is the side slip angle of the tire.

In modeling the tire lateral force, including the effect of normal force is essential, specifically for studying roll dynamics, where the balance of normal forces changes significantly

in harsh maneuvers. However, two points need to be considered. Firstly, the choice of a quadratic function for representing the effect of normal force on the lateral force is not ideal. The relationship between the two forces is so complicated that cannot be perfectly modeled by such a quadratic function. Secondly, the main source of nonlinearity in the tire lateral force, which has significant effects on yaw and roll dynamics, comes from its dependence on the side slip angle, $\alpha$ [3; 118; 119; 1]. With the function in (4.21), the lateral force has a linear relation with the side slip angle, $\alpha$. Figures 4.3 compares the nonlinear Pajecka model with a linear model with respect to the side slip angle. The region indicated in Figure 4.3 as the linear region, where the two models have almost identical values, represents the normal situations of driving. In the nonlinear region, the difference between the values of linear and nonlinear models is fairly large. In the saturated region the two models show a significant difference. Harsh maneuvers happen in either the nonlinear or the saturated regions. Sampson and Cebon also admitted that this assumption of linearity is only reasonable for lateral motions of moderate amplitude [2]. In this research, a Pajecka tire model is used as such a model does not have the limitations mentioned for the tire model in (4.21).

Substituting the values of the tire lateral forces in (4.17), and writing the equations in the state space format, the vehicle dynamic system reads as:

$$\dot{\mathbf{x}}(t) \;=\; \mathbf{f}(\,\mathbf{x}(t), \delta(t)\,) \tag{4.22}$$

where $\mathbf{x} = [\beta,\, r,\, \phi_f,\, \dot{\phi}_f,\, \phi_r,\, \dot{\phi}_r, \phi_{u,f},\, \phi_{u,r}]$ is the state vector, and $\delta$ is the steering input. More details about Pajecka tire model is represented in Appendix B.

## 4.2 Design of a Multi-objective T-S Fuzzy Controller for Yaw Stabilization and Rollover Prevention of Torsionally Rigid Vehicles

The significance of controlling both the yaw and roll motions was discussed in Chapter 1. As mentioned, designing a multi-objective controller is of interest in this research. The

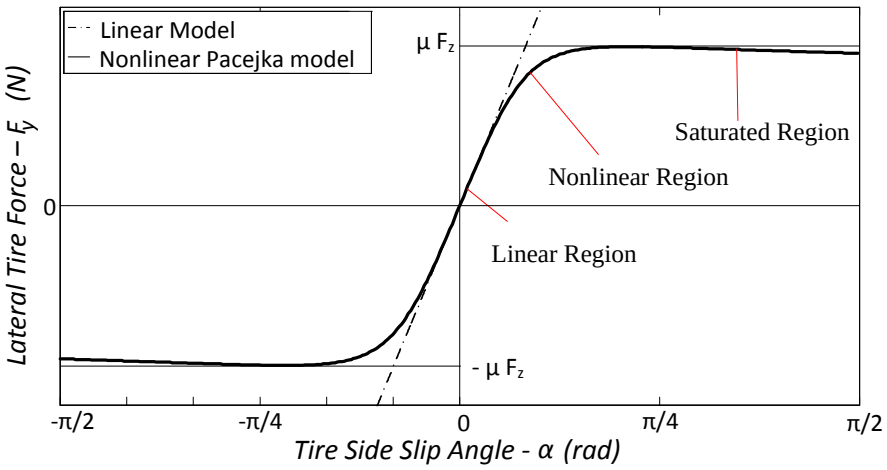


Figure 4.3: The comparison of the linear and nonlinear tire models with respect to the side slip angle $\alpha$

two objectives of the controller are: tracking a desired value for the yaw rate, which provides a better quality of handling and maneuverability, and controlling the value of the rollover index (RI) to decrease the possibility of wheel lift-off, and accordingly rollover. As discussed in introduction, it is practically impossible to attain both of the objectives simultaneously at all times. Thus, there has to be a compromise between meeting each of the objectives.

T-S fuzzy methods have shown a great potential in handling multi-objective controller design problems. To construct a T-S fuzzy model, first the nonlinearities of the system must be identified. As mentioned earlier in Section 4.1.1, the nonlinear terms in the model of (4.1) are the sum of tire lateral forces in the front and rear axles, $F_{y,f}$ and $F_{y,r}$. It is worth mentioning that it is the summation of the tire forces in an axle, $F_y^{axle}$ (let us call it axle force), that plays a role in the dynamics not the individual tire forces. Figure 4.4 shows a schematic of the behaviour of the axle force as a function of the side slip angle, $\alpha$, in a normal driving situation and in the case of wheel lift-off.

The value of the normal forces on tires can change due to the lateral load transfer (LLT) effects, which happens when the vehicle experiences the lateral acceleration. LLT changes the balance of the normal forces on left and right sides of the vehicle according to the following equation:

$$F_{z,i} = F_{z0,i} \pm \frac{m_u a_y h_u + m_s a_{y,s}(h + h_s) + m_s g h_s \phi}{T}, \qquad i\text{=}Left,\ Right \tag{4.23}$$

where $F_{z0,i}$ is the nominal value of the normal force, and $a_y$ and $a_{y,s}$ are the lateral accelerations of the vehicle and the sprung mass, respectively. The rest of the parameters are introduced in Table 4.1. According to (4.23), when the normal force on one side is decreased, the normal force on the other side is increased by the same amount. However, due to the nonlinear relation of $F_y$ and $F_z$, the same statement cannot be said about $F_y$. In other words, when the balance of $F_z$ changes, $F_y$ on one side is not increased as much as it is decreased on the opposite side. This means the axle force, $F_y^{axle}$, does not remain constant and is decreased compared to its maximum value. The maximum value happens when the normal force is balanced on each side of the vehicle. Such a phenomenon causes a loss in $F_y^{axle}$ which is illustrated in Figure 4.4. This loss of force can exceed 20% of the nominal force of an axle. Therefore, $F_y^{axle}$ varies in a range according to the value of the side slip angle, $\alpha$, and the balance of the normal force. The same concept may be used for modelling other nonlinear phenomena in tire dynamics such as its dependence to the road friction coefficient.

It is worth remarking that the vertical acceleration of the sprung and unsprung masses due to the bounce motion can have a negligible effect on the balance of the normal forces which is relatively insignificant in comparison with the LLT effects due to the lateral acceleration.

### 4.2.1 Constructing the Subsystems Using Sector Nonlinearity Approach

The aforementioned nonlinear effects can be captured using a T-S fuzzy model provided that an appropriate set of sectors are selected based on sector nonlinearity approach. The idea of this approach is to find the sectors such that the nonlinear terms remain within them in a local or global region [110]. The proper selection of the sectors is critical for accurate modelling of the system. Another important factor in selecting the sectors is the simplicity

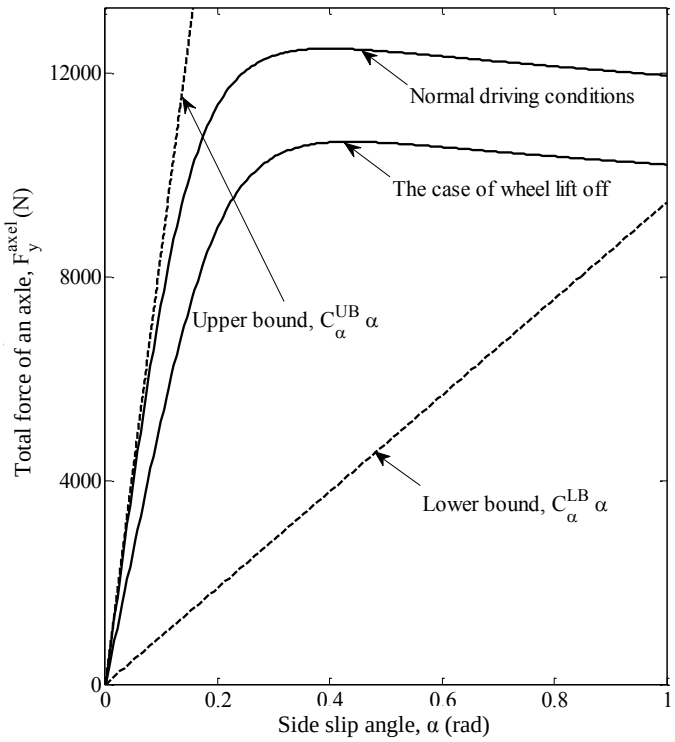


Figure 4.4: Nonlinear behaviour and the loss of force in an axle due to the effects of lateral load transfer

of the model. The best choice must be able to not only represent the essential characteristics of the dynamics, but also to minimize the number of subsystems of the T-S fuzzy model.

In Figure 4.4, the selected sectors for axle forces are depicted by dashed lines. Each of the sectors is used to constitute one of the subsystems of the T-S fuzzy model. The upper bound is almost tangential to the nominal curve, which represents the normal driving conditions. By choosing such an upper bound, when the vehicle is driven in normal conditions a linear model represents the vehicle which is reasonably realistic. If the lower bound has a low enough slope that covers a wide area of the operating region of the lateral force, as shown in Figure 4.4, it is almost guaranteed that the T-S fuzzy model captures all the important characteristics of tire dynamics. The lower bound shown in Figure 4.4 can be representative of different cases, such as the situation that the tire have lower friction coefficient. Another criterion that is considered in this research for the selection of the lower bound is the fine

tuning of the controller's performance. The lower bound is adjusted in a way that each of the controllers come into action at the right time.

With such a choice of the sectors, the T-S fuzzy system has two subsystems which are used for designing two controllers. Figure 4.5 illustrates the block diagram of the proposed control system. The first subsystem is exploited for the design of a controller for the normal driving conditions (controller#1 - CN1) using the upper bound. The second subsystem, which uses the lower bound of the axle force, is used for designing a controller for the cases that the vehicle is close to the verge of wheel lift-off (controller#2 - CN2). In normal driving conditions, the tires have linear behavior, and the lateral load transfer effects are negligible. Thus, as it will be shown in the results, when the vehicle operates in normal driving conditions, the upper bound, which is the tangent line to $F_y^{axle}$ in the nominal condition, can accurately represent the behaviour of the vehicle. The T-S fuzzy system is designed so that in such circumstances the dominant controller is CN1.

However, as the operating points of the tires move away from the linear region, the vehicle experiences high lateral accelerations, and accordingly the effects of LLT are substantial. Under such circumstances, the upper bound will have a considerably larger distance to the true value of the force, while the lower bound will have a smaller distance. In such cases, the dominant controller is CN2 which reduces the value of the rollover index. Such a choice of the sectors provides the fuzzy system with an excellent tool for distinguishing between normal driving conditions and the conditions with high risk of rollover.

**Design of Linear Quadratic Regulator Optimal Controller**

Consider a linear time invariant system as:

$$\begin{cases} \dot{\mathbf{x}}(t) = A\,\mathbf{x}(t) + B\,\mathbf{u}(t) + E_x\,\mathbf{w}(t) \\ \mathbf{y}(t) = C\,\mathbf{x}(t) \end{cases} \tag{4.24}$$

If the output of the above system, $\mathbf{y}(t)$, is required to be regulated, linear quadratic regulator (LQR) system design provides a feedback control input as:

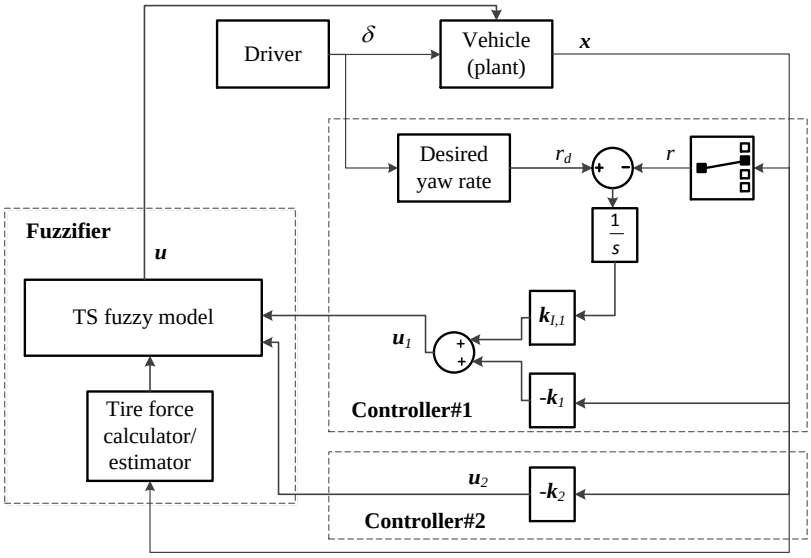


Figure 4.5: The block diagram of the proposed T-S fuzzy controller, and the vehicle system

$$\mathbf{u}(t) = -\mathbf{k}\,\mathbf{x}(t) \tag{4.25}$$

which minimizes the following performance index:

$$J = \int_{t_0}^{\infty} \left[\mathbf{y}^T(\tau)\mathbf{Q}\mathbf{y}(\tau) + \mathbf{u}^T\mathbf{R}\mathbf{u}\right] d\tau = \int_{t_0}^{\infty} \left[\mathbf{x}^T(\tau)\bar{\mathbf{Q}}\mathbf{x}(\tau) + \mathbf{u}^T\mathbf{R}\mathbf{u}\right] d\tau, \quad \bar{\mathbf{Q}} = C^T\mathbf{Q}C \tag{4.26}$$

where $\mathbf{Q}$ and $\mathbf{R}$ are the design parameters and both are positive definite matrices. The index is defined based on the objectives of the specific regulator system. The optimization problem involves solving the following algebraic Riccati equation:

$$A^T Z + Z A - Z B \mathbf{R}^{-1} B^T Z + \bar{\mathbf{Q}} = 0 \tag{4.27}$$

By solving the optimization problem for $Z$, the optimal control law is given by:

$$\mathbf{u}(t) = -\mathbf{R}^{-1} B^T Z\,\mathbf{x}(t) \tag{4.28}$$

and accordingly,

$$\mathbf{k} = -\mathbf{R}^{-1}\, B^T\, Z \tag{4.29}$$

Such a control law guarantees that the cost of output regulation and the control effort are minimized.

### Design of LQR for a Servo System

The standard LQR design procedure described in the previous section can be easily applied to servo systems [2] as well. Here, we describe the application of an LQR to a servo system. If the servo system does not have an integrator, the basic idea is to insert an integrator between the error calculator and the plant. First, the system in (4.24) is modified as follow:

$$\begin{cases} \dot{\mathbf{x}}(t) = A\,\mathbf{x}(t) \;+\; B\,\mathbf{u}(t) \;+\; E_x\,\mathbf{w}(t) \\ \dot{\boldsymbol{\zeta}}(t) = \mathbf{x}_{ref} \;-\; \mathbf{y}(t) = \mathbf{x}_{ref} \;-\; C\,\mathbf{x}(t) \\ \mathbf{u}(t) = -\mathbf{k}\,\mathbf{x}(t) + \mathbf{k}_I\,\boldsymbol{\zeta} \\ \mathbf{y}(t) = C\,\mathbf{x}(t) \end{cases} \tag{4.30}$$

The equations in (4.30) can be combined to form a new dynamic system as:

$$\begin{cases} \begin{Bmatrix} \dot{\mathbf{x}}(t) \\ \dot{\boldsymbol{\zeta}}(t) \end{Bmatrix} = \begin{bmatrix} A & \mathbf{0} \\ -C & \mathbf{0} \end{bmatrix} \begin{Bmatrix} \mathbf{x}(t) \\ \boldsymbol{\zeta}(t) \end{Bmatrix} + \begin{bmatrix} B \\ \mathbf{0} \end{bmatrix} \mathbf{u}(t) + \begin{bmatrix} E \\ \mathbf{0} \end{bmatrix} \mathbf{w}(t) + \begin{bmatrix} \mathbf{0} \\ 1 \end{bmatrix} \mathbf{x}_{ref} \\ \mathbf{y}(t) = C\,\mathbf{x}(t) \end{cases} \tag{4.31}$$

Assume that the reference input is a step function. If the closed loop system is asymptotically stable, $\mathbf{x}(\infty)$, $\boldsymbol{\zeta}(\infty)$, $\mathbf{u}(\infty)$ approach constant values. Besides, at steady state conditions, $\boldsymbol{\zeta}(t) = 0$, or $\mathbf{y}(\infty) = \mathbf{x}_{ref}$. It can be shown that the system of (4.31) is equivalent to the following system:

[2] Here, a servo system is a control system in which the reference value for the controlled states, $\mathbf{x}_{ref}$, is nonzero.

$$\begin{cases} \dot{\mathbf{e}}(t) = \begin{bmatrix} A & \mathbf{0} \\ -C & \mathbf{0} \end{bmatrix} \mathbf{e}(t) + \begin{bmatrix} B \\ \mathbf{0} \end{bmatrix} \mathbf{u}_e(t) + \begin{bmatrix} E \\ \mathbf{0} \end{bmatrix} \mathbf{w}(t) \\ \mathbf{y}(t) = [C \quad \mathbf{0}]\, \mathbf{e}(t) \end{cases} \tag{4.32}$$

where

$$\mathbf{e}(t) = \begin{Bmatrix} \mathbf{x}_e(t) \\ \boldsymbol{\zeta}_e(t) \end{Bmatrix} = \begin{Bmatrix} \mathbf{x}(t) - \mathbf{x}(\infty) \\ \boldsymbol{\zeta}(t) - \boldsymbol{\zeta}(\infty) \end{Bmatrix} \tag{4.33}$$

Equation (4.32) is in the form of a regulator problem of (4.24), and the described method for designing an LQR for a regulator problem in this section can be used for the servo system as well.

**Design of Controller#1 (CN1): Yaw Stabilization of a Torsionally Rigid Vehicle**

The objective of this controller, as mentioned earlier, is to track a specific value of the yaw rate based on the steering command of the driver. This can guarantee that the vehicle moves smoothly and with a fast response along the intended path. The choice of the desired value for the yaw rate depends on the quality of maneuverability that the designer considers for the vehicle. To explain that further, maneuverability is quantified by the definition of understeer/oversteer characteristics of a vehicle. In essence, an understeer vehicle have more resistance to maneuver while an oversteer vehicle is easier to maneuver. For example, if moving along a curve with a constant radius is considered, an understeer vehicle tends to move towards outside of the curve, while an oversteer vehicle tends to move towards inside of the curve. To quantify the understeer/oversteer property of a vehicle, there is a parameter, $K_{us}$, that is defined based on Routh-Hurwitz stability criterion. If $K_{us} < 0$, the vehicle is understeer, and if $K_{us} > 0$, the vehicle is oversteer. Once the value of $K_{us}$ is chosen, the desired value for yaw rate can be determined by the following equation which is based on a simple steady state analysis [118; 119]:

$$r_d = \frac{v_x}{l(1 + K_{us}\, v_x^2)}\delta \tag{4.34}$$

Since the objective of CN1 is tracking a desired value for one of the states of the system, we have a servo problem. Based on the methodology described in this section for designing an LQR for servo systems, the system's equations are defined as (4.30) with

$$\mathbf{u}(t) = M_{z,1}, \quad \mathbf{w}(t) = \delta, \quad C_1 = [0 \quad 1 \quad 0 \quad 0]^T, \quad \mathbf{x}_{ref} = r_d \tag{4.35}$$

where $M_{z,1}$ is the controlling yaw moment of CN1. Substituting these values in (4.30) results in the following equations:

$$\begin{cases} \dot{\mathbf{x}}(t) = A_1\, \mathbf{x}(t) \;+\; B\, M_{z,1} \;+\; E_{x,1}\, \delta \\ \dot{\boldsymbol{\zeta}}(t) = r_d \;-\; y(t) = r_d - r \\ y(t) = C_1 \mathbf{x}(t) = r \end{cases} \tag{4.36}$$

where $A_1$ and $E_{x,1}$ are calculated according to (4.6) by substituting $C_\alpha^{UB}$ for the cornering stiffnesses. The controller is designed to minimize the following performance index:

$$\mathbf{J} = \int_{t_0}^{\infty} \left(q_1\, (r - r_d)^2 + R_1\, M_{z,1}^2\right) \tag{4.37}$$

By solving the optimal control problem, the gains of CN1 are found as follow:

$$\hat{\mathbf{k}} = [\mathbf{k}_1 \mid -\mathbf{k}_I] = [436.6 \quad 1222 \quad 3.3 \quad 7.7 \mid 3162.3] \tag{4.38}$$

**Design of Controller#2 (CN2): The Rollover Index Control of a Torsionally Rigid Vehicle**

The objective of the second controller is to decrease the chance of wheel lift-off, which is a necessary condition for a rollover incident. A wheel of a vehicle lifts off the ground when the normal force on it is equal to zero. There are different measures to evaluate and monitor

a vehicle propensity to rollover. Such methods can be categorized into static or steady-state rollover metrics [125], the dynamic stability measures like ZMP-based [126; 127] and force-angle-based measures [128], and finally energy-based stability measure [129]. In this research, to quantify the situation of a vehicle in terms of wheel lift-off an index, known as the rollover index (RI), is defined which indicates the ratio of the normal force on each side of the vehicle. The RI is defined as follow:

$$RI = \frac{F_{z,l} - F_{z,r}}{m\,g} = \frac{2}{m\,g\,T}\left( \; (K_{s,f} + K_{s,r})\phi + (C_{s,f} + C_{c,r})\dot{\phi} \; \right) \tag{4.39}$$

The value of the RI varies from $-1$ to $+1$, with $\pm 1$ meaning the occurrence of wheel lift-off, and 0 meaning that the normal forces have nominal values. For example, when a vehicle is moving on a straight line, theoretically there is no LLT, and $F_{z,l} = F_{z,r}$, which means $RI = 0$. In addition, in the case that $F_{z,r} = 0$, all the load of the vehicle is on the other side, i.e. $F_{z,l} = m\,g$, and accordingly $RI = 1$.

The objective of CN2 is to decrease the value of the RI. This is similar to what Dahmani et. al [55] have used as the objective of their controller. Dahmani et. al used this objective for all the working conditions of the vehicle. As discussed in Chapter 1, this objective is neither appropriate nor necessary for normal driving conditions, as the controller aims to minimize the RI at all times. However, in this research, CN2 comes into action only in cases that the vehicle is close to the verge of wheel lift-off.

Now that the objective of CN2 is defined, the next step is to interpret the objective to a control problem. The expression in (4.39) for the RI includes terms of the states of the system. Since the objective is to minimize the RI, we have a regulator problem. The procedure for designing a standard LQR problem is presented in this section. Considering the following definition for matrix $C_2$ and $\mathbf{x}_{ref}$:

$$C_2 = \frac{2}{mgT}\left[0 \;\; 0 \;\; (K_{s,f} + K_{s,r}) \;\; (C_{s,f} + C_{c,r})\right], \quad \mathbf{x}_{ref} = 0 \tag{4.40}$$

the system's equations based on (4.24) is modified as follow:

$$\begin{cases} \dot{\mathbf{x}}(t) = A_2\,\mathbf{x}(t) + B\,M_{z,2} + E_{x,2}\,\delta \\ y(t) = C_2\,\mathbf{x}(t) \end{cases} \tag{4.41}$$

The value of the axle cornering stiffness in (4.6) for calculating $A_2$ and $E_{x,2}$ is equal to the lower bound of the axle force, $C_\alpha^{LB}$ (see Figure 4.4). This is because CN2 is designed to be effective in the situations that the vehicle is close to the margins of wheel lift-off. In such situations, the axle loses some of its force capacity due to the lateral load transfer effects, and the actual value of the lateral force is closer to the lower bound. The controller is designed to minimize the following performance index:

$$\mathbf{J} = \int_{t_0}^{\infty} \left(q_2\,(RI)^2 + R_2\,M_z^2\right) \tag{4.42}$$

where $q_2$ and $R_2$ are constant and the design parameters of the controller. By solving the optimization problem, the gains of CN2 are found as follow:

$$\mathbf{k}_2 = [694.2, \quad 252.6, \quad -1549.5, \quad 35.3] \tag{4.43}$$

### 4.2.2 Constructing the T-S Fuzzy System

The T-S fuzzy system is composed of the following two fuzzy rules:

$$\textbf{Fuzzy rule}\,1: \text{IF } F_y^{axle} \text{ is } C_\alpha^{UB} \text{ THEN}$$
$$\begin{cases} \dot{\mathbf{x}}(t) = A_1\,\mathbf{x}(t) \;+\; B\,M_{z,1} \;+\; E_{x,1}\,\delta \\ \dot{\boldsymbol{\zeta}}(t) = r_d \;-\; y(t) = r_d - r \\ y(t) = C_1\mathbf{x}(t) \end{cases} \tag{4.44}$$

$$\textbf{Fuzzy rule}\,2: \text{IF } F_y^{axle} \text{ is } C_\alpha^{LB} \text{ THEN}$$
$$\begin{cases} \dot{\mathbf{x}}(t) = A_2\,\mathbf{x}(t) \;+\; B\,M_{z,2} \;+\; E_{x,2}\,\delta \\ \dot{\boldsymbol{\zeta}}(t) = -\,y(t) \\ y(t) = C_2\mathbf{x}(t) \end{cases}$$

where $F_y^{axle}$ is the premise variable, and $C_\alpha^{UB}$ and $C_\alpha^{LB}$ are the fuzzy sets. **Fuzzy rule** 1 represents the normal driving conditions, and **Fuzzy rule** 2 represents the situation where the vehicle is close to a wheel lift-off event. The allocation of the control action to the two subsystems is performed using the value of the axle force, $F_y^{axle}$. Therefore, the value of tire forces must be either evaluated using a proper model, or estimated using the existing algorithms for estimating them [56; 130]. In this thesis, Pacejka tire model is used to calculate the values of tire forces at each moment.

Another role of the T-S fuzzy system is to ensure that the two controllers that are designed for different objectives are able to stabilize the system when they are in action simultaneously. This task is performed by casting the two control problems into one LMI, according to the Theorem in Section 2.4. To apply the theorem to the fuzzy system of this research, notice that $M_z$, the controlling yaw moment and the output of the controller, is a function of the states of the system, since both of the subsystems have feedback controllers:

$$M_z = \sum_{i=1}^{r} h_i(\boldsymbol{\kappa})\,M_{z,i} = -\,h_1\,[\mathbf{k}_1\,\mathbf{x}(t) - \mathbf{k}_{I,1}\,(r_d \;-\; x_2(t))] - h_2\,\mathbf{k}_2\,\mathbf{x}(t) \tag{4.45}$$

Thus, writing the subsystems in the form of (4.32), and accordingly the fuzzy system in the form of (2.13), and substituting (4.45) in the equation, the fuzzy system is simplified as:

$$\begin{cases} \dot{\mathbf{e}}(t) = \sum_{i=1}^{2} h_i(\boldsymbol{\kappa}) \left( \begin{bmatrix} A_i - B\,\mathbf{k}_i & B\,\mathbf{k}_{I,i} \\ -C_i & \mathbf{0} \end{bmatrix} \mathbf{e}(t) + \begin{bmatrix} E \\ \mathbf{0} \end{bmatrix} \mathbf{w}(t) \right) \\ \mathbf{y}(t) = \sum_{i=1}^{2} [C_i \quad \mathbf{0}]\, \mathbf{e}(t) \end{cases} \tag{4.46}$$

where $\mathbf{k}_{I,2} = 0$. Now, the fuzzy model is represented in the form of the unforced system of the theorem in Section 2.4. Solving the associated LMI, a matrix $P$, is obtained which guarantees Lyapunov quadratic stability for the T-S fuzzy controller with the two subsystems. The matrix $P$ reads as follow:

$$P = 10^5 \times \begin{bmatrix} 0.0033 & 0.0026 & 0.0742 & 0.0029 & -0.0195 \\ 0.0026 & 0.2053 & 0.1945 & 0.0053 & -0.0270 \\ 0.0742 & 0.1945 & 2.9134 & 0.0868 & -0.8100 \\ 0.0029 & 0.0053 & 0.0868 & 0.0087 & -0.0237 \\ -0.0195 & -0.0270 & -0.8100 & -0.0237 & 0.3747 \end{bmatrix} \tag{4.47}$$

This proves that the system of the two controllers can stabilize the plant with zero initial conditions.

## 4.3 Design of a Multi-objective T-S Fuzzy Controller for Yaw Stabilization and Rollover Prevention of Torsionally Flexible Vehicles

In this section, a similar methodology described in the previous section is applied to a nonlinear system of a torsionally flexible vehicle dynamics. The difference comes from the models of the dynamics of the two types of vehicles. The model of a TFV, described in Section 4.1.2, is significantly more complicated than the model of a TRV. This model has an 8-dimensional state space form, as opposed to the model of the TRV which has a 4-dimensional state space form. Besides, the torsional flexibility in the frame makes the model

more complex. Such a property leads to having different values of the rollover index in the front and rear axles. Therefore, in the case of a TFV, there are two rollover indexes that must be controlled: the RI in the front axle, $RI_f$, and the RI in the rear axle, $RI_r$.

The control technique that is used in this case is the same as the case of a TRV. This is to say that in normal driving conditions, the important property is maneuverability and yaw rate following. The control of the rollover index becomes the priority when the vehicle is approaching the limits of wheel lift-off.

The balance of the normal forces in the axles changes according to the lateral accelerations and the roll dynamics of the front and rear parts:

$$\begin{aligned} F^i_{z,f} &= F^i_{z0,f} \pm \frac{m_{u,f}a_{y,f}h_{u,f} + m_{s,f}a_{y,s,f}(h_{u,f}+h_{s,f}) + m_{s,f}g(h_{u,f}+h_{s,f})(\phi_f+\phi_{t,f})}{T} \\ F^i_{z,r} &= F^i_{z0,r} \pm \frac{m_{u,r}a_{y,r}h_{u,r} + m_{s,r}a_{y,s,r}(h_{u,r}+h_{s,r}) + m_{s,r}g(h_{u,r}+h_{s,r})(\phi_r+\phi_{t,r})}{T} \\ & \quad i\text{=}\textit{Left, Right} \end{aligned} \tag{4.48}$$

Based on the values of the normal loads, the values of tire lateral forces are also determined. With the same rationale used for defining the sectors of the nonlinear terms in the previous section, the value of axle force is bounded within an upper bound and a lower bound for the TFV. Likewise, the upper bound is used for representing the normal driving conditions, and the lower bound is used for representing the situations close to wheel lift-off. Controller#1 is designed following the same procedure, with matrix $C_1$ as:

$$C_1 = [0 \quad 1 \quad 0 \quad 0 \quad 0 \quad 0 \quad 0 \quad 0] \tag{4.49}$$

Using the methodology described in Section 4.2.1, the gains of CN1 are found as follow:

$$\hat{\mathbf{k}} = 10 \times [-195.9,\ 272.3,\ -62.9,\ -16.5,\ -47.2,\ -21.1,\ -36.1,\ -86.4,\ 1732.1] \tag{4.50}$$

For designing controller#2, first, the rollover indexes must be defined. With a simple dynamic analysis, the expressions of the rollover indexes can be obtained as follow:

$$
\begin{aligned}
RI_f &= \frac{F_{z,f}^L - F_{z,f}^R}{F_{z,f}^L + F_{z,f}^L} = \frac{2}{mgT}\left(-K_b(\phi_f - \phi_r) - l_b(\dot{\phi}_f - \dot{\phi}_r) - K_f\phi_f - l_f\dot{\phi}_f\right) \\
RI_r &= \frac{F_{z,r}^L - F_{z,r}^R}{F_{z,r}^L + F_{z,r}^L} = \frac{2}{mgT}\left(K_b(\phi_f - \phi_r) + l_b(\dot{\phi}_f - \dot{\phi}_r) - K_r\phi_r - l_r\dot{\phi}_r\right)
\end{aligned} \tag{4.51}
$$

Due to the flexibility in the frame, the values of the lateral accelerations and accordingly the roll angles and the roll rates are different in the front and rear portions. As a result, the values of the rollover indexes are different in the front and rear. This means that there are two rollover indexes that must be monitored and controlled in order to avoid wheel lift-off. Thus, the resulting control problem is multi-output with $RI_f$ and $RI_r$ as the outputs. To form the control problem, matrix $C_2$ is written as follow:

$$
C_2 = \frac{2}{m\,g\,T}\begin{bmatrix} 0,\ 0,\ -(K_f + K_b),\ -(l_b + l_f),\ K_b,\ l_b,\ 0,\ 0 \\ 0,\ 0,\ K_b,\ l_b,\ -(K_b + K_r),\ -(l_b + l_r),\ 0,\ 0 \end{bmatrix} \tag{4.52}
$$

Following the procedure described in Section 4.2.1, the gains of CN2 are found as:

$$
\mathbf{k}_2 = 10 \times [34.3,\ 383.2,\ -68,\ -15.2,\ -43.9,\ -18.9,\ -52.7,\ -112.8,\ 2236.1] \tag{4.53}
$$

Using the fuzzy rules of (4.44), the controlling yaw moment is calculated by (4.45). Writing the fuzzy system in the unforced form of (4.46), the Theorem in Section 2.4 can be implemented to guarantee Lyapunov quadratic stability by solving the associated LMI. The matrix $P$ is found as follow:

$$P = 10^4 \times \begin{bmatrix} 0.55 & -0.01 & 0.01 & 0.02 & -0.01 & 0.02 & -0.06 & -0.11 & 0.30 \\ -0.01 & 0.03 & -0.01 & 0.00 & 0.00 & 0.00 & 0.00 & 0.00 & 0.01 \\ 0.01 & 0.00 & 0.92 & 0.02 & -0.43 & -0.01 & -0.05 & -0.20 & -0.04 \\ 0.02 & 0.00 & 0.02 & 0.02 & -0.02 & -0.01 & -0.10 & 0.07 & 0.01 \\ -0.01 & 0.00 & -0.42 & -0.02 & 0.59 & 0.03 & 0.05 & -0.09 & -0.01 \\ 0.02 & 0.00 & 0.00 & -0.01 & 0.03 & 0.02 & 0.07 & -0.12 & 0.01 \\ -0.07 & 0.00 & -0.05 & -0.10 & 0.05 & 0.07 & 0.71 & -0.32 & 0.00 \\ -0.11 & 0.00 & -0.20 & 0.07 & -0.09 & -0.12 & -0.32 & 1.12 & 0.02 \\ 0.30 & 0.01 & -0.04 & 0.01 & -0.01 & 0.01 & 0.00 & 0.02 & 1.94 \end{bmatrix} \tag{4.54}$$

## 4.4 Stability Analysis of the Vehicle Systems with the T-S Fuzzy Controllers

As discussed in Section 1.3, results of stability analysis can be used to evaluate and compare the performance of different controllers. The stability analysis of the Theorem in Section 2.4 proves that the fuzzy systems are able to stabilize the vehicles provided that the initial conditions of the states of the system are zero. This restriction on initial conditions is not desirable if one intends to investigate system or structural stability analyses. A useful alternative tool for stability analysis, which does not have such a limitation, is the concept of Lyapunov exponents. The proposed method in Chapter 3 is the basis for the stability analysis of the vehicle systems with the fuzzy controllers in this research.

To perform system stability analysis the initial conditions must be disturbed in a reasonable range of states of the system whereas to conduct a structural stability analysis the disturbance must be in parameters of the system. The first step is to investigate what are the most effective initial conditions or parameters on the stability of the system. Based on our observation in this research, the steering angle, $\delta$, the yaw rate, $r$, and the side slip angle, $\beta$,

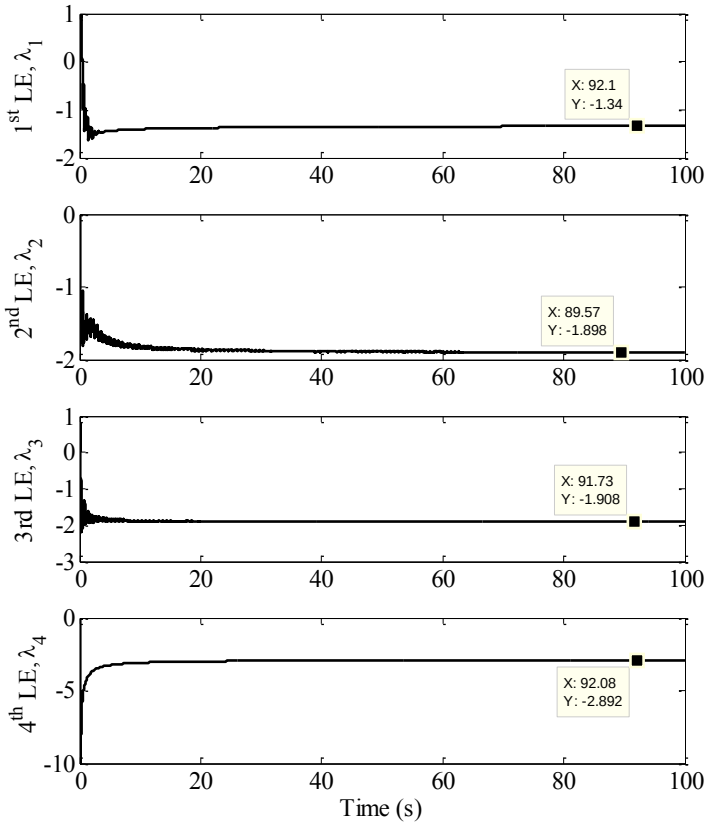


Figure 4.6: Convergence of Lyapunov exponents of the vehicle system with control Strategy#1 with nonzero initial conditions

have the most significant effects on stability. It should be noted that $\delta$ is a parameter of the system while $r$ is one of the states. Although it is not conventional to combine the results of system and structural stability analyses, in this research the results of such analyses are shown in $\delta - r$ plane. The author believes this is a more informative way to present the results of the stability analysis. It will be shown in Chapter 5 that the other states of the system do not have major effects on stability.

It can be easily seen that the equilibrium of a vehicle system of the form of (4.7) is a fixed point which is dependent of the steering angle, $\delta$. As mentioned in Section 2.1, for a system to have a stable fixed point, Lyapunov exponents must be negative. However, in this research, another measure for evaluating the performance of the control systems is their capability of preventing rollover. Thus, a constraint in finding the stability regions is placed

which is the occurrence of wheel lift-off. We adopt *constrained stability region* as the name of the identified regions because of the extra constraint. Therefore, for a set of initial conditions and parameters to be considered inside the constrained stability regions two conditions must be met: first, Lyapunov exponents of the system must be negative, and second, the rollover index must be maintained within the limits of wheel lift-off, i.e., $|RI| < 1$.

However, performing the stability analysis has a challenge which is calculating Lyapunov exponents. Due to the complexities in the vehicle models finding the analytical form of the Jacobian matrix of the system with the controller included in the closed loop is impractical. Thus, Lyapunov exponents of the vehicle systems with the multi-objective controller are calculated using the new approach described in Section 3.3. For the TRV model, with the steering command, $\delta = 0.12\,rad$, and nonzero initial conditions as $\mathbf{x}_0 = \{-0.1, \quad 0.15, \quad 0, \quad 0\}^T$, the values of Lyapunov exponents are as follow:

$$\boldsymbol{\lambda} = \{-1.34, \quad -1.90, \quad -1.90, \quad -2.89\}^T$$

Lyapunov exponents of the system converge to their steady state values after a long enough time. The time history of the process of calculating Lyapunov exponents for such a system are plotted in Figure 4.6. However, it should be noted that the values of Lyapunov exponents can change if the parameters of the dynamic system vary. For example, by changing the value of the steering angle, $\delta$, the values of Lyapunov exponents of the system can be different.

## 4.5 Summary

The models that are used in this thesis for simulating the lateral and roll dynamics of torsionally rigid and torsionally flexible vehicles are described in this chapter. A discussion about the tire dynamics is also provided which highlights the necessity of: 1) using a proper tire model to represent the important properties of the dynamics of the tire, and 2) using a sophisticated control algorithm to capture those important properties. The structure of the controller is described in detail for both vehicle systems, TRVs and TFVs. Finally, the

method for stability analysis, described in Chapter 3, is used for analyzing the two dynamic systems. The details of applying the method to the vehicle systems is also represented in this chapter.

# Chapter 5

# Results and Discussion

The supporting results for the proposed controllers in the previous chapter are discussed in detail here. For both of the TRV and the TFV, the performance of the associated T-S fuzzy controller is explored by comparing the results to the associated single-objective controller and the associated uncontrolled system. The single-objective controller focuses only on yaw stabilization. As mentioned before, yaw rate following can be in favor of wheel lift-off when it operates in harsh situations. On the other hand, the proposed controller, as a multi-objective controller, satisfies another major safety concern which is rollover prevention. The results of this chapter demonstrate such behaviours of the systems with the single-objective and the multi-objective controllers. For each type of vehicle, three maneuvers are selected to compare the controlled and the uncontrolled systems. In addition, results of stability analysis followed by detailed discussions are presented as well.

| Controller | Objective | operating region |
|---|---|---|
| ST1/CN1 | maneuverability | normal driving |
| ST1/CN2 | rollover prevention | close to wheel lift-off |
| ST2/CN1 | maneuverability | normal driving |
| ST2/CN2 | maneuverability | close to wheel lift-off |

Table 5.1: The objective and operating regions of the controllers of each strategy

## 5.1 Yaw Stabilization and Rollover Prevention of a Torsionally Rigid Vehicle Using the Proposed T-S Fuzzy Control Scheme

In this section, the performance of a torsionally rigid vehicle with and without the proposed controller is discussed in three case studies. These cases demonstrate the ability of the proposed controller to meet both of the objectives when the vehicle drives in a normal driving condition, close to a wheel lift-off situation, and a maneuver with fast changes in dynamics. The controller is compared with the uncontrolled vehicle, as well as the same vehicle equipped with a single-objective controller with focus only on yaw stabilization.

In the figures of this chapter, the three systems are labelled as: *Strategy#1 (ST1)*, representing the proposed controller and depicted by solid lines, *Strategy#2 (ST2)*, representing the single-objective controller and depicted by dotted-dashed lines, and *Uncontrolled system*, depicted by dashed lines. ST1 and ST2 use the same controller (CN1) for normal driving conditions which focuses on maneuverability. However, they use different controllers for wheel lift-off situations. In such conditions, ST1 has a rollover prevention controller (ST1/CN2), while ST2 utilizes a controller for yaw stabilization and control (ST2/CN2). ST2/CN2 is a similar controller to ST2/CN1 designed using the process described in section 4.2.1. The difference is that instead of using $A_1$ and $E_{x,1}$ in (4.36), $A_2$ and $E_{x,2}$ of (4.41) are used which represent the situations close to wheel lift-off. A summary about the strategies and their associated controllers is provided in Table 5.1.

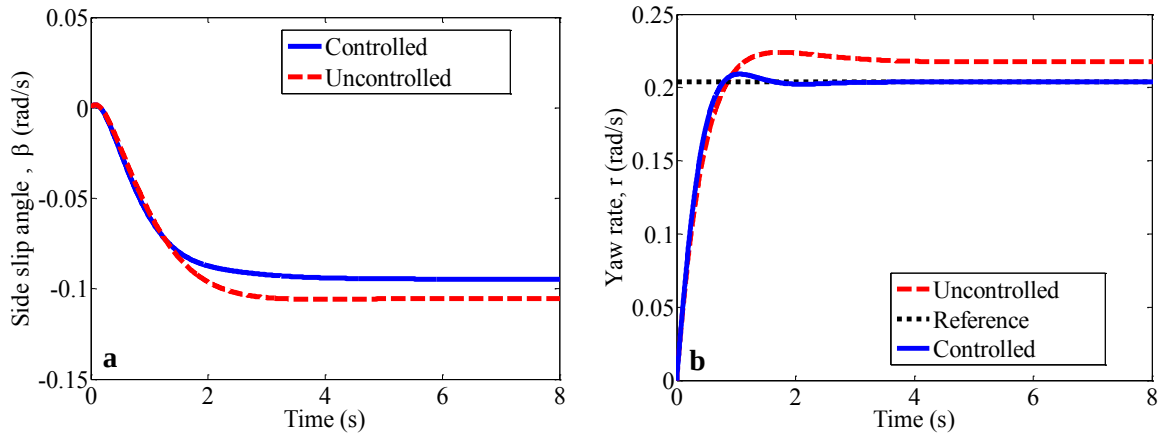


Figure 5.1: a) The side slip angle, $\beta$, and b) the yaw rate, $r$, of the TRV in a moderate maneuver

### 5.1.1 Response to a Moderate Step Steering Input

The first case study is a moderate maneuver where the vehicle operates in the middle of the range of normal driving condition and wheel lift-off. As discussed before, the T-S fuzzy controller is designed so that CN2 does not come into action effectively until wheel lift-off is about to happen. The purpose of this case study is to demonstrate the above behavior. Based on allocation of the fuzzy system, ST1 and ST2 use the same controller (CN1) for such situations, which is focused on maneuverability. Thus, the results of the two fuzzy systems are almost identical. Therefore, only the response of the vehicle with ST1 is compared to that of the uncontrolled vehicle.

In order to show the transient behaviour of CN1, in this case study the steering command, $\delta$, is a step function with the value of $0.35\,rad$. As mentioned before, the rollover index quantifies the situations between moving straight to wheel lift-off by providing a value in the interval $[-1,\ 1]$. For this maneuver, as illustrated in Figure 5.2-a, the value of the RI remains fairly unchanged at $-0.58$ for the controlled vehicle, which shows that the vehicle operates in the middle of the range of straight line motion and wheel lift-off. The objective of the controller in such situations is to maintain the yaw rate at a predefined value based on the driver's command in a fast and smooth manner. The desired value of the yaw rate is specified

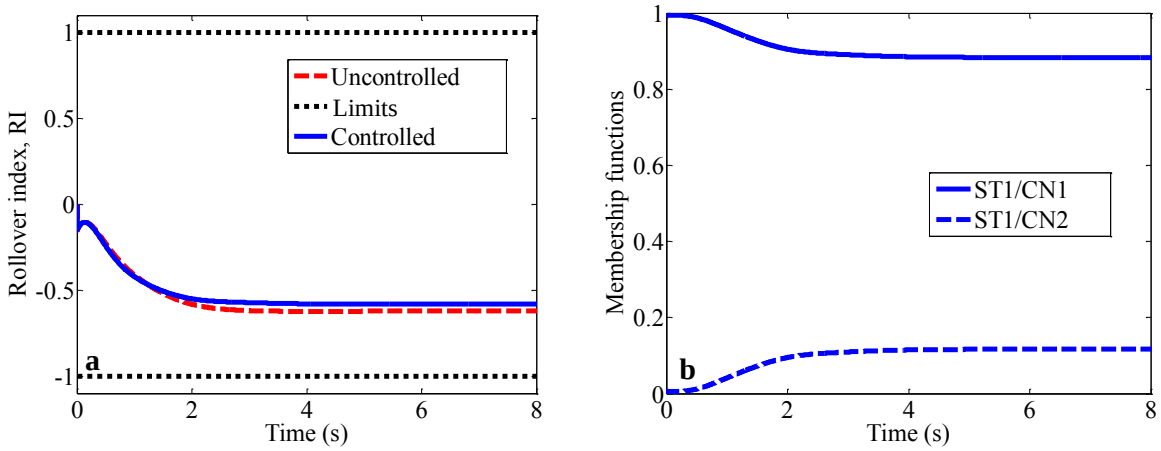


Figure 5.2: a) The membership functions, MFs, of subsystems of the fuzzy system and b) the rollover index, $RI$, of the TRV in a moderate maneuver

using (4.34) which in this maneuver is $0.204\,rad/s$ as the steering command, $\delta$, is constant. As shown in Figure 5.1-b, the controlled vehicle (the solid line) follows the desired value (the dotted line) with a strong transient performance as follow: the rise time, $t_r = 0.785\,s$, the overshoot $MP = 2.65\%$, and the settling time $t_s = 1.26\,s$. This shows that the controller successfully attains the first objective. On the other hand, the yaw rate of the uncontrolled vehicle (the dashed line) settles down at a higher value than the desired value which results in a steady state error. Apart from the steady state error, the other observation from this figure is that the uncontrolled vehicle is slow in response. With respect to the steady state value of its yaw rate response, the uncontrolled vehicle has the following transient performance: the rise time $t_r = 1.34\,s$, the overshoot $MP = 4.69\%$, and the settling time $t_s = 2.54\,s$.

It is worth mentioning that the membership functions (MF) of ST1/CN1 is close to 1 (0.89), while that of ST1/CN2 is close to zero (0.11), as shown in Figure 5.2-b. This means that since the vehicle is performing a moderate maneuver, the fuzzy system gives the priority to CN1. Such an allocation of controllers provides a strong performance for yaw stabilization with minimal interference in the driver's intention. The side slip angle, $\beta$, settles down approximately in $0.1\,rad/s$, as shown in Figure 5.1-a, which shows that tires are in the nonlinear region.

In summary, as the vehicle operates in the middle of the range of the RI, the fuzzy system gives the priority to yaw stabilization. The controlled system has an excellent performance in meeting the objective. Conversely, the uncontrolled vehicle is not fast in response and creates a steady state error.

### 5.1.2 Response to a Harsh Step-like Steering Input

The second case study is a steady state turn where the vehicle is close to the verge of wheel lift-off. The purpose of this case study is to demonstrate the performance of the different strategies in controlling the vehicle. The behaviours of ST1 and ST2 in this example are distinctly different. The performance of the two T-S fuzzy systems together with the uncontrolled vehicle are compared in Figures 5.3 - 5.7. The steering command in this case is a combination of a ramp function which reaches its maximum in $0.5\,s$ and a step function as illustrated in Figure 5.3-a.

With such a steering command, the single-objective controller attains its objective, which is tracking a desired value of yaw rate (see Figure 5.4-a the dotted-dashed curve). However, as depicted in Figure 5.5, with such a strategy, the rollover index of the vehicle (the dotted-dashed curve) exceeds its limits, which means that the tires of one side are lifted off the ground. Conversely, the multi-objective controller has some error in tracking a desirable value of the yaw rate (Figure 5.4-a, the solid line). However, it manages to keep the wheels of the vehicle on the ground. Figure 5.5 shows that unlike ST2, the multi-objective controller manages to maintain the value of the RI within the limits (see the solid line). This shows that the multi-objective controller is able to prioritize the objectives according to the conditions of the vehicle.

It is also worth mentioning that the value of the side slip angle, $\beta$, in Figure 5.3-b is more than $0.2\,rad$, which means that the operating point of the tire is in the saturation region (see Figure 4.4). Since the value of the lateral acceleration is lower in the case of ST1 (see Figure 5.4-b), the value of the roll angle is significantly lower as well (see Figure 5.6-a), where the

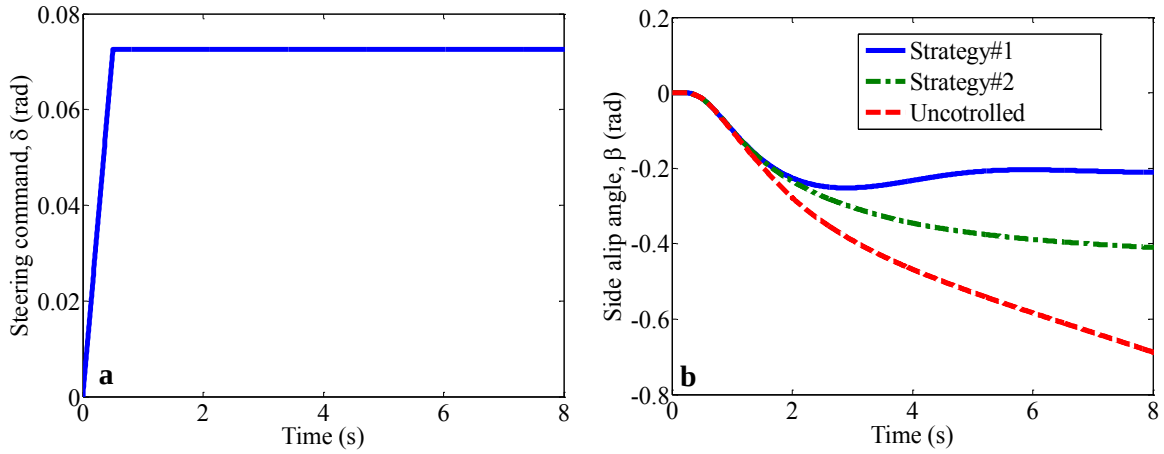


Figure 5.3: a) The steering angle, $\delta$, and b) the side slip angle, $\beta$, of the TRV in a harsh step-like maneuver

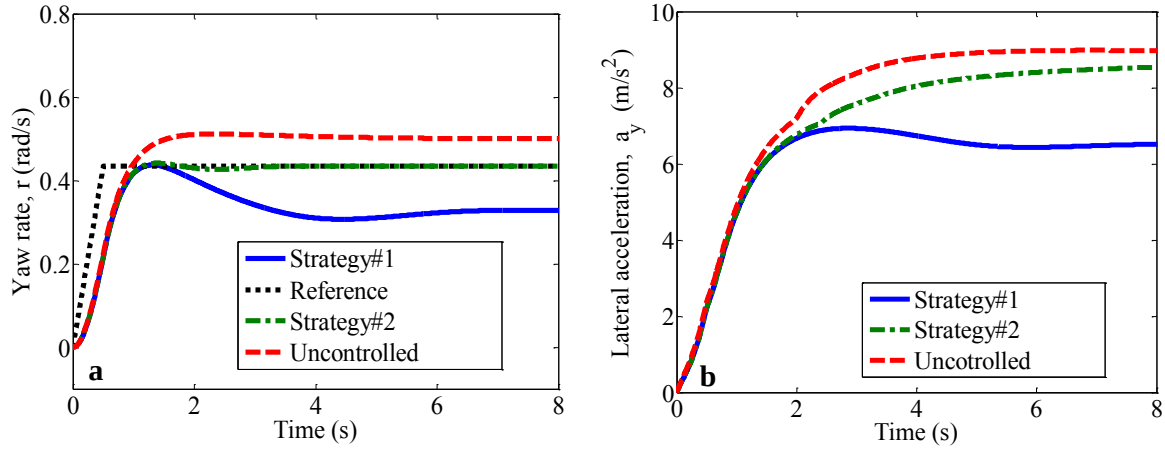


Figure 5.4: a) The yaw rate, $r$, and b) the lateral acceleration, $a_y$, of the TRV in a harsh step-like maneuver

roll angle remains static at around $22\,rad$. The steady state value of the roll angle for ST2 is about $0.31\,rad$. As shown in Figure 5.6-b, the roll rates of the two controlled vehicles have also the same manner up to the point that the T-S fuzzy controller of ST1 changes the priority to rollover prevention. At this time, at about $t = 2\,s$, the roll rate of ST1 oscillates until it settles down at zero. The membership functions (MFs) of the two controllers of ST1 and ST2 are depicted in Figure 5.7-b, where the MF of ST1/CN2 and ST2/CN2 are almost 1 whereas those of ST1/CN1 and ST2/CN1 are almost zero after the transient period. This

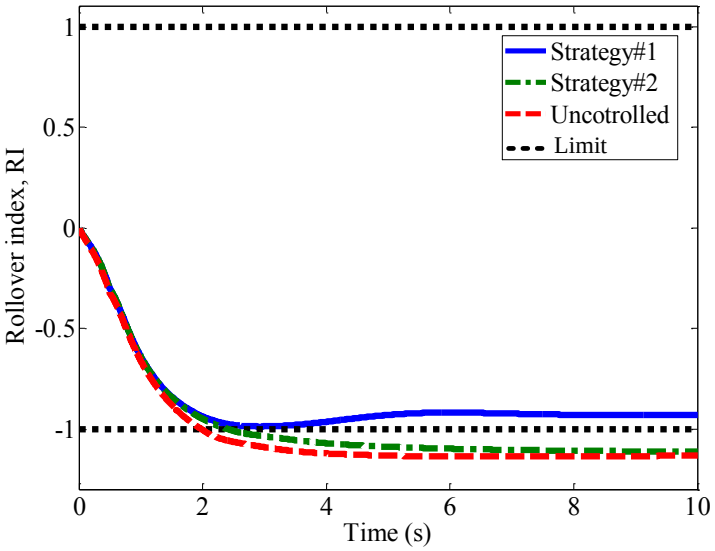


Figure 5.5: The rollover index, $RI$, of the TRV in a harsh step-like maneuver.

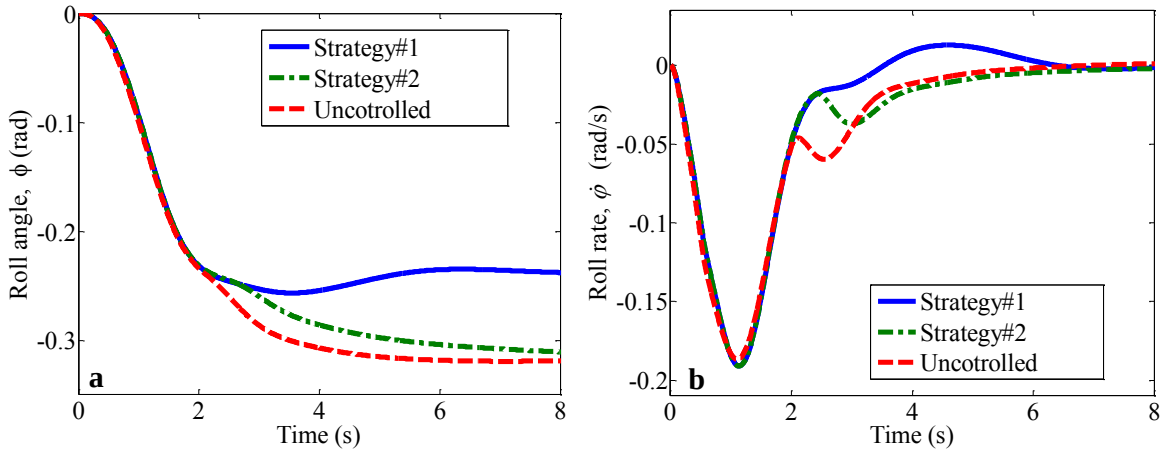


Figure 5.6: a) The roll angle, $\phi$, and b) the roll rate, $\dot{\phi}$, of the TRV in a harsh step-like maneuver

mean that at such a situation, the T-S fuzzy system changes the priority smoothly from CN1 to CN2 as the operating region of the tire is the nonlinear or the saturation region.

It is worth mentioning that at steady state conditions, a number of characteristics of the uncontrolled vehicle and ST2 such as the roll angle, the RI, and the lateral acceleration are close to each other. The reason for this fact is that the tire is in the saturation region (the value of $\beta$ is bigger than $0.4\,rad$). In this region, a change in the value of $\beta$ does not

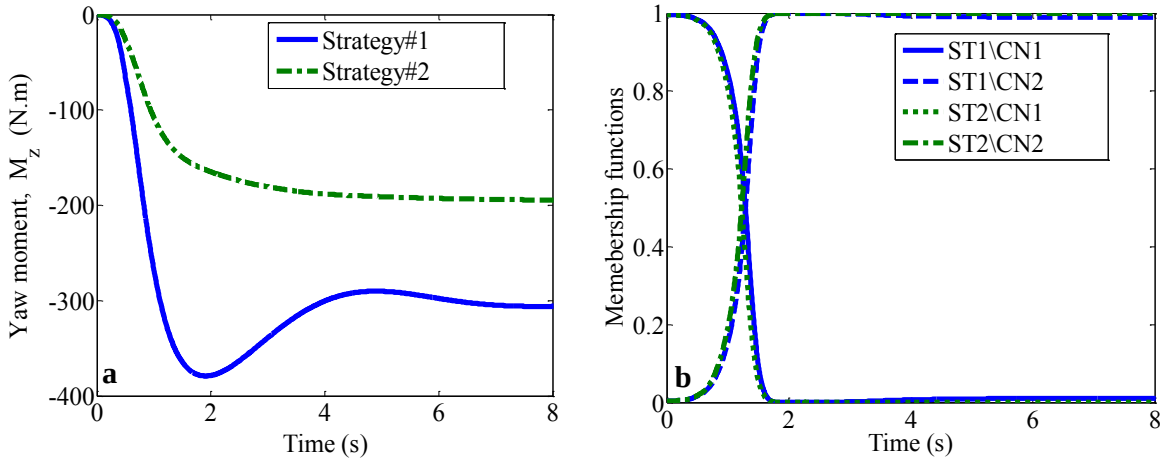


Figure 5.7: a) The membership function, MF, and b) the yaw moment $M_z$ of the TRV in a harsh step-like maneuver

significantly affect the value of lateral forces, which play the main role in the dynamics.

The control efforts of ST1 and ST2 are illustrated in Figure 5.7-a where the yaw moment levels off at $-306\,N.m$ for ST1, and at $-194.5\,N.m$ for ST2. Obviously, since ST1 reduces the yaw rate to a smaller value, the value of its control effort is higher.

This case study demonstrates that it is not possible to attain the two objectives of the control problem when the vehicle is close to the limits of wheel lift-off. The priority must be given to mitigating rollover as controlling the yaw rate can be in support of the wheel lift-off event. The multi-objective controller properly performs this task while the single-objective controller fails to keep the wheels of the vehicle on the ground. The performance of the uncontrolled vehicle is extremely poor.

### 5.1.3 Response to a Fish-hook Steering Input

Fish-hook is a well-known maneuver that is used for examining a vehicle's susceptibility to maneuver-induced on-road rollover [131]. The steering command for a typical fish-hook maneuver is shown in Figure 5.8-a. This case study is designed so that it causes the vehicle to approach the margins of wheel lift-off. The responses of the vehicles to such a maneuver are illustrated in Figures 5.8 - 5.11.

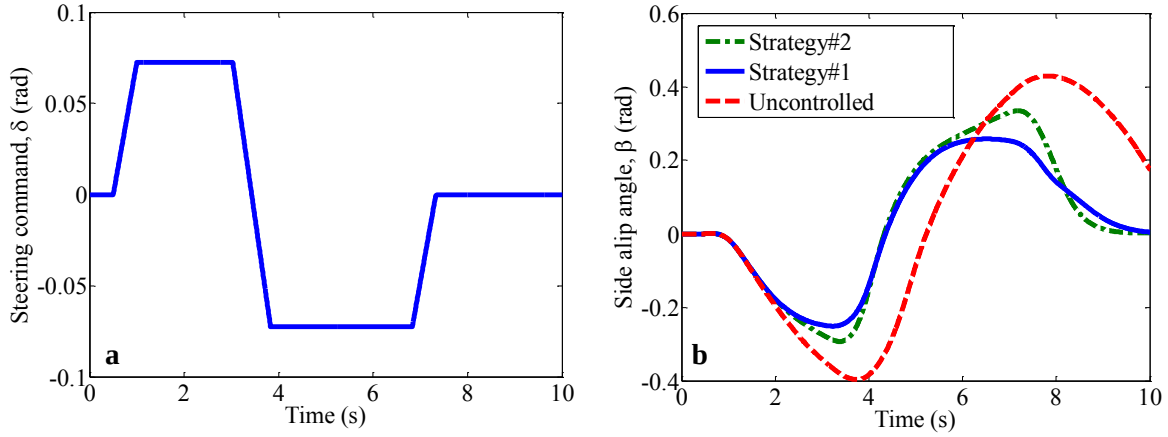


Figure 5.8: a) The steering angle, $\delta$, and b) the side slip angle, $\beta$, of the TRV in a fishhook maneuver

As the peak values of the side slip angles, shown in Figure 5.8-b, are more than $0.2\,rad$, the operating points of the tires are in transition between the linear, the nonlinear, and the saturated regions. Like the previous case study, although ST2 has a strong performance in tracking the desired value of the yaw rate (Figure 5.9-a the dotted-dashed curve), the value of the RI exceeds the limits two times in this maneuver (Figure 5.10 the dotted-dashed curve). On the other hand, despite the fact that ST1 does not follow the desired value of the yaw rate perfectly (Figure 5.9-a the solid line), it maintains the value of the RI within the limits at both of the times that the RI becomes close to the margins (Figure 5.10 the solid line). Figure 5.9-b shows that if the second objective, preventing wheel lift-off from happening is intended, the maximum lateral acceleration must not exceed $7\,m/s^2$ for the TRV of this study.

The poor performance of the uncontrolled vehicle is magnified in this case study. As mentioned before, the uncontrolled vehicle is particularly slow in response. This can be seen in the yaw rate following of the uncontrolled vehicle (Figure 5.9-a the dashed line) which is eminently unsatisfactory. Besides, the roll angle and the roll rate responses show the lag of the uncontrolled vehicle in comparison with the vehicles equipped with controllers (the dashed curves in Figure 5.11). Last but not least, the RI of the uncontrolled vehicle stays outside of the boundary for a long time in both of the wheel lift off event (Figure 5.10 the

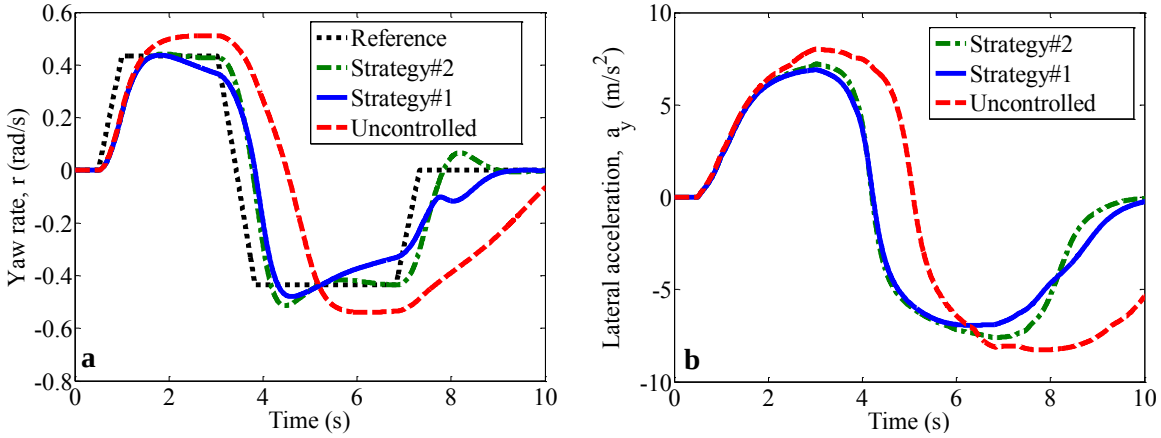


Figure 5.9: a) The yaw rate, $r$, and b) the lateral acceleration, $a_y$, of the TRV in a fishhook maneuver

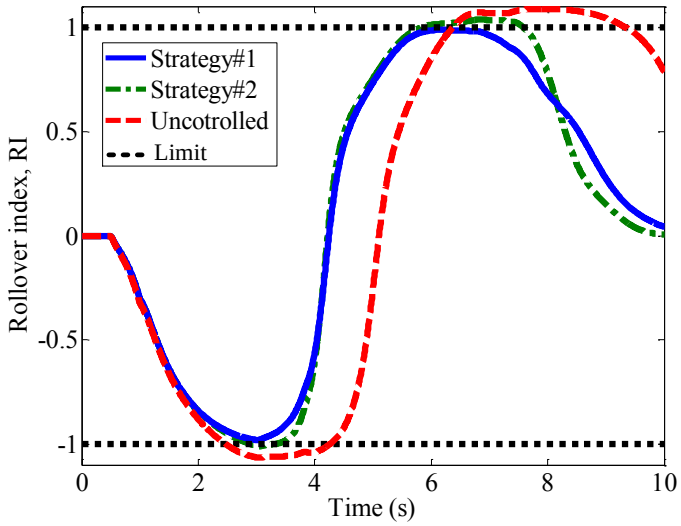


Figure 5.10: The rollover index of the TRV in a fishhook maneuver

dashed line).

Although both of the controlled systems have acceptable transient responses, wheel lift-off occurs with ST2 two times in this maneuver, while ST1 has an excellent performance in keeping the wheels of the vehicle on the ground. The poor performance of the uncontrolled vehicle shows the necessity and significance of using a controller that can address both of the issues of a fast and stable yaw rate response as well as resistance to rollover.

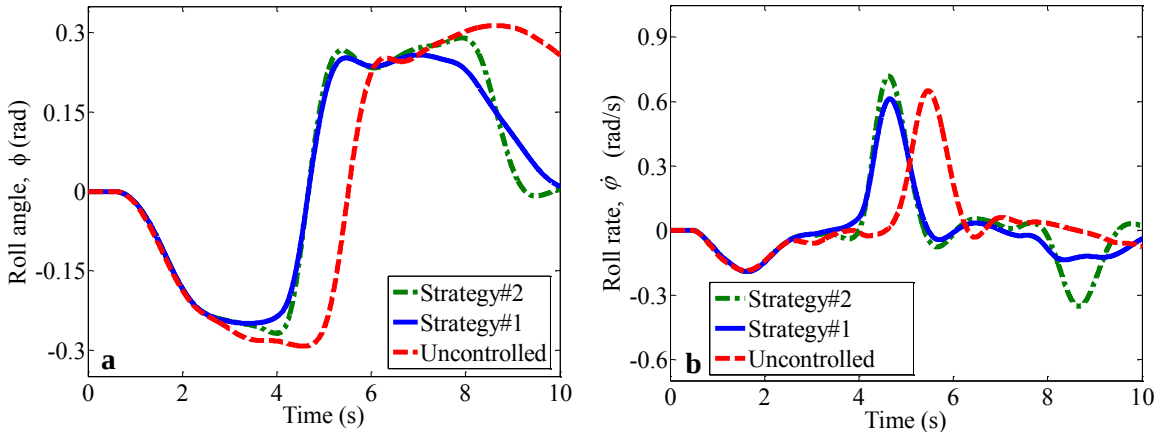


Figure 5.11: a) The roll angle, $\phi$, and b) the roll rate, $\dot{\phi}$, of the TRV in a fishhook maneuver

### 5.1.4 Stability Analysis Using the Proposed Method of Identifying BoAs

In order to compare the performance of the controllers in terms of stability, both system and structural stability analyses are performed in this study. The stability analyses are performed using the proposed methods for identifying boundaries of BoAs of dynamical systems in Chapter 3. As mentioned in Section 4.4, to demonstrate the results of stability analysis, the stability regions are shown in $\delta - r$ plane for different values of $\beta$ as illustrated in Figure 5.12 - 5.13. In finding the stability regions a constraint on the value of the rollover index is considered which is $|RI| < 1$. This is to ensure that the wheels of the vehicle do not lift off the ground. For the points inside these regions it is guaranteed that the system is stable, and wheel lift-off does not happen.

Figure 5.12 depicts the constrained stability regions for negative values of $\beta$, and Figure 5.13 shows those for positive values of $\beta$. In both figures, the stability regions with $\beta = 0$ are shown by thicker lines as the basis for comparison. The constrained stability region of the system with $\beta = 0$ and ST1 is considerably larger than that of the system with ST2. However, as the absolute value of the side slip angle, $\beta$, increases, the constrained stability regions of ST1 start to shrink from one side, although they are still larger than those of

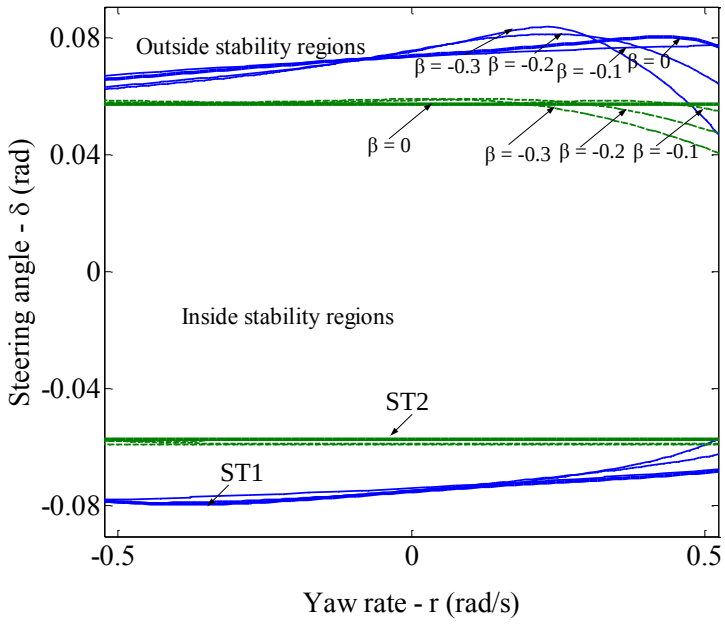


Figure 5.12: The constrained stability regions for the vehicle system with ST1 and ST2 for negative values of the side slip angle, $\beta\,(rad)$

ST2. Conversely, ST2 is less sensitive to the changes in initial conditions as the associated constrained stability regions do not change significantly in size.

Results of the stability analysis indicate that the proposed multi-objective controller provides a better performance in terms of stability and preventing wheel lift-off from happening. Although ST1 is more sensitive to the perturbations in the side slip angle, it provides larger constrained stability regions, which means that the vehicle is more robust to rollover propensity with the proposed controller. It is worth mentioning that based on our observations both ST1 and ST2 are robust to changes in the values of the roll angle, $\phi$, and the roll rate, $\dot{\phi}$. For brevity, we do not include the results that supports this fact. A detailed discussion about the negligible effect of changes in the roll angles will be presented in section 5.2.5 for TFVs.

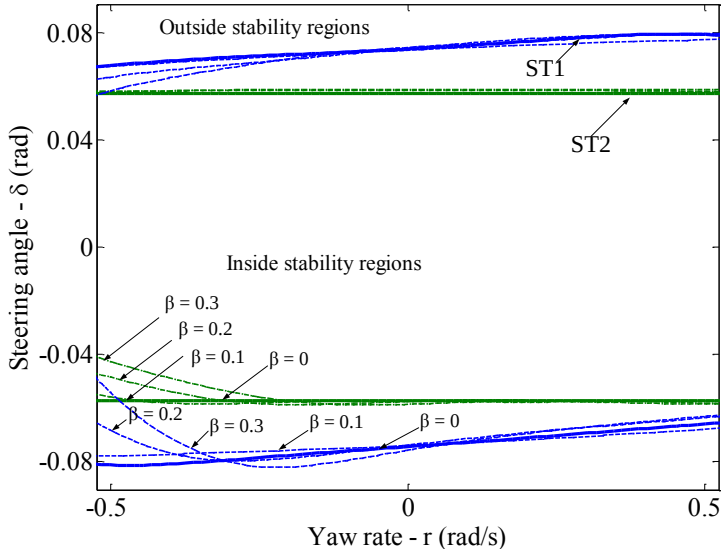


Figure 5.13: The constrained stability regions for the vehicle system with ST1 and ST2 for positive values of the side slip angle, $\beta\,(rad)$

## 5.2 Yaw Stabilization and Rollover Prevention of a Torsionally Flexible Vehicle Using the Proposed T-S Fuzzy Control Scheme

The proposed control scheme is applied to the model of a torsionally flexible vehicle, presented in Section 4.1.2, for the purpose of yaw stabilization and rollover avoidance. The response of the system with the designed controller for the TFV is also illustrated using three steering command functions: a moderate step steer input, a step-like input at the verge of wheel lift-off, and a double lane change input. The abbreviations of Table 5.1 are used in these cases as well. The step-like and double lane change maneuvers are similar to the maneuvers that are used in [2]. The results are compared with the results of the system with the single-objective controller as well as the uncontrolled vehicle.

### 5.2.1 Validation of the Model

The model that is developed in this thesis is based on the model used in [2]. However, there are some differences in the two models, and the main difference is in the tire model. In this research we have used a comprehensive Pacejka nonlinear tire model while the model used in [2] is linear with respect to the side slip angle. However, the results of the two models are comparable in moderate maneuvers. Table 5.2 summarizes the steady sate responses of the two models to a step steering command with the value of $\delta = 0.056\,rad$. The results are in a good agreement.

| Parameter/state | Description | Model in [2] | The developed model |
|---|---|---|---|
| $\delta$ | The steering angle | $0.056\,rad$ | $0.056\,rad$ |
| $a_y$ | The lateral acceleration | $3.8\,m/s^2$ | $3.9\,m/s^2$ |
| $\phi_f$ | The roll angle in the front | $-0.056\,rad$ | $-0.064\,rad$ |
| $\phi_r$ | The roll angle in the rear | $-0.082\,rad$ | $-0.095\,rad$ |

Table 5.2: Comparison of the results of the developed model and the results of the model in [2]

### 5.2.2 Response to a Moderate Step Steering Input

The purpose of this step steering command is to demonstrate the performance of the controller in normal driving conditions. As mentioned before, in such situations the objective that is given the priority by the T-S fuzzy control scheme is maneuverability. This can be noticed by looking at Figure 5.15-a where the MF of ST1/CN1 is 0.92 in the steady state situation while the MF of ST1/CN2 is 0.08. Similar to the case of the TRV, since the T-S fuzzy controller uses the same controller for normal driving conditions, only the results of ST1 are illustrated.

The steering command is a step function at the value of $0.05\,rad$. The side slip angle of the vehicle settles down at $0.061\,rad$ which means that the tires are in the nonlinear region as shown in Figure 5.14-a. The responses of the controlled vehicle and the uncontrolled vehicle in terms of yaw rate following are compared in Figure 5.14-b. The desired value for

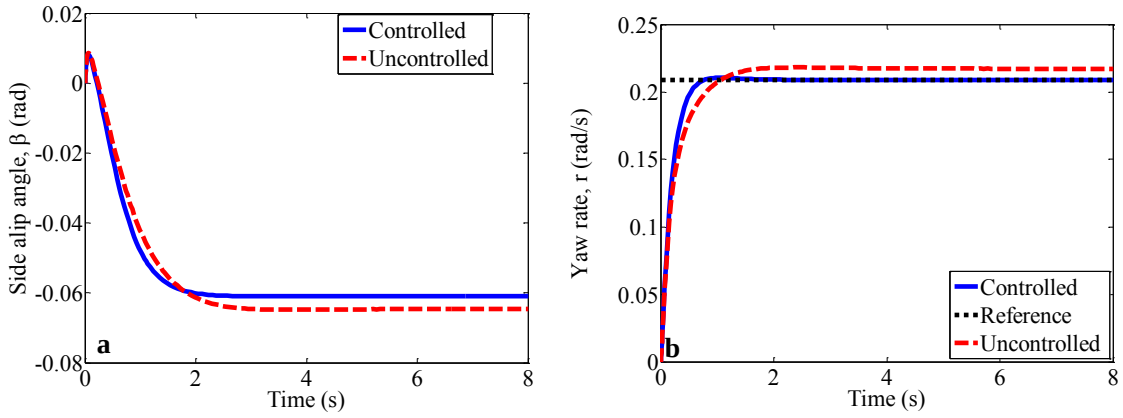


Figure 5.14: a) The side slip angle, $\beta$, and b) the yaw rate, $r$, of the TFV in a moderate maneuver

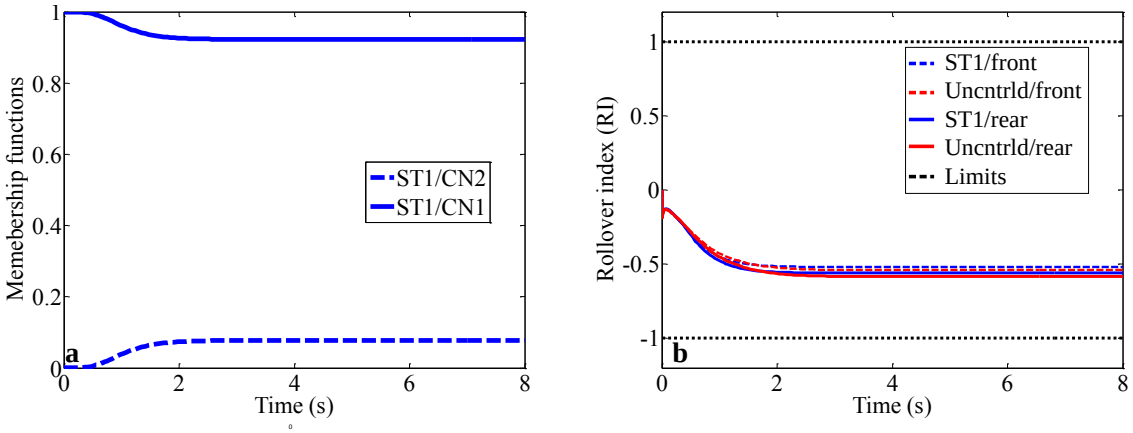


Figure 5.15: a) The membership functions, MFs, and b) the rollover index, $RI$, of the TFV in a moderate maneuver

the yaw rate is $0.21 rad/s$ in this maneuver. The uncontrolled vehicle is considerably slow in response and has more than $4\,\%$ steady state error with respect to the desired value for the yaw rate. The rise time for the uncontrolled vehicle is $t_r = 1.77\,s$, comparing with its steady state value, which is not satisfactory. On the other hand, the controlled vehicle shows an excellent performance in tracking the desired value, with the rise time of $t_r = 0.78\,s$, and the overshoot of $MP = 0.76\,\%$.

The rollover indexes of the front and rear axles are shown in Figure 5.15-b. The steady state values of the RIs for the controlled vehicle are 0.52 and 0.56 for the front and rear

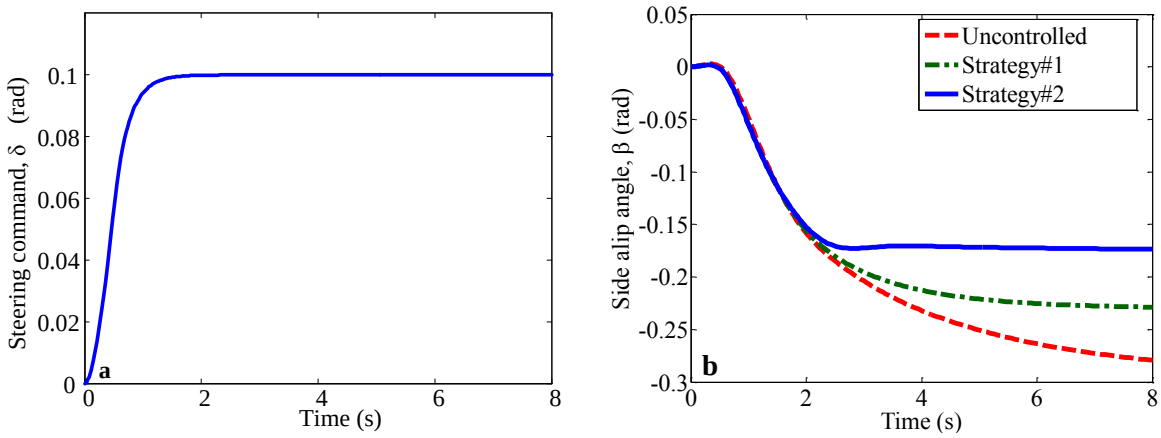


Figure 5.16: a) The steering angle, $\delta$, and b) the side slip angle, $\beta$, of the TFV in a harsh maneuver

axles, respectively. This also indicates that the vehicle operates in the middle range between a straight line motion and a wheel lift off situation.

### 5.2.3 Response to a Harsh Step-like Steering Input

The purpose of using a harsh step-like command is to demonstrate the behavior of the controlled and uncontrolled systems in situations near wheel lift off. To make the maneuver more realistic the steering angle is ramped from zero to the maximum value, $0.1\,rad$, over a period of $0.5\,s$. To represent the limited bandwidth of the driver, as Sampson has suggested, the step-like function is filtered at the cut-off frequency of $\omega_c = 4\,rad/s$, using the following low pass filter [2]:

$$F(s) = \frac{\omega_c}{s + \omega_c} \tag{5.1}$$

This results in a function illustrated in Figure 5.16-a. As shown in Figure 5.16-b, the values of all of the side slip angles are greater than $0.15\,rad$, which means that the tires are in the nonlinear or the saturated regions. In such situations, the model of the normal driving conditions does not represent the behavior of the vehicle. Therefore, based on the allocation of the T-S fuzzy scheme, rollover prevention takes the priority over maneuverability. Such

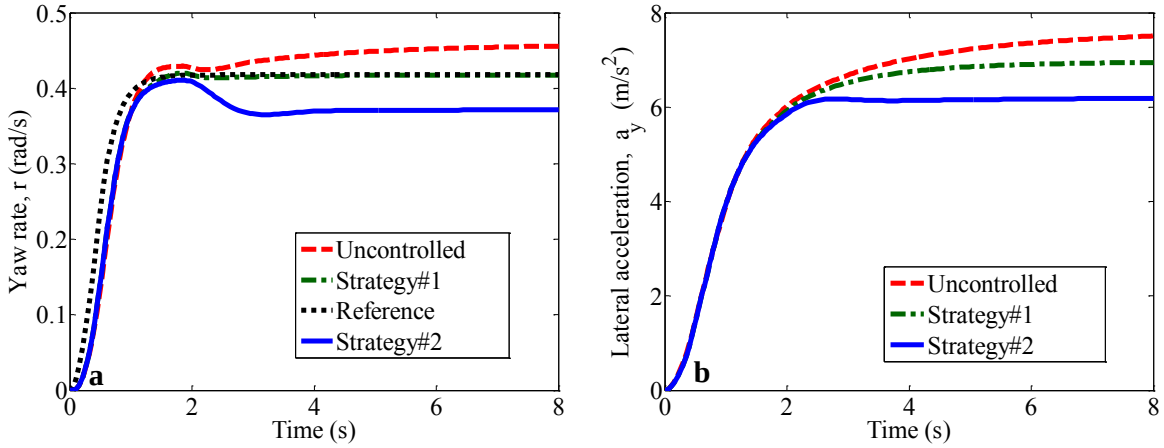


Figure 5.17: a) The yaw rate, $r$, and b) the lateral acceleration, $a_y$, of the TFV in a harsh maneuver

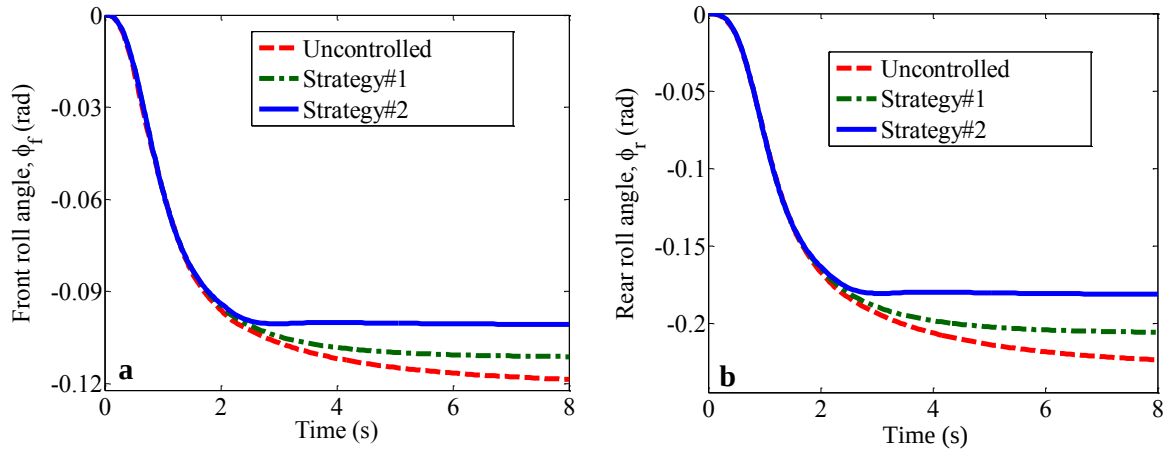


Figure 5.18: a) The front roll angle, $\phi_f$, and b) the rear roll angle, $\phi_r$, of the TFV in a harsh maneuver

an allocation of the controllers is illustrated in Figure 5.21-b where after the transient period in the beginning of the maneuver, the MF of CN2 is almost 1 while that of CN1 is almost zero.

The performance of the vehicles in terms of yaw rate following is illustrated in Figure 5.17-a. Based on the steering command, the steady state value for the desired yaw rate is $0.42\,rad/s$. The vehicle with ST1 tracks the desired value with an excellent performance. The vehicle with ST2 have the same performance in the transient time (until about $t = 1.3\,s$)

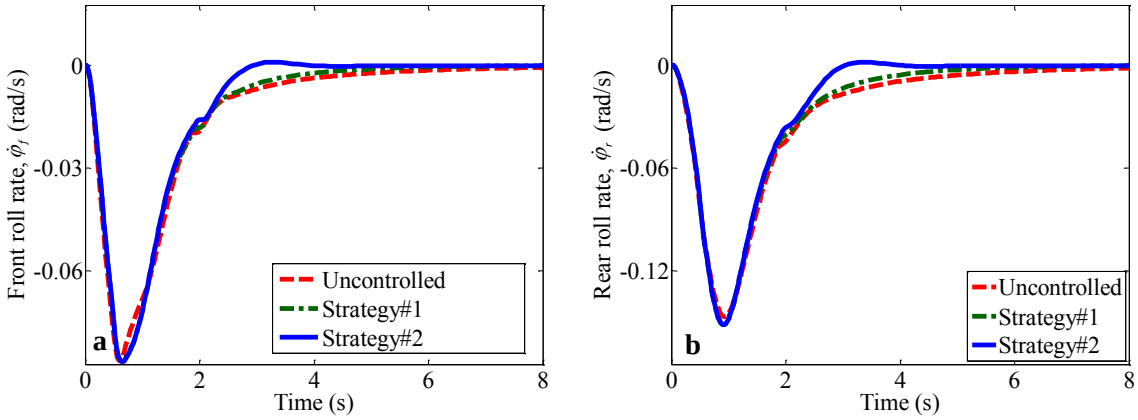


Figure 5.19: a) The roll rate in the front, $\dot{\phi}_f$ and b) the roll rate in the rear, $\dot{\phi}_r$, of the TFV in a harsh maneuver

as ST1 and ST2 use the same controller during this period. However, the vehicle with ST2 does not follow the desired value after that time, and the controller decreases the yaw rate to a steady state value of $0.37\,rad/s$. This is because the value of the rollover indexes are close to the limits and the controller with ST1 prevents the vehicle to reach the margins. The maximum absolute value of the rollover indexes for the vehicle with ST2 is 0.96, while those of the other vehicles pass the limits, as illustrated in Figure 5.22. As a result of the reduction in the value of the yaw rate, the maximum value of the lateral acceleration for the vehicle with ST1 is $6.18\,m/s^2$,, as shown in Figure 5.17-b with the solid line, which is smaller than those of ST2 and the uncontrolled vehicle.

The steady state values of the roll angles are significantly different in the front and rear parts of the vehicle with $\phi_f = -0.10\,rad$ and $\phi_r = -0.18\,rad$ for the vehicle with ST1, as shown in Figure 5.18. This highlights the necessity of using a model that includes the torsional compliance in the frame. The front and rear roll rates are shown in Figure 5.19 where the curves in the solid lines, associated with the vehicle with ST1, deviate from the other two curves due to the change in the objective from yaw rate following to rollover resistance. The values of the chassis roll angles are small in comparison with the sprung mass roll angles, with $\phi_{u,f} = -0.04\,rad$ and $\phi_{u,r} = -0.04\,rad$, as shown in Figure 5.20. Similarly, the values of the yaw moments, $M_z$, also depicted in Figure 5.21-a, have the same

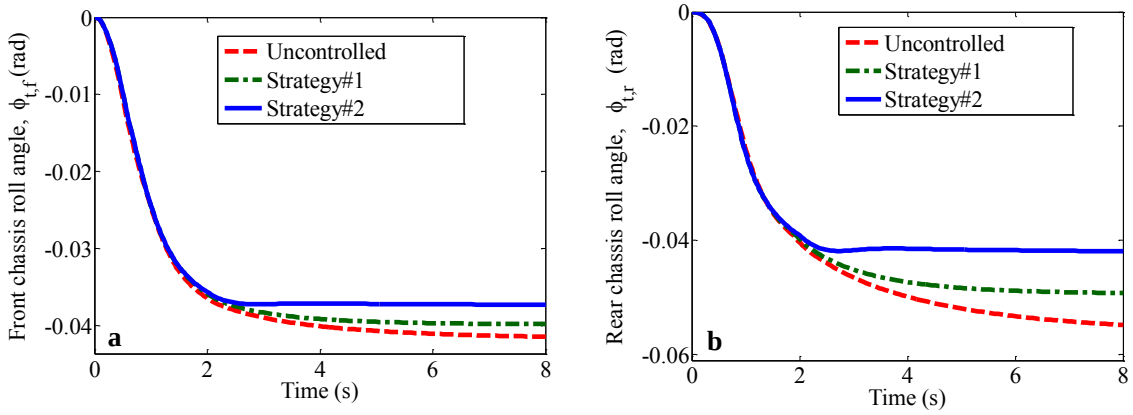


Figure 5.20: a) Th front chassis roll angle, $\phi_{u,f}$, and b) the rear chassis roll angle, $\phi_{u,r}$, of the TFV in a harsh maneuver

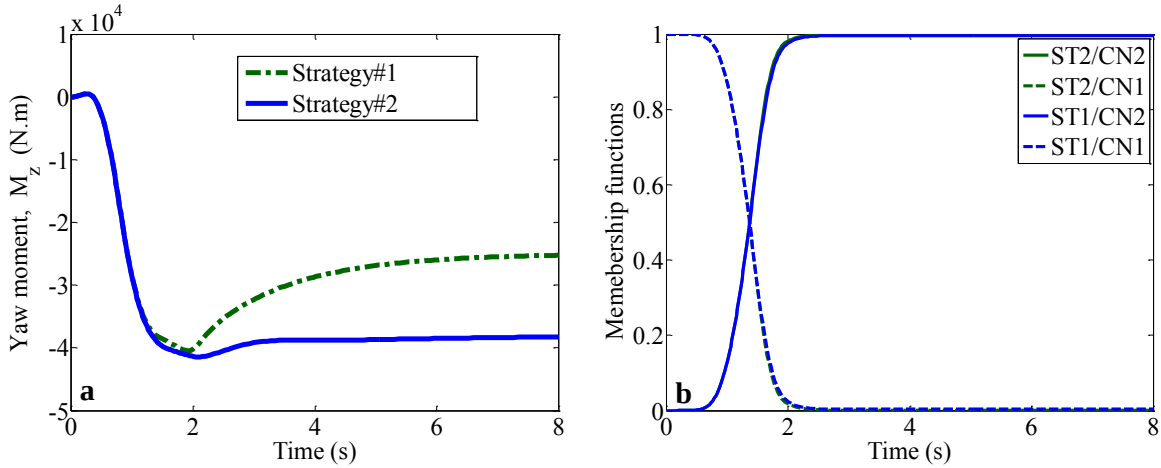


Figure 5.21: a) The membership functions, MFs, and b) the yaw moments, $M_z$, of the TFV in a harsh maneuver

trend until ST1 starts using CN2. After this period, the yaw moment for ST2 decreases because the yaw rate is approaching the desired value. However, since ST1 decreases the yaw rate to a smaller value to maintain the RI within the limits, it requires having a larger yaw moment. The steady state value of the yaw moment for ST1 is $-3.8 \times 10^4\, N.m$. It is worth mentioning that since the vehicle without control tends to have a higher value of the yaw rate (see the dashed line in Figure 5.17-a), the value of $M_z$ for ST1 and ST2 does not approach zero.

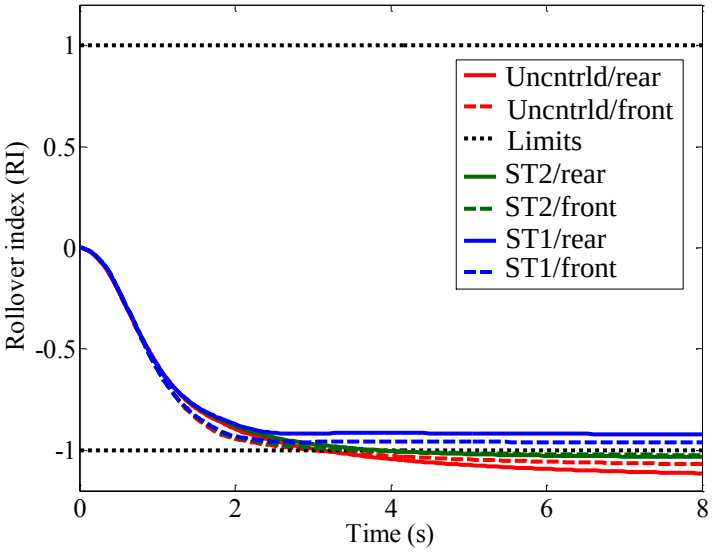


Figure 5.22: The rollover index, $RI$ of the TFV in a harsh maneuver

### 5.2.4 Response to a Double Lane Change Steering Input

One of the popular tests of heavy vehicles to evaluate their transient performance in emergency cases like an obstacle avoidance is the double lane change maneuver [2]. In this section, using a double lane change steering command the performances of the two control strategies and the uncontrolled vehicle are compared. The double lane change maneuver is chosen to have a peak value of $0.14\,rad$ to ensure that the vehicle operates at the limits of wheel lift-off. The steering command consists of two full sine waves, back-to-back, which are filtered at the cut-off frequency of $\omega_c = 4\,rad/s$, using (5.1). The resulting steering command is shown in Figure 5.23-a, which is similar to what has been used in [2] for testing the performance of the controllers.

Figure 5.23-b shows the changes in the values of the side slip angle for the three vehicle systems. The absolute peak values in this figure are, $|\beta| \approx 0.2\,rad/s$ for ST1, and about $0.3\,rad/s$ for ST2 and the uncontrolled vehicle. This means that the tires of all three vehicles are either in the nonlinear or the saturated regions at time instances that the side slip angle is maximum/minimum. Therefore, the performances of ST1 and ST2 are distinguishable.

Yaw rate following performance of the vehicles are compared in Figure 5.24-a. Similarly,

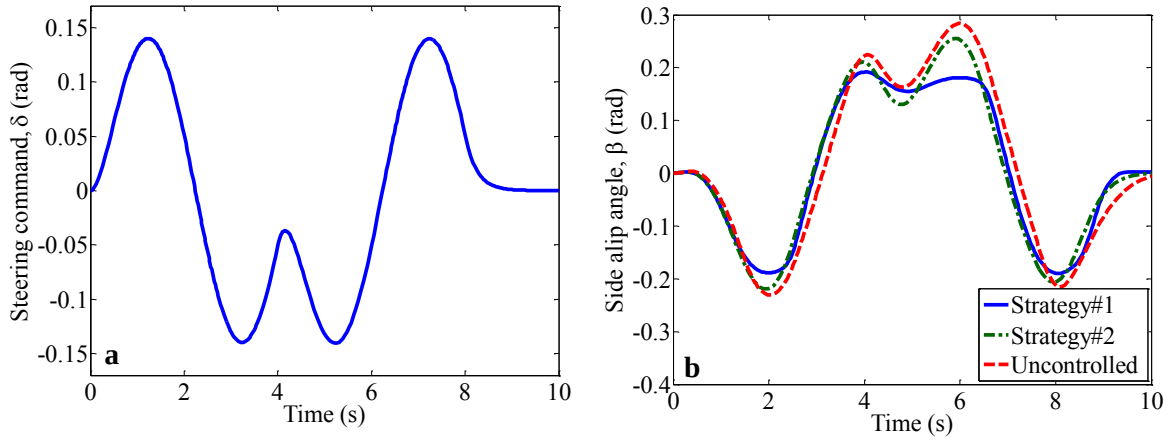


Figure 5.23: a) The steering angle, $\delta$, and b) the side slip angle, $\beta$, of the TFV in a double lane change maneuver

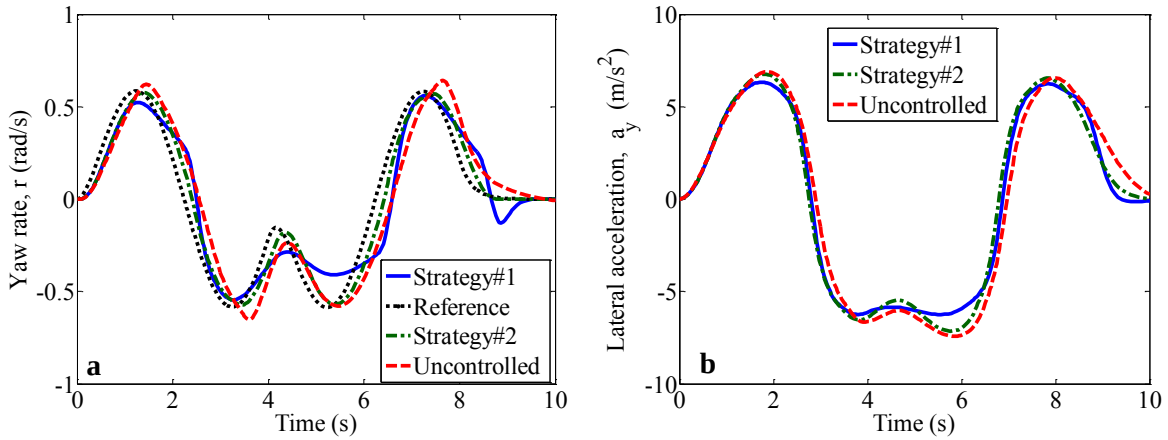


Figure 5.24: a) The yaw rate, $r$, and b) the lateral acceleration, $a_y$, of the TFV in a double lane change maneuver

the vehicle with ST2 has the best behavior in terms of following the desired value for the yaw rate. The vehicle with ST1 has the same performance until about $t = 1.5\,s$, but the two curves deviate from each other when the desired yaw rate becomes closer to the peak value. Clearly, the reason behind such a behavior is that the rollover indexes approach their limits at those instances. At such situations, the fuzzy system with ST1 gives the priority to rollover avoidance and keeps the values of the RIs within the limits, as illustrated in Figure 5.28. Conversely, ST2 and the uncontrolled vehicle fail to maintain the RIs within the bounds. The peak value of the lateral acceleration for ST2 is $6.325\,m/s^2$ which is illustrated in Figure

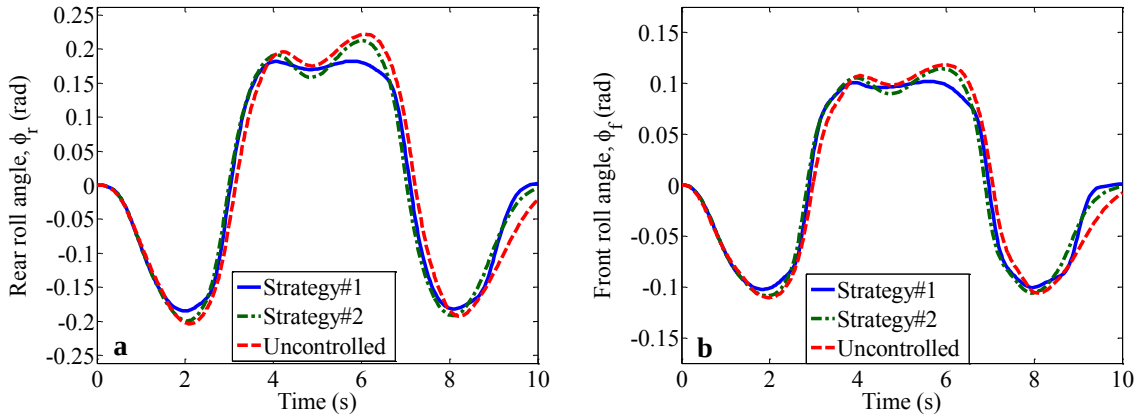


Figure 5.25: a) The front roll angle, $\phi_f$, and b) the rear roll angle, $\phi_r$, of the TFV in a double lane change maneuver

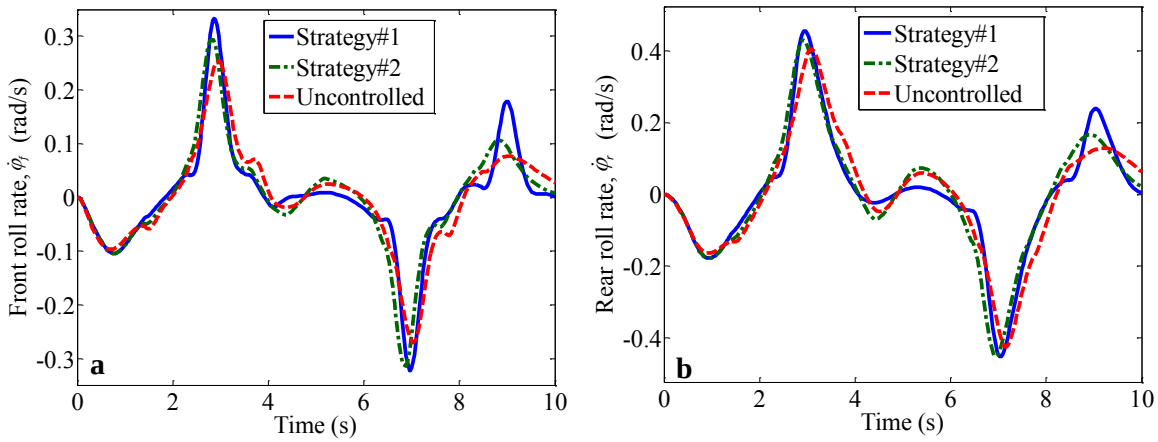


Figure 5.26: a) The roll rate in the front, $\dot{\phi}_f$, and b) the roll rate in the rear, $\dot{\phi}_r$, of the TFV in a double lane change maneuver

5.24-b in the solid line. This shows that in order to keep the value of the RIs within the limits the value of the lateral acceleration must not be greater than $6.5\,m/s^2$ for the TFV of this study.

Figures 5.25 and 5.27 represent the values of the roll angles. The difference between the values of the front and rear parts of the vehicle is noticeable. For example, the peak value of the front roll angle is $|\phi_f|_{max} = 0.10\,rad$, while that of the rear roll angle is $|\phi_r|_{max} = 0.18\,rad$. That shows the significance of including flexibility of the frame in the model of the system's dynamics.

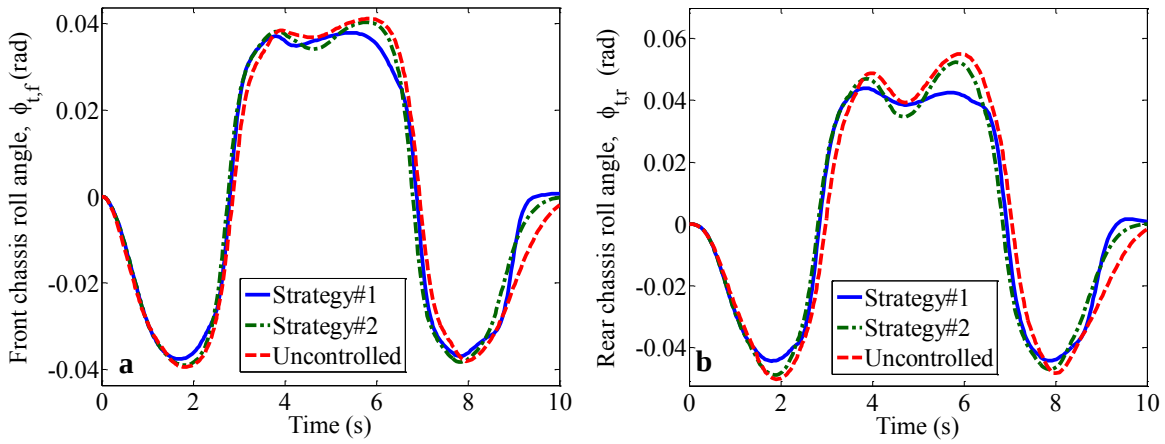


Figure 5.27: a) The front chassis roll angle, $\phi_{u,f}$, and b) the rear chassis roll angle, $\phi_{u,r}$, of the TFV in a double lane change maneuver

The values of the front and rear roll rate are illustrated in Figure 5.26. The peak values of the roll rates are slightly larger for ST1 than for ST2. The reason is that when ST1/CN2 is given the priority, it reduces the values of the RIs, and accordingly the lateral acceleration and the roll angles. Due to the transition in the control objective, the changes in the values of the roll angles for the multi-objective controller are faster than those for the single-objective controller (see Figures 5.25). Therefore, the roll rates have slightly higher values for ST1. Figure 5.26 also highlights the slow dynamics of the uncontrolled vehicle in comparison with the controlled vehicles. This can be observed in the peak values of the roll rates where the uncontrolled vehicle has a shift at the times that the peaks happen.

### 5.2.5 Stability Analysis

In this section, a comprehensive system and structural stability analysis is provided for vehicles with fuzzy controller ST1 and ST2. The results of such analyses can indicate the robustness of the controllers to changes in the parameters or states. Such changes are most likely to happen for vehicle systems in real life. In addition, the size of the stability regions can be indicative of the advantage of a control system over another control system. Similar to the case of the TRV, stability regions are found in the plane of the yaw rate and the

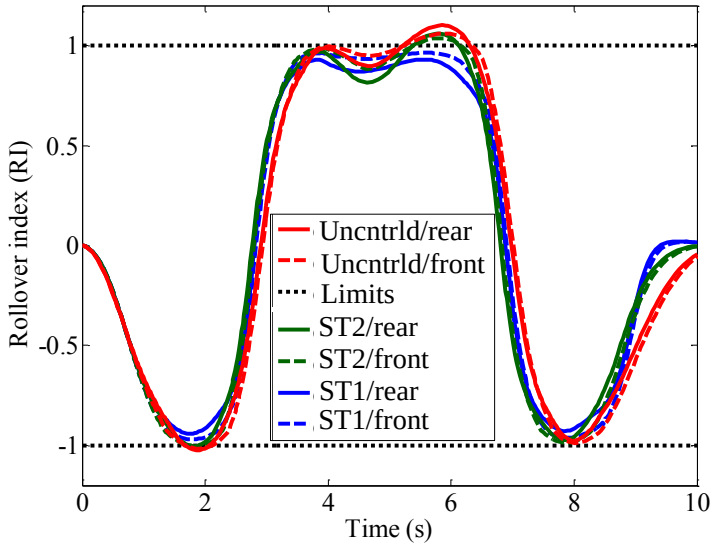


Figure 5.28: The rollover index of the TFV in a double lane change maneuver

steering command, $r - \delta$. The perturbations on initial conditions and parameters of the system change the size of such stability regions.

### Effect of Changes in Initial Conditions on the Stability Region of the Controlled Systems

The effect of changes in initial conditions on the size of stability regions are explored in this section. Since the side slip angle plays an important role in vehicle lateral dynamics, the perturbations in its value can affect stability of the system. Figures 5.29 and 5.30 show the effect of changes in the initial value of the side slip angle on the stability region. Similar to the case of the TRV, the effect of perturbations in the side slip angle, $\beta$, is maximum in the areas that it has an opposite sign to the sign of the yaw rate, $r$, and the steering angle, $\delta$. For instance, as illustrated in Figure 5.29, when $\delta$ and $r$ are both negative, with positive initial values for $\beta$, the stability regions shrink. Likewise, when $r$ and $\delta$ are positive, and $\beta$ is negative, the stability regions become smaller. Figure 5.31 depicts the two situations. The case **a/b** in Figure 5.31 represents a situation when the vehicle is turning right/left, as $r$ is positive/negative, and it is skidding towards the outside of the turn, as $\beta$ is negative/positive.

These cases symbolize situations with excessive lateral accelerations. For the other situations, the effect of the initial values of $\beta$ on the stability regions is minor. Although ST1 is more sensitive to the changes in initial values of the side slip angle, it shows more robustness as the associated stability regions are significantly larger than those associated with ST2.

The effect of changes in initial values of the roll angles and the roll rates on stability of the system is insignificant. In this study, the values of the front and rear roll angles were changed in wide ranges and the effect of these changes on the stability of the system were observed. Even for the case that the vehicle is close to the limits of wheel lift-off, there was no change in the stability regions. For instance, Figures 5.32 and 5.33 compare the performance of the fuzzy controller of ST1 in two cases: with $[\beta,\, r]|_{t=0} = [-0.25,\, 0.41]$ and zero initial conditions for the roll angles, and with initial conditions as:

$$[\beta,\, r,\, \phi_f,\, \phi_r,\, \phi_{u,f},\, \phi_{u,r}]|_{t=0} = [-0.25,\, 0.41,\, -0.17,\, -0.17,\, -0.004,\, -0.004]$$

This selection of initial conditions is based on the results of the harsh maneuver in the previous section where the vehicle is on the verge of wheel lift-off. The maximum absolute values of the rollover index with the zero initial values for the roll angles is 0.97 as depicted with the solid line in Figure 5.32. With the above nonzero initial conditions for the roll angles the maximum value reaches only 0.98. Besides, the roll angles have the same steady state values in both of the cases as illustrated in the figures.

**Effect of Changes in Mass Properties on the Stability Region of the Controlled Systems**

Mass properties of vehicles are prone to change in different loading conditions. Such changes can be dramatic for heavy vehicles as their weight can vary significantly with the loads that they carry. Therefore, it is imperative to investigate the effect of changes in mass properties on the performance of controllers. The effects of increasing the sprung mass of the vehicle as well as changes in the location of center of gravity on the stability regions are explored here.

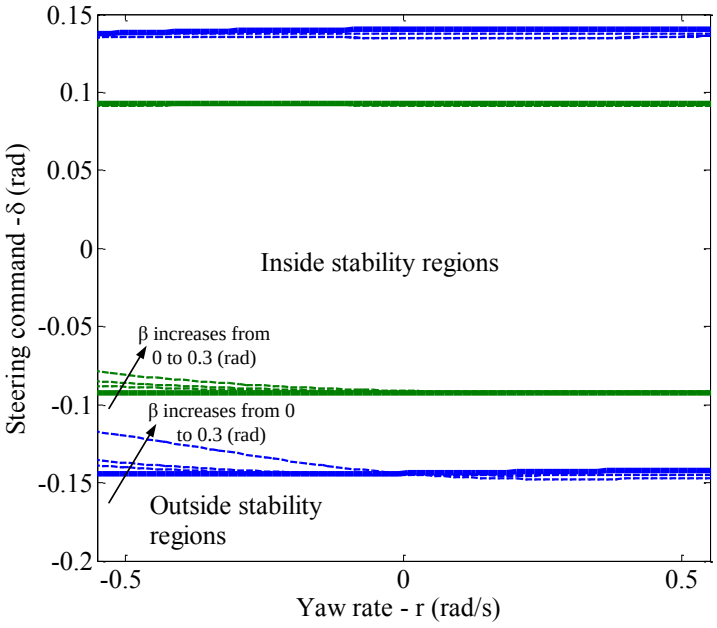


Figure 5.29: Constrained stability region for the TFV in $r - \delta$ plane for positive values of $\beta$

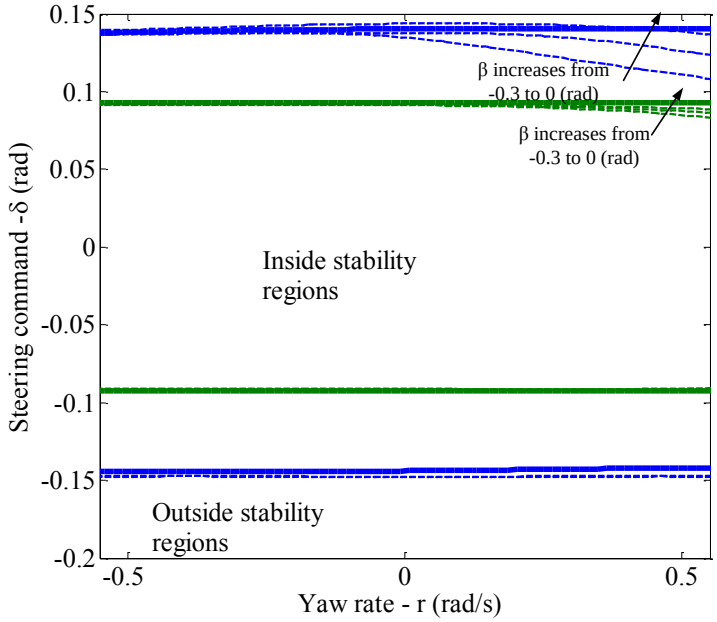


Figure 5.30: Constrained stability region for the TFV in $r - \delta$ plane for negative values of $\beta$

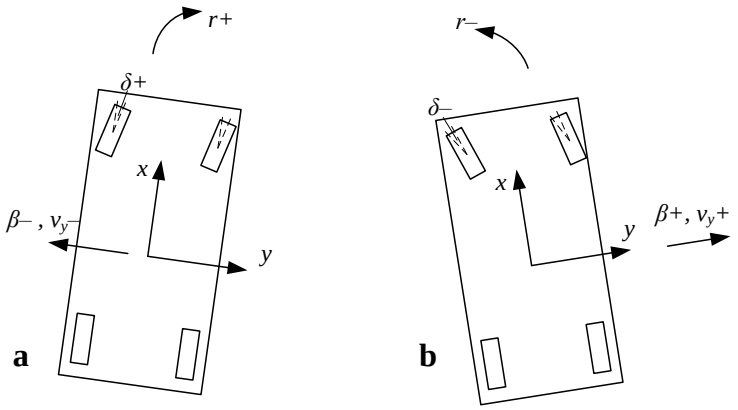


Figure 5.31: The situations with a high lateral acceleration

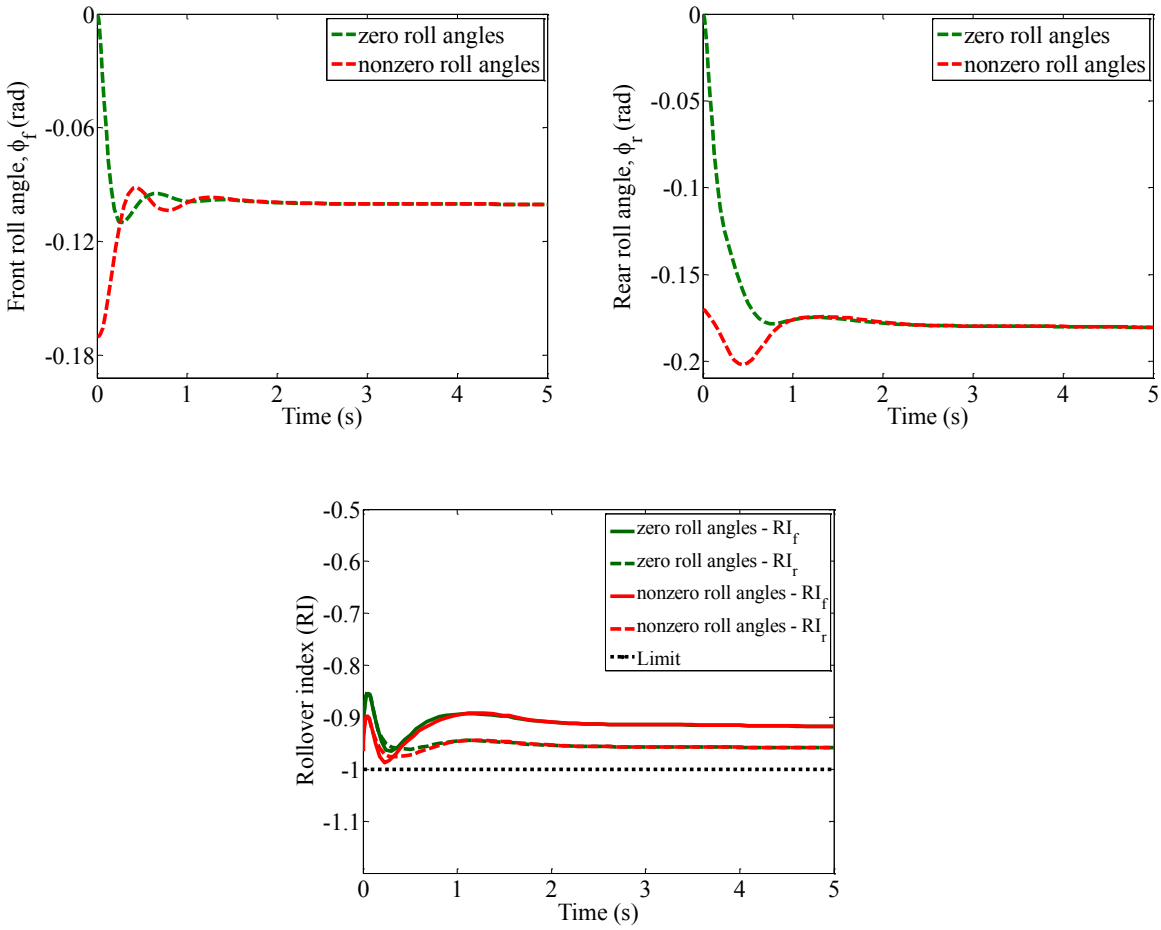


Figure 5.32: The front roll angle, $\phi_f$, the rear roll angle, $\phi_r$, and the RI in a situation with a high lateral acceleration

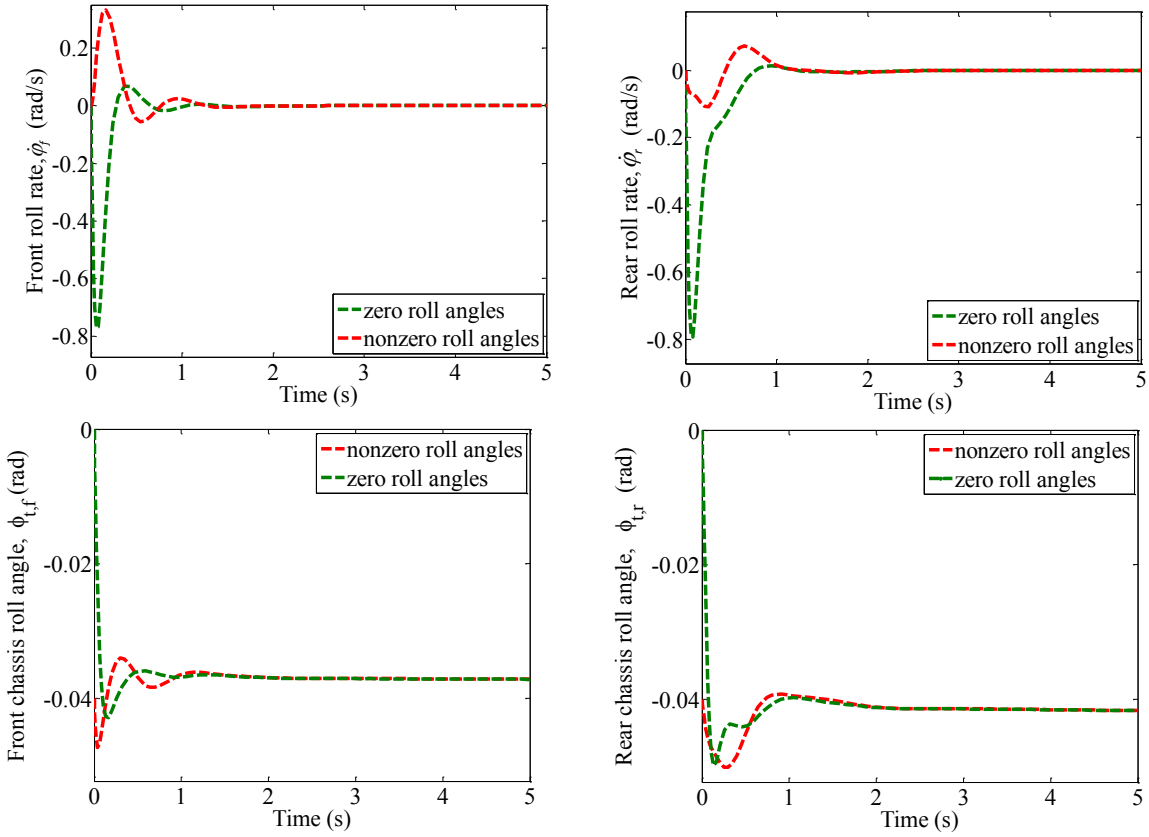


Figure 5.33: The front roll rate, $\dot{\phi}_f$, the rear roll rate, $\dot{\phi}_r$, the rear chassis roll angle, $\phi_{u,f}$, and the front chassis roll angle, $\phi_{u,r}$ in a situation with a high lateral acceleration

The sprung mass of the vehicle is increased by 7%, 14%, and 20% and the results are depicted in Figure 5.34. The size of the stability region with the nominal mass properties decreases with the increase in the sprung mass of the vehicle. Obviously, any increase in the mass of the vehicle can change the values of the accelerations of the masses, which affect stability of the system.

Another important mass property is the location of center of gravity along the longitudinal axis. This property has a direct effect on yaw stability. In general, it can be said that if the C.G. is moved toward the front of the vehicle, yaw stability is improved. Results of the stability analysis are in an agreement with this hypothesis. Figure 5.35 shows the variations in the size of the stability region by changes in the location of the C.G. in the longitudinal direction. The longitudinal location is changed by $-75\,cm$ to $+75\,cm$ with $25\,cm$ increments,

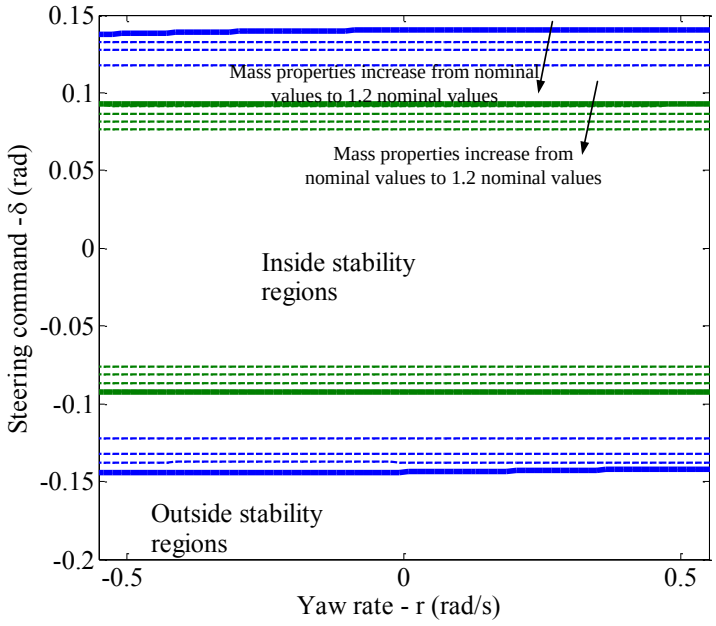


Figure 5.34: Constrained stability region for the TFV in $r - \delta$ plane with perturbations in the mass of the vehicle

while the wheel base of the vehicle is not changed. For both of the strategies the size of the stability region increases by moving the C.G. towards the front, and decreases by moving it towards the back of the vehicle.

### Effect of Changes in Torsional Compliance on the Stability Region of the Controlled Systems

Torsional compliance is another important property of TFVs that play a significant role in their dynamics. The effect of changes in torsional compliance on the stability of the system is discussed in this section. To investigate the effect of both decrease and increase in the torsional compliance, the torsional compliance is multiplied by factors of 0.1, 0.2, 5 and 10 as shown in Figure 5.36. The effect of such changes are not significant. Although it can be seen that as the frame becomes stiffer, i.e., the torsional compliance increases, the size of stability region increases as well. This is because with a more rigid body, the torsion in the frame decreases and the values of the rollover indexes in the front and rear axles will be the

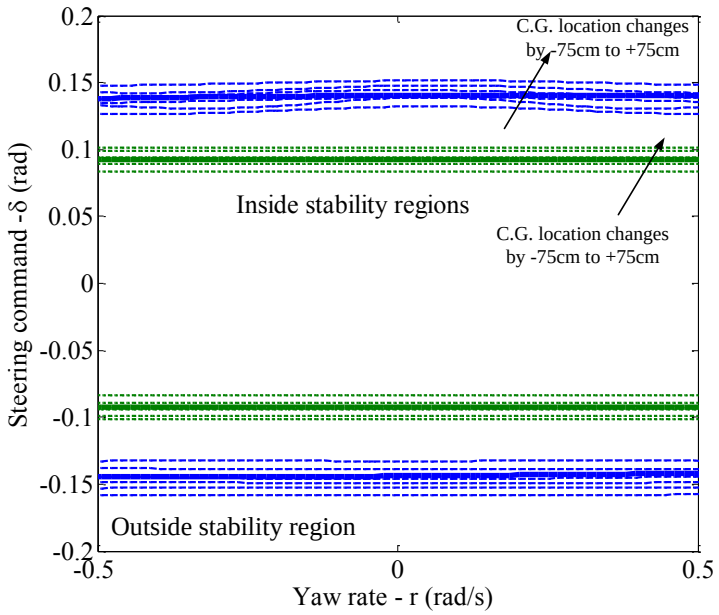


Figure 5.35: Constrained stability region for the TFV in $r - \delta$ plane with perturbations in the location of the C.G.

same. Conversely, as the torsional compliance decreases, i.e., the frame becomes less rigid, the size of the stability region decreases. In such a case, the torsion in the frame increases and the difference between the rollover indexes will decrease, which has a negative effect on stability.

## 5.3 Summary

A T-S fuzzy controller is proposed in this research which integrates yaw stabilization and rollover prevention. A comprehensive Pacejka tire model is employed to represent tire dynamics. The sectors of the tire forces are chosen based on sector nonlinearity approach and fine tuning of the controller. With the proper choice of the sectors, the T-S fuzzy system is able to perfectly capture all the nonlinearities in the system, and prioritize the objectives.

The T-S fuzzy controller is implemented to a model of a torsionally rigid vehicle as well as a model of a torsionally flexible vehicle. The performances of the controllers are examined using three case studies for each type of vehicle. For both types of the vehicles, the first case

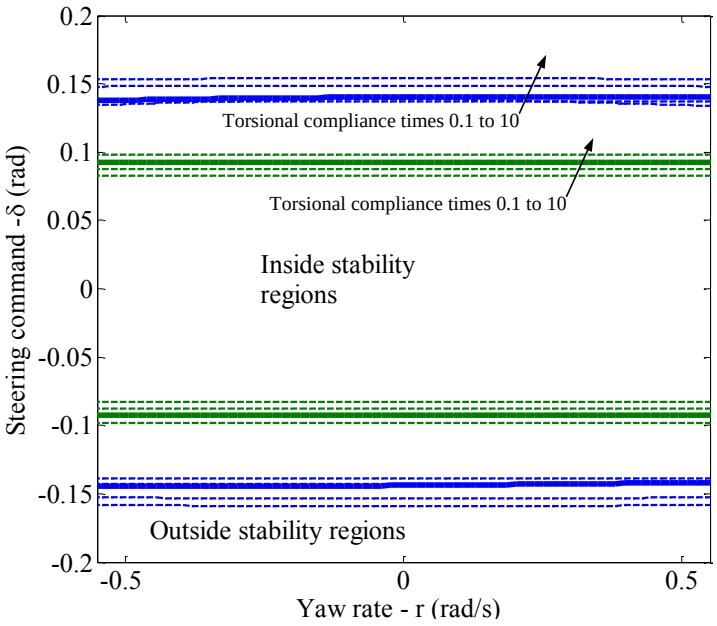


Figure 5.36: Constrained stability region for the TFV in $r - \delta$ plane with perturbations in the torsional compliance of the frame

studies indicate that when the vehicles operate in normal driving conditions, the controller assists the driver to track a desired value of the yaw rate in a fast manner with minimal interference in the driver's decision. However, when the vehicles approach the limits of wheel lift-off, there is a contradiction between the two objectives, tracking a desired value of the yaw rate and rollover prevention. In such circumstances, the priority must be given to rollover mitigation. The second and third case studies show that with such an allocation of priorities, the proposed T-S fuzzy controller manages to maintain the rollover index within the limits. Conversely, the single-objective controller fails to keep the wheels of the vehicle on the ground, although it has satisfactory performance in tracking the desired yaw rate. The third case studies also magnify the fact that the uncontrolled vehicle has an extremely poor performance in both yaw rate following and rollover prevention.

Designing and tunning the T-S fuzzy controller is more complicated in the case of the TFV. One of the reasons is simply because the TFV model has more DOFs than the TRV model. Besides, due to the torsional compliance in the frame of the TFV, the rollover indexes

in the front and rear axles of the vehicle are different. Therefore, the problem of designing CN2 is a multi-output control problem which requires more efforts in tunning the controller.

Although T-S fuzzy provides a stability proof, it is restricted to zero initial conditions. A comprehensive stability analysis using the proposed method in Chapter 3 is provided in this research which compares the performance of the systems in terms of stability. In finding stability regions, wheel lift-off is considered as a constraint. Therefore, for all the points inside the constrained stability regions it is guaranteed that Lyapunov exponents are negative and wheel lift-off does not occur. The constrained stability regions of the proposed controller are significantly larger than those of the single-objective controller.

# Chapter 6

# Conclusions and Future Works

## 6.1 Conclusions

In spite of the fact that there has been extensive research in the field of vehicle safety, tragic events still happen. The objective of this research is to come up with tools for stability analysis and control of yaw and roll dynamics of ground vehicles to contribute in safer operation of such vehicles. To attain this objective, several tasks have been performed.

1) Finding the boundaries of stability regions of the attractors of a dynamical system is challenging. The first task was developing a stability analysis tool that is capable of finding such boundaries for highly nonlinear dynamical systems. Among the current methods, NLB methods are mostly dependent on initial conditions, but normally have low computational loads. LFB methods have strong mathematical basis, but are applicable only to specific problems; once the system becomes complex, it is not feasible to use such methods. On the other hand, the concept of Lyapunov exponents can be applied to highly nonlinear systems with complex boundaries of BoAs; however, the high computational load is a drawback with using Lyapunov exponents.

A new and innovative approach has been proposed in this research that introduces an intelligent algorithm to target the boundaries in an efficient way, and avoids unnecessary calculations. The performance of the method has been demonstrated with three case stud-

ies including system stability and structural stability analyses. The results show that the proposed method can be exploited for complex nonlinear systems in a highly effective and efficient way. For the three case studies represented in Section 3.2, the method reduces the computations by more than 70% in comparison to the primary method of calculating Lyapunov exponents for all the points in the grid.

It is also crucially significant if one can find a way to represent the boundaries of a BoA with a mathematical expression. With the aid of SVMs, known as one the most efficient machine learning algorithms, the collected data is classified, and a function can be found to represent the boundary. This is an extremely valuable advantage in applications like control engineering or monitoring purposes.

2) Designing a reliable controller for yaw stabilization and rollover prevention of ground vehicles was the next task of this research. As illustrated in the results, maintaining both of the above objectives can be contradictory at some instances. In addition, each of the objectives are important at specific situations. Therefore, there must be a compromise between satisfying the two objectives. Furthermore, since the models that are used in this research are highly nonlinear, using the conventional control methods is not practical. T-S fuzzy approaches are capable of solving multi-objective control problems with highly nonlinear plants like the problem of this research.

A T-S fuzzy controller is proposed in this research which integrates yaw stabilization and rollover prevention of ground vehicles. A comprehensive Pacejka tire model, which captures most of the important nonlinearities of tire dynamics, is used as the basis for constructing the T-S fuzzy system based on sector nonlinearity approach. With the proper choice of sectors, the T-S fuzzy system is able to perfectly capture all the nonlinearities in the system.

The proposed controller is applied to a model of a TRV, as well as a model of a TFV. The performance of the controller is examined using three maneuvers for each type of vehicle. In normal driving conditions, the T-S fuzzy controllers assist the driver to perfectly track the desired value of the yaw rate. In harsh maneuvers, the proposed controllers aim at preventing wheel lift-off from happening. The single-objective T-S fuzzy controllers fail to

keep the wheels of the vehicles on the ground.

3) Although T-S fuzzy approach provides a stability proof, it is restricted to zero initial conditions. A comprehensive stability analysis using the proposed method for identifying boundaries of BoAs of the vehicles systems has been provided which compares the performance of the systems in terms of stability. In finding stability regions, wheel lift-off is considered as a constraint. The effects of perturbations in different initial conditions and parameters, such as the side slip angle, the roll angles, and the mass properties, on stability of the systems are explored. However, the most important result is the effect of torsional compliance on the stability of the vehicles. If the torsional compliance is decreased, i.e., the vehicle's frame is less rigid, the stability regions shrink. Conversely, if it is increased, i.e., the frame becomes stiffer, the stability regions become larger. The constrained stability regions of the proposed multi-objective controllers are significantly larger than those of the single-objective controllers.

4) An extension of the existing model of the dynamics of TFVs is presented in this research. A nonlinear tire model with respect to the side slip angle, $\alpha$, has been employed. The use of the nonlinear tire model is imperative since prior to a wheel lift-off event the system's behavior is highly nonlinear. The results of the model are comparable to those of Sampson and Cebon's model [2].

## 6.2 Future Works

Based on the observations of this research, the following research works are recommended:

1) There is a practical possibility to improve the model proposed by Sampson and Cebon [2] for TFVs. Although the separation of the masses of the vehicle into the front and rear portions can be a realistic assumption in some cases, in general the load is distributed throughout the vehicle. Developing a model that can describe the dynamics of such vehicles, in which both of the distributed load and torsional compliance effects are considered, is a significant improvement to this model.

2) The proposed method for identifying boundaries of BoAs can also be enhanced. Exploring the use of more advanced statistical approaches such as Markov chain Monte Carlo (MCMC) is recommended.

3) There is also the possibility of improvement in the simulation of this research. A model in a commercial software like ADAMS, CarSim, or TruckSim can be an appropriate choice. However, the torsional compliance of the frame is not included in all the existing software. TruckSim has presented a model considering this effect, which is fairly expensive.

4) The control algorithm can be improved as well. One possible choice of future work is to consider the effects of uncertainties in the parameters of the system. The parameters of a vehicle system can have different values than their nominal values due to many issues or conditions, such as inaccurate measurements, significant changes in loading conditions, changes due to wear and tear, etc. A suitable enhancement in the control method is to use robust or adaptive algorithms. Besides, the performance of the proposed controller is not ideal with respect to roll dynamics. Integrating roll motion control with the other two objectives can be an incremental improvement to the proposed controller.

5) Lastly, the performance of the controller can be examined by an appropriate experimental set up. As mentioned before, one advantage of T-S fuzzy methods is that in spite of the fact that they can represent highly complex systems, they are simple and easy to implement.

# Appendix A

# Routh-Hurwitz Analysis of the Follower-Loaded Double Pendulum

To find the boundaries of structural stability regions, in [123; 122], the nonlinear system of (3.23) are linearized around the equilibrium point to be able to use Routh-Hurwitz analysis which is a linear approach. The linearization leads to the following characteristic equation:

$$a_0\,\lambda^4 + a_1\,\lambda^3 + a_2\,\lambda^2 + a_3\,\lambda + a_4\ = 0 \tag{A.1}$$

where

$$\begin{aligned} a_0 &= 2, \\ a_1 &= 7c, \\ a_2 &= 2p(\alpha - 2) + c^2 + 7 \\ a_3 &= c(3p(\alpha - 1) + 2), \\ a_4 &= (3 - p)p(\alpha - 1) + 1 \end{aligned} \tag{A.2}$$

Based on the coefficients of the characteristic equation, Routh criteria provides conditions for stability of the system. The coefficients of the characteristic equation, which are given in (A.2), are functions of $p$ and $\alpha$, the two parameters of this study. Thus, the conditions given by Routh-Hurwitz criteria are functions of $p$ and $\alpha$, as well.

The first condition of Routh's criteria is that in the presence of at least one positive

coefficient, all the coefficients of the characteristic equation must be positive. Since it is trivial that $a_0 > 0$ and $a_1 > 0$, this condition results in the following inequalities:

$$\begin{aligned} &2p(\alpha-2)+c^2+7>0 \\ &c(3p(\alpha-1)+2)>0, \\ &(3-p)p(\alpha-1)+1>0 \end{aligned} \tag{A.3}$$

To find the other conditions, the coefficients of the characteristic equation are arranged as the following pattern:

$$\begin{array}{llll} \lambda^4 & a_0 & a_2 & a_4 \\ \lambda^3 & a_1 & a_3 & 0 \\ \lambda^2 & b_1 & b_2 & 0 \\ \lambda^1 & c_1 & c_2 & 0 \\ \lambda^0 & d_1 & 0 & 0 \end{array} \tag{A.4}$$

where

$$\begin{aligned} b_1 &= \frac{a_1\,a_2 - a_0\,a_3}{a_1} \\ b_2 &= \frac{a_1\,a_4 - a_0\,a_5}{a_1} = a_4 \\ c_1 &= \frac{b_1\,a_3 - a_1\,b_2}{b_1} = \frac{a_1\,a_2\,a_3 - a_0\,a_3^2 - a_1^2\,a_4}{a_1\,b_1} \\ c_2 &= \frac{b_1\,a_5 - a_1\,b_3}{b_1} = 0 \\ d_1 &= \frac{c_1\,b_2 - b_1\,c_2}{a_1} = a_4 \end{aligned} \tag{A.5}$$

Routh's stability criteria states that the number of roots of the characteristic equation with positive real parts is equal to the number of changes in sign of the coefficients of the first column of the array in (A.4). Therefore, since $a_0 > 0$ and $a_1 > 0$, the necessary conditions that all the roots of (A.1) lie in the left-half $s$ plane are:

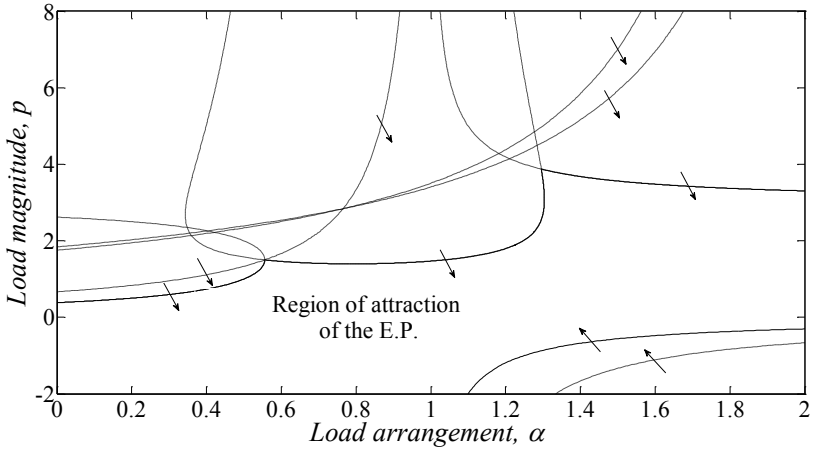


Figure A.1: The result of Routh-Hurwitz analysis of the follower-loaded double pendulum system. The RoA, which is separated from the rest of the space by the solid thick lines, is the outcome of several conditions.

$$
\begin{aligned}
b_1 &= \frac{a_1\, a_2 - a_0\, a_3}{a_1} > 0 \\
c_1 &= \frac{a_1\, a_2\, a_3 - a_0\, a_3^2 - a_1^2\, a_4}{a_1\, b_1} > 0 \\
d_1 &= a_4 = (3-p)p(\alpha - 1) + 1 > 0
\end{aligned}
\tag{A.6}
$$

Equations (A.6) and (A.3) provide five necessary and sufficient conditions that the equilibrium point is stable. These conditions are plotted in the $p - \alpha$ plane, illustrated in Figure A.1. The intersection of all the regions identified by every individual of the conditions is the region in which the equilibrium is stable. This region is indicated in the figure, which has the boundaries with solid lines.

# Appendix B

# Pacejka Magic Formula Tire Model

Pacejka Magic formula is a mathematical model that estimates the forces and moments of tire accurately. Being based on numerous complicated experiments, the tire model includes many parameters and expressions, which creates a complex function for modeling tire behavior. The general form of the pure slip version of Magic formula is as follow [3]:

$$F_{yo}^{*} = D_y \sin[C_y \, arctan B_y \, \alpha_y - E_y(B_y \, \alpha_y - aractan(B_y \, \alpha_y))] + S_{Vy} \tag{B.1}$$

In (B.1), $\alpha_y$, $C_y$, and $D_y$ are given by the following equations:

$$\alpha_y = \alpha^{*} + S_{Hy} \tag{B.2a}$$

$$C_y = p_{Cy1} \, \lambda_{Cy} \tag{B.2b}$$

$$D_y = \mu_y \, F_z \, \zeta_2 \tag{B.2c}$$

where $\alpha^{*}$ and $S_{Hy}$ read as:

$$\alpha^{*} = V_{cx} \tan\alpha \tag{B.3a}$$

$$\gamma^{*} = \sin\gamma \tag{B.3b}$$

$$F'_{zo} = \lambda_{F_{zo}} \, F_{zo} \tag{B.3c}$$

$$df_z = \frac{F_z - F'_{zo}}{F'_{zo}} \tag{B.3d}$$

| Parameter | Value | Parameter | value | parameter | value |
|---|---|---|---|---|---|
| $p_{Cy1}$ | 1.193 | $p_{Dy1}$ | -0.990 | $p_{Dy2}$ | 0.145 |
| $p_{Dy3}$ | -11.23 | $p_{Ey1}$ | -1.003 | $p_{Ey2}$ | -0.537 |
| $p_{Ey3}$ | 0.083 | $p_{Ey3}$ | -4.787 | $p_{Ky1}$ | -14.95 |
| $p_{Ky2}$ | 2.130 | $p_{Ky3}$ | -0.028 | $p_{Hy1}$ | 0.003 |
| $p_{Hy2}$ | -0.001 | $p_{Hy3}$ | 0.075 | $p_{Vy1}$ | 0.045 |
| $p_{Vy2}$ | -0.024 | $p_{Vy3}$ | -0.532 | $p_{Vy4}$ | 0.039 |
| $\lambda_{Ey}$ | 1 | $\lambda_{Ky\alpha}$ | 1 | $\lambda_{Ky\gamma}$ | 1 |
| $\lambda_{Hy}$ | 0 | $\lambda_{Vy}$ | 0 | $\lambda_{Cy}$ | 1 |
| $\lambda_{\mu y}$ | 1 | $\lambda_{\mu V}$ | 1 | $\zeta_i, \quad i = 0, 1, ..., 8$ | 1 |

Table B.1: The parameters of the pure slip Pacejka magic formula for lateral force [3]

$$S_{Hy} = (p_{Hy1} + p_{Hy2} df_z)\lambda_{Hy} + p_{Hy3}\,\gamma^*\,\lambda_{Ky\gamma}\,\zeta_0 + \zeta_4 - 1 \tag{B.3e}$$

with $V_{cx}$ being the forward speed.

In (B.1), $E_y$ is calculated by the subsequent equations:

$$\mu_y = (p_{Dy1} + p_{Dy2}\,df_z)(1 - p_{Dy3}\,\gamma^{*2})\frac{\lambda_{\mu y}}{1 + \lambda_{\mu V}\dfrac{V_s}{V_o}} \tag{B.4a}$$

$$E_y = (p_{Ey1} + p_{Ey2} df_z)\,[1 - (p_{Ey3} + p_{Ey4}\gamma^*)\,sgn(\alpha_y)]\,\lambda_{Ey} \tag{B.4b}$$

where $V_s$ and $V_o$ are the speeds of the contact point of the tire to the ground, in $x$ and $y$ directions, respectively.

In (B.1), $B_y$ is obtained by the following equation:

$$K_{y\alpha o} = p_{Ky1} F'_{zo} \sin[2\arctan(\frac{F_z}{p_{Ky2}\,F'_{zo}})]\,\lambda_{Ky\alpha} \tag{B.5a}$$

$$K_{y\alpha} = K_{y\alpha o}(1 - p_{ky3}\,\gamma^{*2})\,\zeta_3 \tag{B.5b}$$

$$B_y = \frac{K_{y\alpha}}{C_y\,D_y} \tag{B.5c}$$

Finally, in (B.1), $S_{Vy}$ is calculated as:

$$S_{Vy} = F_z[(p_{Vy1} + p_{Vy2}\,df_z)\lambda_{Vy} + (p_{Vy3} + p_{Vy4} df_z)\gamma^*\,\lambda_{Ky\gamma}]\lambda'_{\mu y}\,\zeta_2 \tag{B.6}$$

# Appendix C

# Calculations of Support Vector Machine Learning Algorithm

As mentioned in Chapter 2, the decision function has the following format:

$$G(\mathbf{x}) = \sum_{i=1}^{l} \alpha_i \, \gamma_i \, \psi(\mathbf{x}, \mathbf{x}_i) + b \tag{C.1}$$

In the above equation, $\alpha_i$ are Lagrange multipliers, which are positive real numbers. $b$ is the intercept of the hyperplane that separates the two groups. $\gamma_i$ are the labels of the groups, and are $+1$ for the first group, and $-1$ for the second group. $\psi(.,.)$ is the Kernel function, and defines the form of the decision function.

To find the decision function, all the gathered data are given to an optimization algorithm. The outputs of the optimization process are $\alpha_i$ which indicate the importance of each of input data in determining the decision function, $b$ or the bias term of the hyperplane. For some input data that are away from the boundary the associated $\alpha_i$ is equal to zero. The input data that have nonzero Lagrange multipliers, are called support vectors, which are shown as $\mathbf{x}_i$. Having the bias term, and the support vectors and their associated Lagrange multipliers, the decision function can be identified by expanding the Kernel function and substituting these values into (C.1).

As an example, the function found in section 3.2.1 for the Lienard system has the following

Kernel function:

$$\psi(\mathbf{x}, \mathbf{x}_i) \; = \; \mathbf{x}\mathbf{x}_i(1 + \mathbf{x}\mathbf{x}_i) \tag{C.2}$$

Considering that $\mathbf{x} = (x, y)$ and $\mathbf{x}_i = (x_i, y_i)$, the Kernel function is extended as:

$$\psi(\mathbf{x}, \mathbf{x}_i) = \psi(x, y, x_i, y_i) = (x\, x_i)^2 + 2x\, x_i\, y\, y_i + (y\, y_i)^2 + x\, x_i + y\, y_i \tag{C.3}$$

Substituting the values of the support vectors, and their associated $\alpha_i$, and $b$ in (C.1), the decision function reads as:

$$G(\mathbf{x}) = \sum_{i=1}^{l} \alpha_i\, \gamma_i\, [(x\, x_i)^2 + 2x\, x_i\, y\, y_i + (y\, y_i)^2 + x\, x_i + y\, y_i] + b \tag{C.4}$$

Finally, the decision function for the Lienard system is found as:

$$G(\mathbf{x}) = G(x, y) = 14.45x^2 + 3.21x\, y - 0.03x + 12.36y^2 + 0.05y - 13.05 \tag{C.5}$$

# Bibliography


[1] B. Mashadi, M. Majidi, and H. P. Dizaji, "Optimal vehicle dynamics controller design using a four-degrees-of-freedom model," *Proceedings of the Institution of Mechanical Engineers, Part D: Journal of Automobile Engineering*, vol. 224, no. 5, pp. 645–659, 2010.

[2] D. J. Sampson and D. Cebon, "Active roll control of single unit heavy road vehicles," *Vehicle System Dynamics*, vol. 40, no. 4, pp. 229–270, 2003.

[3] H. Pacejka, *Tyre and vehicle dynamics*. Elsevier, 2005.

[4] "Cooperative agreement to support biomechanical research - rollover tasks.," *UNITED STATES DEPARTMENT OF TRANSPORTATION (U.S. DOT) National Highway Traffic Safety Administration (NHTSA)*, 2011.

[5] R. Goodall and W. Kortüm, "Active controls in ground transportation—a review of the state-of-the-art and future potential," *Vehicle System Dynamics*, vol. 12, no. 4-5, pp. 225–257, 1983.

[6] I. ČECH, "A slow-acting in-series active suspension," *Vehicle System Dynamics*, vol. 16, no. 1, pp. 17–26, 1987.

[7] R. Sharp and S. Hassan, "On the performance capabilities of active automobile suspension systems of limited bandwidth," *Vehicle System Dynamics*, vol. 16, no. 4, pp. 213–225, 1987.

[8] A. T. Pham and P. Ugazio, "Basic developments of an active air spring suspension for passenger cars," *SAE Transactions*, pp. 175–181, 1989.

[9] L. Segel, "An overview of developments in road vehicle dynamics: past, present and future," in *Proc. IMechE Conference on Vehicle ride and handling*, pp. 1–12, 1993.

[10] E.-C. von Glasner, E. Göhring, R. Povel, P. Schützner, and A. Mercedes-Benz, "Analysis of intelligent suspension systems for commercial vehicles," *Fuel*, vol. 2011, pp. 12–05, 1993.

[11] R. Lin, D. Cebon, and D. Cole, "An investigation of active roll control of heavy road vehicles," *Vehicle System Dynamics*, vol. 23, no. S1, pp. 308–321, 1994.

[12] G. Frost, M. Howell, T. Gordon, and Q. Wu, "Dynamic vehicle roll control using reinforcement learning," 1996.

[13] C. Winkler, D. Blower, and R. Ervin, "Rollover of heavy commercial vehicles," tech. rep., 1999.

[14] C. Winkler, R. Ervin, and M. Hagan, "On-board estimation of the rollover threshold of tractor semitrailers," in *The dynamics of vehicles on roads and on traks - Supplement to vehicle system dynamics, Volume 33. Proceedings of the 16th IAVSD symposium, held in Pretoria, South Africa, August 30-September 3*, 2000.

[15] R. Goldman, M. El-Gindy, and B. Kulakowski, "Rollover dynamics of road vehicles: Literature survey," *International Journal of Heavy Vehicle Systems*, vol. 8, no. 2, pp. 103–141, 2001.

[16] D. J. M. Sampson, *Active roll control of articulated heavy vehicles.* University of Cambridge UK, 2000.

[17] R. Lang and U. Walz, "Active roll reduction," in *Proc. 3rd International Conference on Vehicle Dynamics and Power Train Engineering*, pp. 88–92, 1991.

[18] R. Sharp and D. Pan, "On the design of an active roll control system for a luxury car," *Proceedings of the Institution of Mechanical Engineers, Part D: Journal of Automobile Engineering*, vol. 207, no. 4, pp. 275–284, 1993.

[19] T. Gordon, "An integrated strategy for the control of a full vehicle active suspension system," *Vehicle System Dynamics*, vol. 25, no. S1, pp. 229–242, 1996.

[20] J. Darling and T. Ross-Martin, "A theoretical investigation of a prototype active roll control system," *Proceedings of the Institution of Mechanical Engineers, Part D: Journal of Automobile Engineering*, vol. 211, no. 1, pp. 3–12, 1997.

[21] A. B. Dunwoody and S. Froese, "Active roll control of a semi-trailer," *Commercial Vehicle*, vol. 2013, pp. 09–08, 1993.

[22] Y. Kusahara, "Feasibility study of active roll stabilizer for reducing roll angle of an experimental medium-duty truck," in *International Symposium on Advanced Vehicle Control (1994: Tsukuba-shi, Japan). Proceedings of the International Symposium on Advanced Vehicle Control 1994*, 1994.

[23] Y. Watanabe and H. Katoh, "Investigation into the turning behaviour of an experimental four-wheel steering medium-duty truck," in *Society of Automotive Engineers, Eighteenth Fisita Congress*, pp. 423–428, SAE, 1990.

[24] Y. Watanabe, Y. Kusahara, N. Hata, S. Hasegawa, *et al.*, "Effect of rear-axle steering on vehicle controllability and stability of a medium-duty truck," *Training*, vol. 2013, pp. 11–18, 1993.

[25] H.-C. Pflug, E.-C. v. Glasner, and R. Povel, "Improvement of commercial vehicles handling and stability by smart chassis systems," *Smart vehicles*, 1995.

[26] R. J. Dorling, *Integrated Control of Road Vehicle Dynamics*. PhD thesis, University of Cambridge, Cambridge, UK, 1996.

[27] R. C. Lin, *An investigation of active roll control for heavy vehicle suspensions.* PhD thesis, University of Cambridge, 1994.

[28] R. Lin, D. Cebon, and D. Cole, "Optimal roll control of a single-unit lorry," *Proceedings of the Institution of Mechanical Engineers, Part D: Journal of Automobile Engineering*, vol. 210, no. 1, pp. 45–55, 1996.

[29] D. J. Sampson and D. Cebon, "Achievable roll stability of heavy road vehicles," *Proceedings of the Institution of Mechanical Engineers, Part D: Journal of Automobile Engineering*, vol. 217, no. 4, pp. 269–287, 2003.

[30] A. J. Miege and D. Cebon, "Optimal roll control of an articulated vehicle: theory and model validation," *Vehicle system dynamics*, vol. 43, no. 12, pp. 867–884, 2005.

[31] P. Gáspár, Z. Szabó, and J. Bokor, "Brake control combined with prediction to prevent the rollover of heavy vehicles," in *Proc. of the IFAC World Congress, Praha*, pp. 79–86, 2005.

[32] P. Gaspar, I. Szaszi, and J. Bokor, "The design of a combined control structure to prevent the rollover of heavy vehicles," *European journal of control*, vol. 10, no. 2, pp. 148–162, 2004.

[33] P. Gaspar and J. Bokor, "A fault-tolerant rollover prevention system based on an lpv method," *International journal of vehicle design*, vol. 42, no. 3, pp. 392–412, 2006.

[34] P. Gaspar, I. Szaszi, and J. Bokor, "Reconfigurable control structure to prevent the rollover of heavy vehicles," *Control Engineering Practice*, vol. 13, no. 6, pp. 699–711, 2005.

[35] S. C. Baslamısl, *LPV modeling and robust control of yaw and roll modes of road vehicles.* PhD thesis, Bogaziçi University, 2007.

[36] N. Yu, S. Muthiah, and B. T. Kulakowski, "The handling characteristics of a transit bus," *International Journal of Vehicle Systems Modelling and Testing*, vol. 2, no. 2, pp. 138–152, 2007.

[37] M. J. L. Boada, B. L. Boada, A. Gauchia Babe, and J. A. Calvo Ramos, "Active roll control using reinforcement learning for a single unit heavy vehicle," *International Journal of Heavy Vehicle Systems*, vol. 16, no. 4, pp. 412–430, 2009.

[38] A. Gauchía, V. Díaz, M. Boada, O. Olatunbosun, and B. Boada, "Bus structure behaviour under driving manoeuvring and evaluation of the effect of an active roll system.," *International Journal of Vehicle Structures & Systems (IJVSS)*, vol. 2, no. 1, 2010.

[39] A. Gauchía, E. Olmeda, F. Aparicio, and V. Díaz, "Bus mathematical model of acceleration threshold limit estimation in lateral rollover test," *Vehicle System Dynamics*, vol. 49, no. 10, pp. 1695–1707, 2011.

[40] D. Cao, S. Rakheja, and C.-Y. Su, "Roll-and pitch-plane coupled hydro-pneumatic suspension: Part 1: Feasibility analysis and suspension properties," *Vehicle system dynamics*, vol. 48, no. 3, pp. 361–386, 2010.

[41] Y. Akhmetov, A. Sandel, L. Maiffredy, D. Rémond, W. Marquis-Favre, and V. Harth, "Reference trajectory generation for control in single-unit heavy vehicle: focus on rollover prevention," *International Journal of Heavy Vehicle Systems*, vol. 20, no. 1, pp. 1–18, 2013.

[42] H. Imine, L. M. Fridman, and T. Madani, "Steering control for rollover avoidance of heavy vehicles," *Vehicular Technology, IEEE Transactions on*, vol. 61, no. 8, pp. 3499–3509, 2012.

[43] H. Imine, A. Benallegue, T. Madani, and S. Srairi, "Rollover risk prediction of heavy

vehicle using high-order sliding-mode observer: Experimental results," *Vehicular Technology, IEEE Transactions on*, vol. 63, no. 6, pp. 2533–2543, 2014.

[44] S. Solmaz, M. Corless, and R. Shorten, "A methodology for the design of robust rollover prevention controllers for automotive vehicles: Part 1-differential braking," in *Decision and Control, 2006 45th IEEE Conference on*, pp. 1739–1744, IEEE, 2006.

[45] D. Bernardini, S. Di Cairano, A. Bemporad, and H. Tsengz, "Drive-by-wire vehicle stabilization and yaw regulation: A hybrid model predictive control design," in *Decision and Control, 2009 held jointly with the 2009 28th Chinese Control Conference. CDC/CCC 2009. Proceedings of the 48th IEEE Conference on*, pp. 7621–7626, IEEE, 2009.

[46] C. E. Beal and J. C. Gerdes, "Model predictive control for vehicle stabilization at the limits of handling," *Control Systems Technology, IEEE Transactions on*, vol. 21, no. 4, pp. 1258–1269, 2013.

[47] M. A. Rodríguez Licea and I. Cervantes, "Robust switched predictive braking control for rollover prevention in wheeled vehicles," *Mathematical Problems in Engineering*, vol. 2014, 2014.

[48] B. Schofield and T. Hagglund, "Optimal control allocation in vehicle dynamics control for rollover mitigation," in *American Control Conference, 2008*, pp. 3231–3236, IEEE, 2008.

[49] R. Rajamani and D. Piyabongkarn, "New paradigms for the integration of yaw stability and rollover prevention functions in vehicle stability control," *Intelligent Transportation Systems, IEEE Transactions on*, vol. 14, no. 1, pp. 249–261, 2013.

[50] B. Schofield and T. Hagglund, "Optimal control allocation in vehicle dynamics control for rollover mitigation," in *American Control Conference, 2008*, pp. 3231–3236, IEEE, 2008.

[51] J. Yoon, S. Yim, W. Cho, B. Koo, and K. Yi, "Design of an unified chassis controller for rollover prevention, manoeuvrability and lateral stability," *Vehicle system dynamics*, vol. 48, no. 11, pp. 1247–1268, 2010.

[52] M. B. Alberding, J. Tjønnås, and T. A. Johansen, "Integration of vehicle yaw stabilisation and rollover prevention through nonlinear hierarchical control allocation," *Vehicle System Dynamics*, vol. 52, no. 12, pp. 1607–1621, 2014.

[53] B. Jiang, Z. Gao, P. Shi, and Y. Xu, "Adaptive fault-tolerant tracking control of near-space vehicle using takagi–sugeno fuzzy models," *Fuzzy Systems, IEEE Transactions on*, vol. 18, no. 5, pp. 1000–1007, 2010.

[54] H. Li, J. Yu, C. Hilton, and H. Liu, "Adaptive sliding-mode control for nonlinear active suspension vehicle systems using t–s fuzzy approach," *Industrial Electronics, IEEE Transactions on*, vol. 60, no. 8, pp. 3328–3338, 2013.

[55] H. Dahmani, A. El Hajjaji, N. Daraoui, *et al.*, "Observer-based robust control of vehicle dynamics for rollover mitigation in critical situations," 2014.

[56] K. Nam, S. Oh, H. Fujimoto, and Y. Hori, "Estimation of sideslip and roll angles of electric vehicles using lateral tire force sensors through rls and kalman filter approaches," *Industrial Electronics, IEEE Transactions on*, vol. 60, no. 3, pp. 988–1000, 2013.

[57] J.-J. E. Slotine, W. Li, *et al.*, *Applied nonlinear control*, vol. 199. Prentice hall New Jersey, 1991.

[58] Y. Sun and C. Q. Wu, "Stability analysis via the concept of lyapunov exponents: a case study in optimal controlled biped standing," *International Journal of Control*, vol. 85, no. 12, pp. 1952–1966, 2012.

[59] D. Koop and C. Q. Wu, "Passive dynamic biped walking part ii: Stability analysis of

the passive dynamic gait," *ASME Computational and Nonlinear Dynamics*, vol. 85, no. 12, pp. 1952–1966, 2012.

[60] I. Śliwa and K. Grygiel, "Periodic orbits, basins of attraction and chaotic beats in two coupled kerr oscillators," *Nonlinear Dynamics*, vol. 67, no. 1, pp. 755–765, 2012.

[61] M. S. de Freitas, R. L. Viana, and C. Grebogi, "Basins of attraction of periodic oscillations in suspension bridges," *Nonlinear Dynamics*, vol. 37, no. 3, pp. 207–226, 2004.

[62] W. Paradis and D. Perlmutter, "Tracking function approach to practical stability and ultimate boundedness," *AIChE Journal*, vol. 12, no. 1, pp. 130–136, 1966.

[63] H. Scofield, "An estimate of the stable initial condition region based on the describing function," *Automatic Control, IEEE Transactions on*, vol. 10, no. 4, pp. 484–485, 1965.

[64] R. Luus and L. Lapidus, "An averaging technique for stability analysis," *Chemical Engineering Science*, vol. 21, no. 2, pp. 159–181, 1966.

[65] K. Loparo and G. Blankenship, "Estimating the domain of attraction of nonlinear feedback systems," *Automatic Control, IEEE Transactions on*, vol. 23, no. 4, pp. 602–608, 1978.

[66] E. Cruck, R. Moitie, and N. Seube, "Estimation of basins of attraction for uncertain systems with affine and lipschitz dynamics," *Dynamics and Control*, vol. 11, no. 3, pp. 211–227, 2001.

[67] T.-C. Wang, S. Lall, and M. West, "Polynomial level-set methods for nonlinear dynamical systems analysis," in *Proc. Allerton Conf. on Communication, Control, and Computing, Allerton, IL*, 2005.

[68] R. Genesio, M. Tartaglia, and A. Vicino, "On the estimation of asymptotic stability regions: State of the art and new proposals," *Automatic Control, IEEE Transactions on*, vol. 30, no. 8, pp. 747–755, 1985.

[69] A. Levin, "An analytical method of estimating the domain of attraction for polynomial differential equations," *Automatic Control, IEEE Transactions on*, vol. 39, no. 12, pp. 2471–2475, 1994.

[70] H.-D. Chiang and J. S. Thorp, "Stability regions of nonlinear dynamical systems: A constructive methodology," *Automatic Control, IEEE Transactions on*, vol. 34, no. 12, pp. 1229–1241, 1989.

[71] B. Tibken and Y. Fan, "Computing the domain of attraction for polynomial systems via bmi optimization method," in *American Control Conference, 2006*, pp. 6–pp, IEEE, 2006.

[72] G. Chesi, A. Garulli, A. Tesi, and A. Vicino, "Lmi-based computation of optimal quadratic lyapunov functions for odd polynomial systems," *International Journal of Robust and Nonlinear Control*, vol. 15, no. 1, pp. 35–49, 2005.

[73] A. Levin, "An analytical method of estimating the domain of attraction for polynomial differential equations," *Automatic Control, IEEE Transactions on*, vol. 39, no. 12, pp. 2471–2475, 1994.

[74] A. Balestrino, A. Caiti, E. Crisostomi, and S. Grammatico, "R-composition of lyapunov functions," in *Control and Automation, 2009. MED'09. 17th Mediterranean Conference on*, pp. 126–131, IEEE, 2009.

[75] Y. Ohta, "Piecewise linear estimate of attractive regions for linear systems with saturating control," in *Proc. of AMS*, 2002.

[76] B. E. Milani, "Piecewise-affine lyapunov functions for discrete-time linear systems with saturating controls," *Automatica*, vol. 38, no. 12, pp. 2177–2184, 2002.

[77] T. Hu and Z. Lin, "Properties of the composite quadratic lyapunov functions," *Automatic Control, IEEE Transactions on*, vol. 49, no. 7, pp. 1162–1167, 2004.

[78] G. Chesi, "Rational lyapunov functions for estimating and controlling the robust domain of attraction," *Automatica*, 2013.

[79] B. Tibken, "Estimation of the domain of attraction for polynomial systems via lmis," in *Decision and Control, 2000. Proceedings of the 39th IEEE Conference on*, vol. 4, pp. 3860–3864, IEEE, 2000.

[80] O. Hachicho and B. Tibken, "Estimating domains of attraction of a class of nonlinear dynamical systems with lmi methods based on the theory of moments," in *Decision and Control, 2002, Proceedings of the 41st IEEE Conference on*, vol. 3, pp. 3150–3155, IEEE, 2002.

[81] D. F. Coutinho, C. E. de Souza, and A. Trofino, "Stability analysis of implicit polynomial systems," *Automatic Control, IEEE Transactions on*, vol. 54, no. 5, pp. 1012–1018, 2009.

[82] Z. W. Jarvis-Wloszek, *Lyapunov based analysis and controller synthesis for polynomial systems using sum-of-squares optimization*. PhD thesis, University of California, 2003.

[83] A. Papachristodoulou, *Scalable analysis of nonlinear systems using convex optimization*. PhD thesis, Citeseer, 2005.

[84] G. Chesi, "Robust domain of attraction: computing and controlling estimates with non-polynomial lyapunov functions," in *Control Applications (CCA), 2012 IEEE International Conference on*, pp. 1086–1091, IEEE, 2012.

[85] W. Tan and A. Packard, "Stability region analysis using polynomial and composite polynomial lyapunov functions and sum-of-squares programming," *Automatic Control, IEEE Transactions on*, vol. 53, no. 2, pp. 565–571, 2008.

[86] H. E. Nusse, J. A. Yorke, and B. R. Hunt, *Dynamics: numerical explorations*, vol. 101. Springer, 1998.

[87] S. Sadri and C. Wu, "Stability analysis of a nonlinear vehicle model in plane motion using the concept of lyapunov exponents," *Vehicle System Dynamics*, vol. 51, no. 6, pp. 906–924, 2013.

[88] H. E. Nusse, J. A. Yorke, and B. R. Hunt, *Dynamics: numerical explorations*, vol. 101. Springer, 1998.

[89] Y. Sun and C. Q. Wu, "A radial-basis-function network-based method of estimating lyapunov exponents from a scalar time series for analyzing nonlinear systems stability," *Nonlinear Dynamics*, vol. 70, no. 2, pp. 1689–1708, 2012.

[90] J. Cusumano and B. Kimble, "A stochastic interrogation method for experimental measurements of global dynamics and basin evolution: Application to a two-well oscillator," *Nonlinear Dynamics*, vol. 8, no. 2, pp. 213–235, 1995.

[91] M. S. Zakynthinaki, J. R. Stirling, C. A. Cordente Martínez, A. L. Díaz de Durana, M. S. Quintana, G. R. Romo, and J. S. Molinuevo, "Modeling the basin of attraction as a two-dimensional manifold from experimental data: Applications to balance in humans," *Chaos: An Interdisciplinary Journal of Nonlinear Science*, vol. 20, no. 1, pp. 013119–013119, 2010.

[92] M. S. Zakynthinaki, A. López, C. A. Cordente, J. A. Ospina Betancurt, M. S. Quintana, and J. Sampedro, "Detecting changes in the basin of attraction of a dynamical system: Application to the postural restoring system," *Applied Mathematics and Computation*, vol. 219, no. 17, pp. 8910–8922, 2013.

[93] A. Wolf, J. B. Swift, H. L. Swinney, and J. A. Vastano, "Determining lyapunov exponents from a time series," *Physica D: Nonlinear Phenomena*, vol. 16, no. 3, pp. 285–317, 1985.

[94] V. I. Oseledec, "A multiplicative ergodic theorem. lyapunov characteristic numbers for dynamical systems," *Trans. Moscow Math. Soc*, vol. 19, no. 2, pp. 197–231, 1968.

[95] G. Benettin, L. Galgani, A. Giorgilli, and J.-M. Strelcyn, "Lyapunov characteristic exponents for smooth dynamical systems and for hamiltonian systems; a method for computing all of them. part 1: Theory," *Meccanica*, vol. 15, no. 1, pp. 9–20, 1980.

[96] K. Ramasubramanian and M. Sriram, "A comparative study of computation of lyapunov spectra with different algorithms," *Physica D: Nonlinear Phenomena*, vol. 139, no. 1, pp. 72–86, 2000.

[97] D. P. Kroese and J. C. Chan, "Common statistical models," in *Statistical Modeling and Computation*, pp. 101–120, Springer, 2014.

[98] D. J. MacKay, "Introduction to monte carlo methods," in *Learning in graphical models*, pp. 175–204, Springer, 1998.

[99] C. M. Bishop and N. M. Nasrabadi, *Pattern recognition and machine learning*, vol. 1. springer New York, 2006.

[100] L. L. Carter and E. D. Cashwell, "Particle-transport simulation with the monte carlo method," tech. rep., Los Alamos Scientific Lab., N. Mex.(USA), 1975.

[101] C. Andrieu, N. De Freitas, A. Doucet, and M. I. Jordan, "An introduction to mcmc for machine learning," *Machine learning*, vol. 50, no. 1-2, pp. 5–43, 2003.

[102] C.-F. Lin and S.-D. Wang, "Fuzzy support vector machines," *Neural Networks, IEEE Transactions on*, vol. 13, no. 2, pp. 464–471, 2002.

[103] T. Joachims, *Text categorization with support vector machines: Learning with many relevant features*. Springer, 1998.

[104] J. A. Suykens and J. Vandewalle, "Least squares support vector machine classifiers," *Neural processing letters*, vol. 9, no. 3, pp. 293–300, 1999.

[105] W. M. Campbell, D. E. Sturim, and D. A. Reynolds, "Support vector machines using gmm supervectors for speaker verification," *Signal Processing Letters, IEEE*, vol. 13, no. 5, pp. 308–311, 2006.

[106] C. Shawe-Taylor and S. Schölkopf, "The support vector machine," 2000.

[107] J. Platt *et al.*, "Sequential minimal optimization: A fast algorithm for training support vector machines," 1998.

[108] R.-E. Fan, P.-H. Chen, and C.-J. Lin, "Working set selection using second order information for training support vector machines," *The Journal of Machine Learning Research*, vol. 6, pp. 1889–1918, 2005.

[109] L. Bottou and C.-J. Lin, "Support vector machine solvers," *Large scale kernel machines*, pp. 301–320, 2007.

[110] K. Tanaka and H. O. Wang, *Fuzzy control systems design and analysis: a linear matrix inequality approach*. John Wiley & Sons, 2004.

[111] Z. Lendek, T. M. Guerra, R. Babuška, and B. De Schutter, *Stability analysis and nonlinear observer design using Takagi-Sugeno fuzzy models*, vol. 262. springer, 2010.

[112] J.-C. Lo and M.-L. Lin, "Observer-based robust $h_\infty$ control for fuzzy systems using two-step procedure," *Fuzzy Systems, IEEE Transactions on*, vol. 12, no. 3, pp. 350–359, 2004.

[113] Y.-Y. Cao and P. M. Frank, "Robust $h_\infty$ disturbance attenuation for a class of uncertain discrete-time fuzzy systems," *Fuzzy Systems, IEEE Transactions on*, vol. 8, no. 4, pp. 406–415, 2000.

[114] J. Yoneyama, "Robust h control analysis and synthesis for takagi–sugeno general uncertain fuzzy systems," *Fuzzy sets and systems*, vol. 157, no. 16, pp. 2205–2223, 2006.

[115] L. Perko, *Differential equations and dynamical systems*. Texts in applied mathematics, Springer-Verlag, 1991.

[116] Z. Feng, "Exact solutions to the liénard equation and its applications," *Chaos, Solitons & Fractals*, vol. 21, no. 2, pp. 343–348, 2004.

[117] A. Maccari, "Vibration control for parametrically excited lienard systems," *International Journal of Non-Linear Mechanics*, vol. 41, no. 1, pp. 146–155, 2006.

[118] T. D. Gillespie, "Fundamentals of vehicle dynamics (r-114)," *SAE International, March*, 1992.

[119] A. Goodarzi and A. Armion, "Integrated fuzzy-optimal motorcycle dynamic control," *Vehicle System Dynamics*, vol. 48, no. S1, pp. 505–524, 2010.

[120] Y. E. Ko and J. M. Lee, "Estimation of the stability region of a vehicle in plane motion using a topological approach," *International Journal of Vehicle Design*, vol. 30, no. 3, pp. 181–192, 2002.

[121] Y. Ko and C. Song, "Vehicle modeling with nonlinear tires for vehicle stability analysis," *International Journal of Automotive Technology*, vol. 11, no. 3, pp. 339–344, 2010.

[122] J. S. Jensen, "Non-linear dynamics of the follower-loaded double pendulum with added support-excitation," *Journal of sound and vibration*, vol. 215, no. 1, pp. 125–142, 1998.

[123] J. Thomson, "Chaotic dynamics of the partially follower-loaded elastic double pendulum," *Journal of sound and vibration*, vol. 188, no. 3, pp. 385–405, 1995.

[124] J. Kiusalaas, *Numerical methods in engineering with MATLAB®*. Cambridge university press, 2010.

[125] J. P. Chrstos and D. A. Guenther, "The measurement of static rollover metrics," *SAE Tech. Paper Series*, vol. 920582, no. 3, p. 4, 1992.

[126] S. Lapapong and S. Brennan, "Terrain-aware rollover prediction for ground vehicles using the zero-moment point method," in *American Control Conference (ACC), 2010*, pp. 1501–1507, IEEE, 2010.

[127] S. Lapapong, A. Brown, K. Swanson, and S. Brennan, "Zero-moment point determination of worst-case manoeuvres leading to vehicle wheel lift," *Vehicle System Dynamics*, vol. 50, no. sup1, pp. 191–214, 2012.

[128] E. Papadopoulos and D. A. Rey, "The force-angle measure of tipover stability margin for mobile manipulators," *Vehicle System Dynamics*, vol. 33, no. 1, pp. 29–48, 2000.

[129] S. B. Choi, "Practical vehicle rollover avoidance control using energy method," *Vehicle System Dynamics*, vol. 46, no. 4, pp. 323–337, 2008.

[130] Y.-H. Hsu, S. M. Laws, and J. C. Gerdes, "Estimation of tire slip angle and friction limits using steering torque," *Control Systems Technology, IEEE Transactions on*, vol. 18, no. 4, pp. 896–907, 2010.

[131] "Consumer information; new car assessment program; rollover resistance, national highway traffic safety administration." `http://www.nhtsa.gov/cars/rules/rulings/rollfinal/index.html#roll9`. 49 CFR Part 575 [Docket No. NHTSA-2001-9663; Notice 3] RIN 2127-AI81.